

Nuclear and Particle Physics through Quantum Sensing Using Cold Atoms and Molecules

Akio Kawasaki

National Metrology Institute of Japan (NMIJ), National Institute of Advanced Industrial Science and Technology (AIST),
1-1-1 Umezono, Tsukuba, Ibaraki 305-8563, Japan

(*Electronic mail: akio.kawasaki@aist.go.jp)

As techniques for manipulating single atoms and molecules developed, quantum technologies witnessed drastic advancements. These technologies are now so mature that they can be applied to various fields. One of such fields is nuclear and particle physics, which were conventionally investigated with high energy accelerators. In general, quantum sensing enables high-precision measurements, opening ways to investigate high-energy phenomena that slightly modify energy levels of low-energy systems by higher-order perturbations. In other cases, such high-precision measurements are sensitive to faint low-energy interactions between the low-energy system and exotic fields. These measurements open new parameter spaces to explore in conventionally investigated topics, e.g., variations of fundamental constants, dark matter, fifth force, parity violation, CP-violation, supersymmetric theories, and other physics beyond the Standard Model. Additionally, such measurements can serve as confirmations for existing results from completely different systems, or surpass existing results using smaller-scale experiments. The field of atomic and molecular physics oriented to nuclear and particle physics motivations evolved significantly. This paper provides an overview of the field of nuclear and particle physics through high-precision quantum measurements using atoms and molecules.

I. INTRODUCTION TO QUANTUM SENSING AND ITS APPLICATION TO HIGH ENERGY PHYSICS

Quantum sensing is defined in the following three ways, as described carefully in Ref.¹.

- (i) a measurement of a physical quantity that utilizes quantized energy levels as a detector.
- (ii) a measurement of a physical quantity that relies on the superposition of quantum states.
- (iii) a measurement of a physical quantity that employs quantum entanglement to enhance its sensitivity.

Among these three definitions, the most strict and certain definition of quantum sensing is (iii), because quantum entanglement is a phenomenon that never occurs in classical physics. However, entangled states, e.g., a squeezed state and a Schrödinger's cat state, are typically difficult to generate, and examples of measurements with entangled states are limited.

Definition (i) is broader and the most commonly used. In some cases, a quantum system and its classical limit are described in the same way. In such cases, when quantum sensing is discussed, the system is typically in a state where the energy separation between quantum states is comparable to the total energy of the system. For example, a harmonic oscillator can be described both classically and quantum mechanically. As a quantum sensor, excitation up to at most a few motional quanta is assumed. In other words, quantum sensing as defined by (i) is measurements involving a quantum system that can be well approximated to a two-level or, at most, few-level system. Even for a few-level system, in the context of atomic physics, a light field resonant with a specific pair of states is frequently assumed, and thus a two-level system is the most important configuration for quantum sensing.

Definition (ii) is also broad. An example of superposition of quantum states is that between a two-level system in an atom. While simply using a two-level system is within the scope of definition (i), superposition is a procedure to enhance the

measurement. Definition(ii) focuses on the methodology of the measurement, rather than the object used as the detector. In this sense, definition (ii) is different from definition (i).

In this paper, quantum sensing is broadly regarded as measurements defined by (i) and (ii) and deal with definition (iii) when relevant examples are available. There are many physical realization of quantized energy levels. Examples are superconducting qubits^{2,3}, mechanical harmonic oscillators including micro- or nanoparticles and suspended mirrors^{4,5}, spin systems in solid state materials such as nitrogen-vacancy centers⁶⁻⁸, cold atoms⁹ and molecules¹⁰ that are often trapped, and trapped ions^{11,12}. Among them, this paper focuses on cold atoms, molecules, and ions. Typically cooled down by laser cooling techniques, they are isolated from the environment very well. Rapidly-developing trapping and manipulation techniques provide ways to control the quantum state of a single atom, ion, or molecule independently and arbitrarily. This capability makes these systems suitable as quantum sensors.

The energy scale where atoms can be controlled using laser is on the order of 1 eV. This energy scale is orders of magnitude smaller than the typical energy scale for nuclear and particle physics, which is 100 keV or more. The difference between these two energy scales is bridged by the precision measurements that quantum sensors can perform. High-energy phenomena manifest in low-energy system as higher-order perturbations, slightly changing the energy levels of the low-energy system compared to the case without such high-energy phenomena. High precision measurements can detect such slight differences. The most important aspect of applying quantum sensing to nuclear and particle physics is thus the precise measurement of the energy difference of a two-level system affected by the high energy phenomena.

The low energy phenomena such as electromagnetic forces can become backgrounds when extracting such high-energy phenomena in a low-energy system. To discriminate such backgrounds properly, multiple measures are employed. In

addition, it is essential to have a proper theory that can extract high-energy phenomena from the slight energy shifts. The following discussions are centered at how to select an appropriate two-level system to extract a desired high-energy phenomenon, and how to cancel all backgrounds that can potentially mimic the signal.

This paper first briefly summarize how to prepare atomic and molecular systems useful for quantum sensors. As the real system, atomic clocks are first discussed. This is partly because the basis of the precision measurements lies in precision spectroscopy of atomic levels, and atomic clocks are the state-of-the-art for this field. Moreover, atomic clocks serve as platforms for exploring nuclear and particle physics through precision measurements. The systematic shifts and uncertainties discussed here provide typical factors to consider in other types of precision spectroscopy. The discussion is then followed by searches for variation of fundamental constants. This shows what atomic clocks are sensitive to as quantum sensors, also serving as a good introduction to why the next two topics are important: highly charged ion (HCI) clocks and nuclear clocks. These two clocks are not only promising candidate for next-generation optical clocks, but also as quantum sensors for variation of fundamental constants and some other high-energy phenomena. Although nuclear clocks are technically not an atomic system, they are included in the discussion due to their technical proximity. A somewhat related topic is searches for ultralight dark matter, where periodic modulation of fundamental constants are interpreted as signals of ultralight dark matter. After this, searches for a new force between an electron and a neutron through isotope shifts are discussed. These measurements also serve as precise measurements of the nuclear structure. Then Searches for atomic parity violation is mentioned, which involves interactions between the nucleus and an electron by the weak force. In the end, searches for electric dipole moment (EDM) in an electron and nuclei are described. EDMs have direct implications for supersymmetric theories that can have a energy scale of > 10 TeV.

II. TYPICAL PROCEDURE TO UTILIZE ATOMS AND MOLECULES FOR QUANTUM SENSORS

In this section, experimental procedures for preparing atoms as quantum sensors is briefly summarized. These are typical procedures, and in some cases, for example molecular beam experiments for electron EDM searches, the procedures of cooling and trapping are completely different.

Trapping atoms begins with creating an atomic beam. The method depends on the vapor pressure of the atoms. For low-vapor-pressure atoms like Yb or Sr, an atomic oven heated to a few hundred $^{\circ}\text{C}$ is used to generate an atomic beam. The resulting atomic beam has a center velocity of a few hundred m/s. For alkali atoms, which have relatively high vapor pressure, atomic dispensers are also used. These atoms have to be slowed down. A Zeeman slower¹³ is sometimes implemented for this purpose. In a Zeeman slower, a circularly-polarized laser beam slightly off-resonant from a broad atomic transition propagates to the opposite direction of the atomic beam.

Atoms in a certain velocity range resonant with the laser light due to the Doppler effect are decelerated. To keep these atoms resonant to the laser as they slow down, a spatially-varying magnetic field is applied, which shifts the atomic resonance by the Zeeman effect.

Sufficiently slow atoms can be trapped by a magneto-optical trap (MOT)¹⁴. A MOT is formed by a combination of circularly polarized light and a quadrupole magnetic field. In the standard configuration, counter-propagating light with σ^+/σ^- polarization red-detuned from a broad-linewidth transition provide a dissipation term. The quadrupole magnetic field induces a position-dependent scattering rate, creating an approximately harmonic potential. This potential attracts atoms to the center of the trap, and the dissipative force pull atoms to the center of the trap. As a result, the atoms are slowed, cooled, and confined in the trap. For a transition with a linewidth of $\Gamma = 2\pi \times 5$ MHz, the Doppler limited temperature is $\hbar\Gamma/2k_B = 0.12$ mK. For atoms with Zeeman sublevels in the ground state, polarization gradient cooling¹⁵ simultaneously functions to cool atoms down below this limit. With narrower-linewidth transitions, atoms can be cooled down to ~ 1 μK .

Typically, atoms are next transferred from the MOT to an optical lattice. An optical lattice is a trap for atoms made by pairs of counter-propagating laser beams that form a standing wave. Because of ac Stark shift, atoms are attracted to the most (least) intense part of the light field when the trapping laser is red (blue) detuned from broad-linewidth transitions¹⁶. Depending on the number and configuration of the pairs of the counterpropagating laser beams, one-, two-, or three-dimensional lattice can be formed.

In the optical lattice, atoms can be further cooled down. Various methods for cooling at this stage have been demonstrated, such as evaporative cooling¹⁷, sideband-resolved Raman cooling^{18–20}, cooling with a narrow-linewidth transition²¹, and Sisyphus cooling²². For precision spectroscopy, the goal of this cooling is to put all atoms at the motional ground state. This ensures that the transition frequency does not shift due to the excitation or de-excitation of the motional state. The resulting temperature is very low, sometimes 100 nK or less.

The final stage of state preparation is to initialize all atoms into a single internal state. The ground state of an atom generally has several sublevels, such as Zeeman sublevels and hyperfine structures. In general, atoms are distributed over these states, and to utilize them as quantum sensors, all atoms need to be put in a single state. Optical pumping²³ is the simplest procedure to initialize all atoms in an ensemble to a single state. The actual procedure depends on the system. For example, if the ground state has several Zeeman sublevels with different m_F and no hyperfine structure, where m_F is the magnetic quantum number for total angular momentum F , irradiating the atoms with σ^+ -polarized light resonant with a broad-linewidth transition puts all atoms into the highest m_F state. More sophisticated techniques such as stimulated Raman adiabatic passage (STIRAP)^{24,25}, rapid adiabatic passage^{26,27}, and coherent population trapping²⁸ are also widely used for state preparations.

After the state preparation is completed, atoms finally undergo the measurement sequence. While the measurement sequence depends on the specific experiment, there are two basic procedures for a sequence. To describe these sequences, a two-level system with an energy difference of $\hbar\omega_0$ is assumed. This system is driven by a laser of frequency $\omega = \omega_0 + \delta$ and intensity characterized by Rabi frequency Ω . Detailed formalism can be found in textbooks on atomic physics²⁹.

The first sequence is the Rabi sequence. In this sequence, resonant light drives the two-level system. When the initial state is at the ground state $|g\rangle$, the final state $|f\rangle$ after a pulse of duration t satisfies $|\langle e|f\rangle|^2 = \frac{\Omega^2}{\Omega^2 + \delta^2} \sin^2 \frac{\sqrt{\Omega^2 + \delta^2}t}{2}$, where $|e\rangle$ is the excited state. When $\omega = \omega_0$ and $\Omega t = \pi$, $|f\rangle$ is purely $|e\rangle$. Such a pulse to drive from $|g\rangle$ to $|e\rangle$ is called a π pulse. When the pulse length is half as long as the π pulse, $|f\rangle = (|g\rangle + |e\rangle)/\sqrt{2}$, and this pulse is called a $\pi/2$ pulse. The relative phase between $|g\rangle$ and $|e\rangle$ in $|f\rangle$ can be controlled by adjusting the phase offset of the driving light field. If ω_0 is perturbed by external fields, the nominal pulse length might not result in the desired final state. To mitigate this, composite pulses, which are intensively studied in the field of nuclear magnetic resonance (NMR)^{30–32}, can be applied to laser spectroscopy.

The second basic sequence is the Ramsey sequence. In this sequence, atoms are initially prepared in the ground state. First, a $\pi/2$ pulse is applied, putting atoms in a superposed state $(|g\rangle + |e\rangle)/\sqrt{2}$. Then atoms are left for a period of τ_R , which is referred to as the interrogation time. During this period, if ω drifts from ω_0 , its accumulation $\Delta\phi = \int_0^{\tau_R} (\omega - \omega_0)dt$ is recorded as a phase shift between the atomic system and the laser. $\Delta\phi$ is read out by another $\pi/2$ pulse and subsequent proper state detection of $|g\rangle$ and $|e\rangle$. Both the Rabi sequence and the Ramsey sequence are used to measure the frequency offset between the laser system and the atomic system to lock the laser to the atomic resonance. Also, the Ramsey sequence is frequently used to detect phase drift $\Delta\phi$ caused by external fields or hypothetical phenomena.

III. ATOMIC CLOCK

A. Introduction

1. Components of clocks

Modern stable clocks, including atomic clocks, consist of three main components: an oscillator, a counter, and a reference. The periodic motion of the oscillator is counted by the counter, which displays the time. For the stability purpose, the oscillator is locked to the reference. In an atomic clock, these components are physically realized as a stable laser, frequency comb, and an atomic transition, respectively. The frequency of the stable laser is tuned to the resonant frequency of an atomic transition, so that the response of atoms as a result of interrogation by the laser serve as a signal for feedback to stabilize the laser frequency. Because the atomic transition serves as the ultimate source of stability, a deep understanding of the behavior of atoms is essential for improving uncertainty

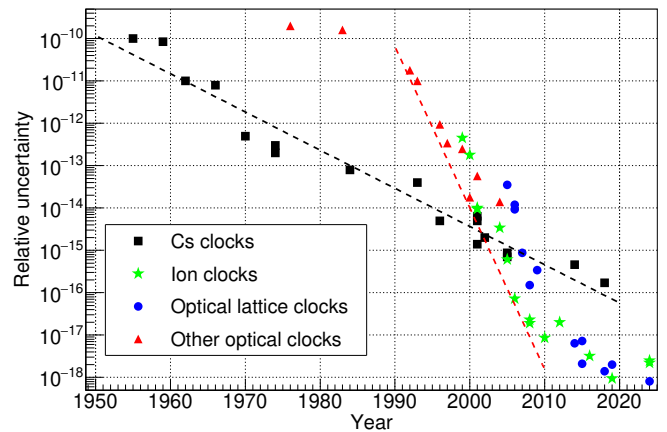


FIG. 1. Historical development of the relative uncertainty of atomic clocks: the black dotted line shows the average improvement in the uncertainty for the Cs clocks, and the red dotted line shows approximate development of the uncertainty for the best optical clocks.

for an atomic clock.

A good reference should minimize relative frequency fluctuation $\Delta\nu/\nu_0$, where $\nu_0 = \omega_0/2\pi$ is the frequency of an atomic transition and $\Delta\nu$ is its uncertainty. Such minimization is typically achieved by using a forbidden transition, i.e., a transition that cannot be driven by the electric dipole (E1) interaction. In addition, for atomic clocks, it is important to select an atomic resonance that is insensitive to external perturbations. It should also be noted that the physics of selected atomic transition and a laser to drive it is well modeled as a two-level system driven by a light field. This two-level system is regarded as the quantized energy levels when the atomic clock is regarded as a quantum sensor. Various sources of the perturbation on the resonant frequency of the transition are shown in this paper. For a clock, such perturbations are sources of uncertainties, but when it is regarded as a sensor, the system is regarded to be sensitive to the source of perturbations.

Historically, a microwave transition between $m_F = 0$ states of two hyperfine levels in the ground state of alkali atoms such as Cs and Rb was used as the atomic transition. This transition is a magnetic dipole (M1) transition, and its linewidth is not limited by the natural lifetime of the state but other effects, such as the relaxation due to collisions with other atoms. The uncertainty for the Cs clock has improved by six orders of magnitude over decades, as shown in Fig. 1. With the advent of laser spectroscopy, optical clocks developed much more quickly than microwave clocks. One of the advantages of optical clocks is five orders of magnitude larger ν . $\Delta\nu$ can be limited by some external factors, such as the coherence time of the laser and lifetime of atoms in a trap due to residual gas collision, and is not necessarily the natural linewidth of the transition itself, resulting in $\Delta\nu/\nu_0$ smaller than microwave clocks.

Optical clocks are sorted into two types. One is the optical lattice clock, and the other is the ion clock. An optical lattice clock interrogates thousands of atoms trapped in an optical lat-

tice, and an ion clock is conventionally operated with a single ion trapped in a Paul trap. Initially, the ion clock developed as the best optical clock. The optical lattice clock was proposed in 2003³³, and first demonstrated in 2005³⁴. Around this time, the relative uncertainty of optical clocks started to surpass that of microwave clocks, and since then, optical clocks have improved their uncertainties by three orders of magnitude. So far, the smallest relative uncertainties for the optical lattice clock and the ion clock are about the same, and each clock has its own advantages and disadvantages. Early developments of optical clocks are summarized well in some previous review papers^{35,36}.

2. Allan deviation and the stability of atomic clocks

The stability of atomic clocks is typically described by the Allan deviation $\sigma(\tau)$ ³⁷. It is defined in the following way, and the Allan deviation is in general a good measure of the stability of time-varying signals.

$$\sigma^2(\tau) = \frac{1}{2} \langle (\bar{y}_{n+1} - \bar{y}_n)^2 \rangle = \frac{1}{2\tau^2} \langle (x_{n+2} - 2x_{n+1} + x_n)^2 \rangle, \quad (1)$$

where $\langle \dots \rangle$ denotes the expectation operator, $\bar{y}_n = (x(nT_C + \tau) - x(nT_C))/\tau$, and $x_n = x(nT_C)$ is the n th data that are taken every time in interval T_C . In case where the dominant noise source is the phase noise, flicker frequency noise, white frequency noise, random walk frequency noise, and frequency drift, the Allan deviation scales with τ as τ^{-1} , $\tau^{-1/2}$, τ^0 , $\tau^{1/2}$, and τ , respectively. The stability of the state-of-the-art atomic clocks described by the Allan deviation is limited by quantum mechanical randomness when a superposition state between $|g\rangle$ and $|e\rangle$ is projected onto either $|g\rangle$ or $|e\rangle$. This is called quantum projection noise (QPN)³⁸, and the corresponding stability limit is called standard quantum limit (SQL). The SQL is expressed as

$$\sigma_\tau = \frac{1}{\omega_0 \tau_R} \sqrt{\frac{T_C}{\tau}} \sqrt{\frac{\xi_W^2}{N}}, \quad (2)$$

where T_C is the length of a single cycle of repeated measurements, ξ_W^2 is the Wineland parameter for squeezing³⁹, and N is the number of atoms in the system⁴⁰. For a coherent spin state⁴¹, $\xi_W^2 = 1$, and $\xi_W^2 < 1$ when the spin state is squeezed in the phase direction during the Ramsey sequence. The optimal τ_R is the Ramsay coherence time τ_{Rc} , which for alkaline-earth-like atoms (see Section III B 2) can be calculated as

$$\tau_{Rc} = \frac{2}{\Gamma_e^I + \Gamma_g^I + \Gamma_{12}^R + \Gamma_1^{BBR} (1 + R_0^D/R_1^D)}, \quad (3)$$

where Γ_e^I (Γ_g^I) is the atom loss rate from the trap for the excited (ground) state, Γ_{12}^R is the Raman scattering rate of the trap laser for the excited state, Γ_1^{BBR} is the rate at which the black body radiation (BBR) induces the transition from the excited state to the 3P_1 state via the 3D_1 state, and R_j^D is the branching ratio from the 3D_1 to the 3P_j states.

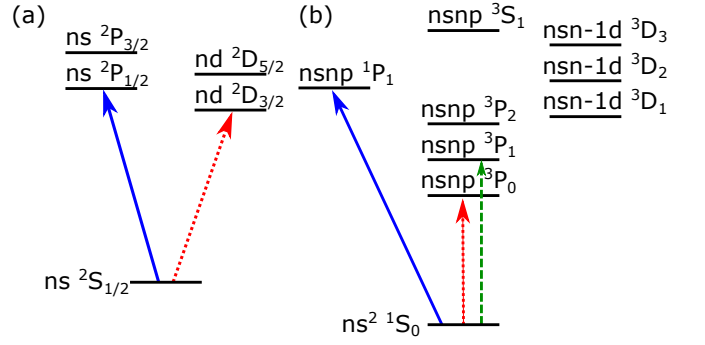


FIG. 2. Typical energy structure of atoms used for atomic clocks: (a) alkali-atom-like structure (b) alkali-earth-like structure: the blue solid lines show the transitions used for laser cooling. The green dashed line in (b) is the transition used for the second-stage laser cooling. The red dotted lines are the clock transitions.

B. Popular atomic species for atomic clocks

For ion clocks and optical lattice clocks, atoms with certain kinds of transitions are preferred. A narrow-linewidth transition is essential to operate a clock. Also, a broad-linewidth transition convenient for laser cooling plays an important role to cool atoms down. Atoms with these transitions can be sorted into the following two types.

1. Alkali-atom-like species

Alkali-atom-like species have a single electron outside of a closed shell, and have a typical energy structure shown in Fig. 2(a). The advantage of this species is the strong transition from the $^2S_{1/2}$ ground state to a 2P excited state suitable for laser cooling. The alkali atoms themselves do not have a narrow-linewidth transition suitable for the clock transition. However, some singly-ionized ions of alkali-earth-like atoms have such narrow-linewidth transitions. The narrow-linewidth transition used as the clock transition is usually from the $^2S_{1/2}$ ground state to a 2D excited state, and it is an electric quadrupole (E2) transition. Example for such ion clocks are Ca^{+42} , Sr^{+43} , Ba^{+44} , Ra^{+45} , and Hg^{+46} . The linewidth of the E2 transition is $\lesssim 1$ Hz, as listed in Table I. An exception is Yb^+ . In addition to the two E2 transitions to 2D states, it also has an electric octupole (E3) transition to an 2F state. Because the E3 transition is a higher-order effect than a E2 transition, the linewidth is as narrow as $3.20(16)$ nHz⁴⁷.

2. Alkaline-earth-atom-like species

Alkaline-earth-like atoms have two valence electrons outside of a closed shell. All electronic spins pair up in the ground state, and the ground state has zero electronic angular momentum. Two electrons provide a wider variety of electronic states than alkali atoms, as shown in Fig. 2(b), some of which are beneficial to atomic clocks. The ground state is a

TABLE I. Major optical clock transitions: λ_{trap} is the magic wavelength for optical lattice clocks. The transitions listed here have small enough uncertainty to be listed in the secondary representation of the second. The units for ν and λ_{trap} are THz and nm, respectively. Note that the clock transition for ^{88}Sr is strictly forbidden, and it is induced by applying a magnetic field.

Atom	Transition	ν_0	$\Delta\nu$	λ_{trap}
$^{27}\text{Al}^+$	$3s^2\ ^1S_0 \rightarrow 3s3p\ ^3P_0$	1121	7.73(53) mHz ⁴⁸	
$^{40}\text{Ca}^+$	$4s\ ^2S_{1/2} \rightarrow 3d\ ^2D_{5/2}$	411	0.186 Hz ⁴⁹	
$^{88}\text{Sr}^+$	$5s^2\ ^1S_0 \rightarrow 4d\ ^2D_{5/2}$	445	0.4 Hz ⁵⁰	
$^{171}\text{Yb}^+$	$6s\ ^2S_{1/2} \rightarrow 5d\ ^2D_{3/2}$	688	2.58(27) Hz ⁵¹	
$^{171}\text{Yb}^+$	$6s\ ^2S_{1/2} \rightarrow 4f^{13}6s^2\ ^2F_{7/2}$	642	3.20(16) nHz ⁴⁷	
$^{199}\text{Hg}^+$	$6s\ ^2S_{1/2} \rightarrow 5d\ ^2D_{5/2}$	1065	1.83(8) Hz ⁵²	
^{87}Sr	$5s^2\ ^1S_0 \rightarrow 5s5d\ ^3P_0$	429	1.35(3) mHz ⁵³	813
^{88}Sr	$5s^2\ ^1S_0 \rightarrow 5s5d\ ^3P_0$	429		813
^{171}Yb	$6s^2\ ^1S_0 \rightarrow 6s6p\ ^3P_0$	518	7.03(6) mHz ⁵⁴	759
^{199}Hg	$6s^2\ ^1S_0 \rightarrow 4f^{13}5d6s(J=2)$	1129	0.1 Hz ³⁵	363

singlet state, and it can be driven to the 1P_1 singlet state via a broad-linewidth E1 transition. This transition is used for the first stage of laser cooling. Among triplet states, the 3P_1 state has a total angular momentum of $J = 1$, and thus the selection rule $\Delta J = 1$ for the transition from the ground state is satisfied, except that the transition is between a singlet and a triplet state. Such an intercombination transition is weakly allowed by spin-orbit coupling (L-S coupling), and thus the transition from the ground state to the 3P_1 state has a narrower linewidth than the transition to the 1P_1 state. The narrow linewidth allows atoms to be cooled down to $\sim 10\ \mu\text{K}$ or less, which is why the transition is used for the second stage of laser cooling.

The transition from the ground state to the 3P_0 state and the 3P_2 state are not allowed by the E1 interaction, even with L-S coupling. Particularly, the transition from the ground state to the 3P_0 state is strictly forbidden, because of $J = 0$ for both the ground state and the excited state. If the nucleus has a nonzero magnetic moment, this mixes the 3P_0 state and the 3P_1 state slightly, making the transition probability from the ground state to the 3P_0 state finite. The mixing is so small that the linewidth is as small as ~ 1 mHz, as summarized in Table I. This narrow linewidth is excellent for the clock transition. Also, thanks to the absence of electronic angular momentum, it is insensitive to magnetic fields, which is advantageous for stability under ambient fields. Note that without a nuclear magnetic moment, a strong magnetic field must be applied to induce the transition.

The 3P_2 state also has a narrow enough linewidth to function as a clock transition. However, because of its sensitivity to magnetic fields, so far, the transition has not been used as intensively as the 3P_0 state for clock operation. This state is used as a probe for many-body physics in quantum degenerate gases^{55–58}. Yb has one more metastable state: the $4f^{13}5d6s^2(J=2)$ state. This state is theoretically predicted to be beneficial for various fundamental physics searches^{59–61}, and recently the direct transitions to this state from the ground state^{62,63} and the $6s6p\ ^3P_0$ state⁶⁴ are observed for the first time. It is expected that the uncertainty on the absolute

frequency measurement will improve to the same level as other clock transitions, and the first report on the analysis for nuclear and particle physics application of this transition is available⁶⁵.

Many atomic species with alkaline-earth-like structure are used for atomic clocks. As for neutral atoms, most alkaline-earth-like atoms have been experimentally investigated: Mg⁶⁶, Ca⁶⁷, Sr⁶⁸, Yb⁶⁹, Cd⁷⁰, and Hg⁷¹. Ba has 3D states at lower energy than that of 3P states, and thus the 3P_0 state cannot serve as the clock transition. So far, only a theoretical proposal is available for Be⁷². The 3P states in Ca has such a narrow linewidth that the 3P_1 state was investigated as the clock transition in the past. Sr and Yb are the two most common atomic species for optical lattice clocks. Recently, the narrow-linewidth transitions in these atoms are also utilized for atom interferometry⁷³ and quantum computation⁷⁴. Some ion clocks also have alkali-earth-like electronic structure. Examples are Al^{+75} , In^{+76} , and Lu^{+77} .

C. Optical lattice clock

An optical lattice clock is an atomic clock where thousands of neutral atoms are trapped in an optical lattice. The trapping laser used for the optical lattice is tuned to a special frequency called the magic frequency (the word magic wavelength is also frequently used when referring to the wavelength)^{33,78}, where the ac Stark shift due to the trapping laser is cancelled out between the ground state and the excited state for the clock transition. Most atoms suitable for the optical lattice clock are alkaline-earth-like atoms, due to the existence of a narrow-linewidth transition in neutral atoms.

The stability of the state-of-the-art optical lattice clock reached 1×10^{-18} in 2013⁷⁹. Thanks to the development of reference cavities that provides a short-term stability for the clock laser, represented by the development of the cryogenic cavity^{80,81}, and the development of methods to analyze two subparts of a single atomic ensemble to cancel out fluctuations originating from the laser instability, the stability at 1 s improved from 3.2×10^{-1679} to 4.4×10^{-1882} in the past decade. Accordingly, the long-term stability improved to 7.6×10^{-2182} . Higher stability enables us to estimate systematic uncertainties in a shorter period of time, and therefore contributes to improving the uncertainty of the clock. An optical lattice clock with a relative uncertainty of 2×10^{-18} was reported in 2015⁸³, and now the best clock has a relative uncertainty of 8×10^{-1968} .

1. Major systematic uncertainties

For a good clock, it is essential to have a precise estimate of systematic uncertainties. Optical lattice clocks are typically stable enough to have small enough statistical uncertainty by increasing the overall average time, and their overall uncertainties are limited by systematic uncertainties. Historically, developments in the uncertainty of optical lattice clocks have been enabled by a better understanding of systematic shifts,

and desire for further understanding of the uncertainties has motivated methods to cancel the shifts in a better way. A good example is the dc Stark shift. When optical lattice clocks were reported for the first time, the dc Stark shift by stray electric fields in an ordinary vacuum chamber was not a major source of the total systematic uncertainty. However, as the total uncertainty for the optical lattice clock improved, the effect of ambient electric fields on the systematic uncertainty was observed⁸⁴. To estimate it precisely, dc Stark shift was carefully measured with a chamber with electrodes inside⁸⁵, and now the inner surface of the viewports, which is an insulator, is coated with indium tin oxide to avoid the accumulation of charge on its surface to suppress the amount of stray electric fields^{85–87}.

One of the major sources of the uncertainty is the BBR shift. The uncertainty comes both from the amount of the BBR atoms experience and the uncertainty in the polarizability of the ground and particularly the excited state. To estimate the polarizability precisely, the transition matrix for the $^3P_0 \rightarrow ^3D_1$ transition, which has the smallest transition frequency among the transition from the 3P_0 state, is carefully measured for Sr⁶⁸ and Yb⁸⁸. To control the amount of the BBR, a metallic shield whose temperature is stabilized is implemented inside a vacuum chamber. The temperature is calibrated at the 1-mK level^{69,83}, confirmed by a Pt thermometer that can be located near location of the atoms. In addition, the inner surface of the vacuum chamber and the shield is coated with carbon nanotube to keep the emissivity of the chamber wall as close to 1 as possible⁸⁹. Surrounding atoms with a cold shield inside a vacuum chamber reduces the amount of BBR at the location of atoms according to the Stefan-Boltzmann law. Such a cryogenic optical lattice clock at 95 K achieved a small BBR uncertainty⁹⁰.

Smaller uncertainty from the BBR shift can also be achieved by using atoms less sensitive to BBR. Hg, Cd, Mg, and Tm are attractive for this reason⁹¹, and Hg, Cd, and Tm clocks are already achieved in several places^{70,71,92,93}. A Mg clock is under development with the clock transition frequency and the magic wavelength already measured^{66,94}.

Another major source of uncertainty originates from the ac Stark shift due to the trapping laser^{68,69}. When the total uncertainty was on the order of 10^{-16} , this was cancelled out by setting a proper magic wavelength^{95,96}. However, with an orders of magnitude smaller uncertainty, higher order effects also need to be considered. First, vector and tensor shifts, which depends on the polarizations of the trapping lasers, come into play^{83,97}. The shift proportional to the trap depth U_0 is formulated as

$$\Delta v^{E1} = (\Delta \kappa^s + \Delta \kappa^v m_F \xi \hat{\mathbf{k}} \cdot \hat{\mathbf{B}} + \Delta \kappa^t \beta) U_0, \quad (4)$$

where $\beta = (3|\hat{\mathbf{e}} \cdot \hat{\mathbf{B}}|^2 - 1)[3m_f^2 - F(F+1)]$, with $\hat{\mathbf{e}}$ and $\hat{\mathbf{k}}$ being the lattice polarization and propagation vectors and $\hat{\mathbf{B}}$ being the bias magnetic field direction. $\Delta \kappa^s$, $\Delta \kappa^v$, and $\Delta \kappa^t$ are the scalar, vector, and tensor components of the shift. For a one-dimensional lattice, properly selecting the relative orientation between the polarization and the magnetic field cancels some of these shifts. However, for a three-dimensional lattice, such

cancellation does not work for all three dimensions. This is the main motivation for having a one-dimensional optical lattice in the state-of-the-art optical lattice clock.

The ac Stark shift including the nonlinear terms for a one-dimensional optical lattice is characterized in the following way:

$$\begin{aligned} \frac{\Delta v_{LS}(u, \delta_L, n_z)}{v_C} &= \left(\frac{\partial \tilde{\alpha}_{E1}}{\partial v} \delta_L - \tilde{\alpha}_{M1E2} \right) (n_z + 1/2) u^{1/2} \\ &\quad - \left[\frac{\partial \tilde{\alpha}_{E1}}{\partial v} \delta_L + \frac{3}{2} \tilde{\beta} \left(n_z^2 + n_z + \frac{1}{2} \right) \right] u \\ &\quad 2\tilde{\beta} \left(n_z + \frac{1}{2} \right) u^{3/2} - \tilde{\beta} u^2, \end{aligned} \quad (5)$$

where $u = U_0/E_R$ with E_R being recoil energy, n_z is the quantum number for the longitudinal vibrational state, $\tilde{\alpha}_{E1}$ is the differential E1 polarizability between the ground state and the excited state of the clock transition, and $\tilde{\alpha}_{M1E2}$ and $\tilde{\beta}$ are the differential multipolarizability and hyperpolarizability, respectively. This includes the effect of the longitudinal temperature of atoms in the lattice in the form of n_z and effects in Eq. 4. The radial temperature T_r can be incorporated by modifying u^j to $(1 + jk_B T_r / u E_R)^{-1} u^j$, where j is the exponent on u for each term in Eq. 5 and k_B is Boltzmann constant. Experimental efforts are also made to cool radial temperature^{21,22}. Analysis with this formalism resulted in the idea of operational magic intensity⁹⁸. Even with these characterizations, the lattice ac Stark shift remains the major source of uncertainty in the best optical lattice clocks. A careful analysis on the order of 10^{-19} is reported for Sr⁹⁹, leading to a relative uncertainty of 9×10^{-19} ⁶⁸. Similar analysis is also going on for Yb¹⁰⁰. An alternative method to suppress the uncertainty from the ac Stark shift is to make use of atoms with small higher-order effects. Particularly, hyperpolarizability for Hg, Cd, and Zn is calculated to be smaller than for Sr and Yb¹⁰¹. These clocks can be potentially useful in the context of the ac Stark shift, in addition to the BBR shift.

The ac Stark effect also shifts the transition frequency due to the clock laser itself. Because irradiation of the clock laser is unavoidable to drive the clock transition, to suppress the shift, long irradiation times with small and uniform intensity are typically selected for the $\pi/2$ pulses. For such operations, simply inducing Rabi flopping is more suitable than the Ramsey sequence where a separate interrogation time is required in addition to $\pi/2$ pulses. As a result, for state-of-the-art optical lattice clocks, it is more common to use a single $\pi/2$ pulse to observe the frequency offset of the clock laser from the atomic system.

The density shift, which is the frequency shift due to atom-atom interactions, is another source of uncertainty. This is proportional to the density of atoms in the lattice, and thus reducing the density of atoms suppresses the uncertainty. Trapping atoms in a three-dimensional optical lattice with excessive atoms removed by reducing the Fermi temperature of the degenerate Fermi gas¹⁰² sets density shift under a good control. The disadvantage of the first method is the increase in QPN due to the small number of atoms, and the second method induces a large uncertainty in the ac Stark shift due to

the tensor shift. Additionally, the edge effect¹⁰³ needs to be carefully treated. Recent reports utilize low-density fermionic gas in large vertical one-dimensional optical lattices. First, a large optical lattice, e.g., characterized by a waist size of 260 μm ⁸², is used to reduce the density of atoms. To achieve this optical lattice, it is common to enhance the trap laser intensity with an intermediate finesse cavity ($F \sim 200, 1300$ ^{69,82}). Delocalization of atoms to reduce the density in this large one-dimensional optical lattice is also performed.^{104,105} Second, immunity of fermionic isotopes to s-wave collisions suppresses the collisional shift. The remaining shift due to p-wave collisions is canceled by inter-layer s-wave collisions induced by the wave function of atoms ranging over a few layers because of low trap depth ($U_0 < 10E_R$)⁸². This achieved the clock of 10^{-19} relative uncertainty⁶⁸.

2. Varieties of optical lattice clocks

As technologies for the optical lattice clock mature, systems oriented to various applications are also developed. These systems are not limited to the conventional optical lattice clock system where a single atomic ensemble is loaded into a single location in an optical lattice.

Transportable optical lattice clocks are developed for the purpose of testing of geodesy and comparing clocks at remote locations. An example of such a clock is a lab on a trailer¹⁰⁶. More compact ones are used to examine the validity of general relativity at an observation tower¹⁰⁷, and efforts to make it even smaller are ongoing. Clock comparison across continents using such transportable clocks was recently reported^{108,109}.

Comparison between atomic clocks is also performed using fiber links. Metrology labs are linked via optical fibers in various places around the world. The longest network is in Europe^{110,111}, and clock comparisons between remote national metrology institutes are performed^{111,112}. Other fiber links are made use of to compare different types of clocks with unprecedentedly small uncertainty¹¹³ and to measure the height based on time delay¹¹⁴.

For differential comparison between atomic ensembles, multiple atomic ensembles are trapped in a single one-dimensional optical lattice. For this purpose, a moving optical lattice can be utilized¹¹⁵. Trapping atoms at up to six spatially different locations is demonstrated, and the relative measurements are used to test general relativity¹¹⁶ and to improve clock stability¹¹⁷. For a fixed optical lattice, two ensembles are trapped by shifting the position of the MOT¹⁰⁵.

Continuous interrogation is beneficial for suppressing the Dick effect^{118,119}, where pulsed interrogation of the atomic system induces instability at the frequency corresponding to the period of a single cycle of the experiment. Also, continuous interrogation allows feedback on the phase, causing the Allan deviation to scale $\sim 1/\tau$ rather than $\sim 1/\sqrt{\tau}$. This contributes to a quicker estimate of systematic shifts. The continuous generation of an ultracold atomic beam for the future development of the continuous optical lattice clock is reported¹²⁰.

The rapidly developing technology of optical tweezer arrays is also applied to atomic clocks^{121,122}. Some tweezer array systems are designed for Sr and Yb^{123–125}, some of which are utilized as atomic clocks. There is a report on the stability using ⁸⁸Sr atoms¹²⁶, but characterization of the uncertainty has not been reported yet. The ability to control atoms individually is advantageous for generating entangled states to enhance the stability, as discussed in the next section.

3. Enhancement of stability by entanglements

The atomic clock system is one of the few systems where enhancement in their performance through quantum entanglement is demonstrated. Early proof-of-principle experiments were performed with microwave clocks using ⁸⁷Rb^{127,128}. These reports utilized spin-squeezed states as the source of entanglement. The first spin-squeezed optical clock is demonstrated with Yb. Spin squeezing was performed on the spin-1/2 system in the ground state of ¹⁷¹Yb¹²⁹, and then transferred to the excited state of the clock transition to demonstrate the improvement in the clock performance⁴⁰. The report⁴⁰ showed the improvement in the stability of the atomic system by 4.4 dB below the SQL with a stability of $\sim 10^{-14}$, limited by the coherence time of the clock laser. The improvement in the clock performance was demonstrated at the stability of $\sim 10^{-17}$ ¹³⁰ with a Sr optical lattice clock. Note that the spin squeezing described here was performed in a cavity quantum electrodynamics (QED) system, where atoms are located in a high-finesse cavity that enhances the coupling between atoms and light.

The improved performance of optical clocks using Greenberger-Horne-Zeilinger (GHZ) states is demonstrated with tweezer array clocks.^{131,132} The GHZ state is generated through a strong interaction between atoms via a Rydberg state. The strongly entangled atoms shows high phase sensitivity, resulting in better clock performance when the Ramsey sequence is used. However, because the GHZ state and other entangled states are more sensitive to decoherence, atomic coherence time decreases and the interrogation time is typically shorter than that for state-of-the-art optical lattice clocks. This cancels the enhancement due to the reduced QPN, so the overall stability of the clock does not necessarily improve with entangled states. Nevertheless, the shorter interrogation time reduces the time required for a single cycle of the clock operation, increasing the bandwidth of the clock measurement. Such an increase can be beneficial when the interrogation time is constrained for some reasons (e.g., for a fountain clock) or for searches for ultralight dark matter with a relatively large masses (see Section VII).

D. Ion clocks

1. State-of-the-Art Systems

In a conventional ion clock, a single ion is trapped in a Paul trap. A Paul trap is designed for trapping charged particles

using an oscillating quadrupole electric field^{133–135}. Because the Paul trap has longer history than the magic-wavelength optical lattice, ion clocks as the frequency standard were developed ahead of optical lattice clocks, as shown in Fig. 1. Although the 1-s stability for the ion clock is not as good as that of optical lattice clocks, their ability for long-term operation allows the ion clocks with smallest relative uncertainties to be comparable to that of optical lattice clocks.

The two ionic species with smallest uncertainties are Al^{+75} and $\text{Yb}^{+136,137}$. Al^{+} is alkaline-earth-like species, while Yb^{+} has an alkali-atom-like electronic structure with an octupole transition where an electron in the $4f$ orbital is excited. Other ionic species with alkaline-earth like structure include Lu^{+77} and In^{+76} . Alkali-atom-like structure with E2 transitions are also investigated, such as $\text{Sr}^{+43,138}$, Ca^{+42} , Ba^{+44} , and Ra^{+45} . Details of some of these clocks are summarized in Table I. For some ions, the wavelength of broad-linewidth transitions suitable for laser cooling is too short for easily available laser systems. In such cases, the laser cooling is performed through sympathetic cooling of another ion trapped in the same Paul trap. The preparation and the detection of the quantum state is also performed by the other ion through the Coulomb coupling of their motional states, which is called quantum logic spectroscopy¹³⁹. For example, in an Al^{+} clock, the Al^{+} ion is sympathetically cooled with an Mg^{+} ion, and quantum logic spectroscopy is performed through the Mg^{+} ion.

2. Systematic Uncertainties

The advantage of the ion clock regarding systematic uncertainties is the absence of the lattice ac Stark shift. Instead, it has uncertainties arising from the micromotion-related Doppler shift. The uncertainty originated from micromotion is the main source of uncertainties in some clocks^{43,75,137}. In fact, the advancements in their accuracies compared to previous-generation apparatuses are achieved by designing a new electrode configuration for their Paul trap to suppress micromotions⁷⁵.

Other uncertainties are generally the same as those in optical lattice clocks. The BBR shift is another dominant source of uncertainty^{42,43,75,76,136–138} and extensively studied. For some ions, papers specifically evaluating the BBR shift are published^{140,141}, and a cryogenic clock is achieved for a Ca^{+} ion clock⁴². Other components, such as the second-order Zeeman shift and the servo error, also contribute to the total uncertainty. Note that conventional ion clocks are free from the collisional shift because a single ion is used for the spectroscopy.

The main disadvantage of ion clocks compared to optical lattice clocks is the large QPN due to the small number of ions in the trap, as opposed to the large number of neutral atoms in optical lattice clocks. To overcome this, spectroscopy schemes better than the Rabi or Ramsey sequence are experimentally implemented. The hyper-Ramsey sequence, first theoretically developed in Ref.¹⁴², is experimentally investigated in an Yb^{+} ion clock¹⁴³. Optimizing the frequency comparison sequence between an ion clock and an optical lattice clock can also improve stability. By linking the zero-

dead-time interrogation of Yb optical lattice clocks coherently to an Al^{+} ion clock, the stability of the frequency comparison was improved by an order of magnitude¹⁴⁴.

The ultimate solution to improve the SQL is to increase the number of ions in the trap. Multi-ion clocks are investigated both theoretically and experimentally. It was theoretically proposed for both Paul traps^{145,146} and Penning traps¹⁴⁷. For Paul traps, a path to reach an uncertainty below 10^{-18} is demonstrated, and the \sqrt{N} scaling of the QPN is reported⁴³. A main source of uncertainty in the multi-ion clock is the quadrupole shift because the ions are not located at the center of a Paul trap. Suppression of this quadrupole shift is demonstrated through dynamic decoupling^{148,149}. Also, quantum logic spectroscopy for multiple ions are demonstrated¹⁵⁰.

IV. VARIATION OF FUNDAMENTAL CONSTANTS

Constancy of fundamental constants is one of the fundamental assumption in modern physics. If a fundamental constant varies over time or space, this is a violation of Einstein's equivalence principle. To observe any variation of fundamental constants, the constants must be dimensionless, because a reference is always necessary to detect such variations. For example, the time variation of proton mass m_p cannot be measured by itself, but the change in the proton-to-electron mass ratio $\mu = m_p/m_e$ can be tested. Other important dimensionless fundamental constants include coupling constants for fundamental interactions, such as the fine structure constant α . Note that the majority of m_p arises from the effect of the strong force, so the variation of μ can also originate from changes in a coupling constant.

There are several mechanisms in physics beyond the Standard Model (BSM) that can induce such variations in the coupling constants of fundamental interactions. In theories with extra dimensions, such as Kaluza-Klein models¹⁵¹, superstring theories¹⁵², and brane world models¹⁵³, the fundamental constants are uniform in the world including higher dimensions, and they are only effectively constant in the $(3+1)$ -dimensional world observable to us. In addition, a field that is introduced to explain the inflation theory can couple to fundamental constants. Typically, this field is a scalar field, due to its simplicity and ability to take a vacuum expectation value without breaking Lorentz invariance.¹⁵⁴

Based on these theoretical backgrounds, intensive astronomical searches for variations of fundamental constants have long been performed¹⁵⁴. Particularly important were observations based on atomic absorption lines which suggested that the fine structure constant α has a different value in the universe with large redshift z .¹⁵⁵ The study claims $\Delta\alpha/\alpha = -0.72(18) \times 10^{-5}$ over $0.5 < z < 3.5$. Assuming a linear time variation, the corresponding drift rate is $\Delta\alpha/\alpha = 1.2(3) \times 10^{-15} \text{ yr}^{-1}$, which should be easily observed in state-of-the-art atomic clocks. Terrestrial searches can be performed under a better control of the environment of atoms than astronomical searches, and thus serve as a good cross-check against astronomical searches.

The search for the time variation of fundamental constants

on Earth is performed by comparing the transition frequencies of two different clock transitions over a long period. Because the dependence of an atomic transition on a fundamental constant differs between transitions, the ratio of the transition frequencies has a nonzero dependence on fundamental constants. Let us take α as an example. The binding energies of energy levels in hydrogen with a principal quantum number n scale $\sim \alpha^2$. The fine structure, which is induced by the L-S coupling, is proportional to α^4 . Therefore, the frequency ratio of these two energy scales is proportional to $\sim \alpha^2$. For precise frequency measurements, narrow-linewidth transitions that are used in atomic clocks are more suitable than broad-linewidth transitions in hydrogen. For multi-electron atoms, the α dependence of a transition is estimated by theoretical calculations of the electronic structure, and it is characterized by a constant K in the following equation:

$$\frac{\delta\nu}{\nu} = \frac{2q}{E_0} \frac{\delta\alpha}{\alpha} = K \frac{\delta\alpha}{\alpha}, \quad (6)$$

where q is the sensitivity parameter to the variation of α and E_0 is the energy difference between the excited state and the ground state. This means that the two-level system for the clock transition functions as the quantum sensor for the variation of α .

Table II summarizes K for major transitions used in atomic clocks, together with some species proposed for future measurements that have particularly large K . For neutral atoms and singly-ionized ions, K relative to the ground state is at most $O(1)$, and highly charged ions (see Sec. V) are necessary to obtain $K > 10$. The nuclear clock transition in ^{229}Th is predicted to be highly sensitive to the variation of α ¹⁵⁶. (see Sec. VI)

The historical advancement in the constraint on the time variation of α is summarized in Fig. 3. The constraint on the time variation of α , i.e., $|\dot{\alpha}/\alpha|$, rapidly improved with the development of atomic clocks. At an early stage, the Hg^+ clock played an important role, and recent best constraints are obtained by Yb^+ ion clocks, both of which have large K . Because the constraint is estimated for a linear drift, frequency ratio measurements over a long period enhance the sensitivity. The recent reports by Yb^+ ion clocks utilize the frequency ratio data spanning more than 10 years. The best constraint reported so far, $\dot{\alpha}/\alpha = 1.8(2.5) \times 10^{-19} \text{ /yr}$ ¹⁶², is four orders of magnitude more stringent than the astronomical report of a potential variation in α .

To increase the sensitivity to the time variation of α in a fixed amount of time, either the stability of an atomic clock or K has to be enhanced. It is noteworthy that the $4f^{13}5d6s^2(J=2)$ state in neutral Yb can enhance the sensitivity^{59–61}. K for this transition is not the largest in Table II, but because optical lattice clocks have higher short-term stability than ion clocks, this state potentially enhances the sensitivity, particularly for short-term variations. Note that the large K 's in the $6s6p^3P_0 \rightarrow 4f^{13}5d6s^2(J=2)$ and $6s6p^3P_2 \rightarrow 4f^{13}5d6s^2(J=2)$ transitions are primarily due to their small transition energy, and the excited state is the same as the $6s^2^1S_0 \rightarrow 4f^{13}5d6s^2(J=2)$ transition. In this case, if an infinitely stable clock is assumed, the ultimate sensitivity to

TABLE II. Sensitivity to the variation of the fine structure constant for major transitions used in atomic clocks. At the end of the table, transitions in HCl with particularly large K and a nuclear clock transition are listed for reference. Ground state hyperfine and RF for Rb and Cs means that the transitions are between hyperfine states in the ground state with energy differences in the radio frequency range.

Atom	Transition	λ (nm)	K	Ref.
Rb	ground state hyperfine	RF	0.34	157
Cs	ground state hyperfine	RF	0.83	157
Al ⁺	$3s^2^1S_0 \rightarrow 3s3p^3P_0$	267	0.008	157
Ca ⁺	$4s^2S_{1/2} \rightarrow 3d^2D_{5/2}$	729	0.15	157
Sr	$5s^2^1S_0 \rightarrow 5s5d^3P_0$	698	0.06	157
Sr ⁺	$5s^2S_{1/2} \rightarrow 4d^2D_{5/2}$	674	0.43	157
Yb	$6s^2^1S_0 \rightarrow 6s6p^3P_0$	578	0.31	157
Yb	$6s^2^1S_0 \rightarrow 6s6p^3P_2$	507	0.56	59
Yb	$6s^2^1S_0 \rightarrow 4f^{13}5d6s^2(J=2)$	431	-3.82	59
Yb	$6s6p^3P_0 \rightarrow 4f^{13}5d6s^2(J=2)$	1695	-15	60
Yb	$6s6p^3P_2 \rightarrow 4f^{13}5d6s^2(J=2)$	2875	-27	61
Yb ⁺	$6s^2S_{1/2} \rightarrow 5d^2D_{5/2}$	411	1.03	157
Yb ⁺	$6s^2S_{1/2} \rightarrow 4f^{13}6s^2F_{7/2}$	467	-5.95	157
Hg ⁺	$6s^2S_{1/2} \rightarrow 5d^2D_{5/2}$	282	-2.94	157
Pr ¹⁰⁺	$5s^25p_{1/2} \rightarrow 5s^24f_{5/2}$	2650(49)	40	158
Pr ¹⁰⁺	$5s^25p_{1/2} \rightarrow 5s^24f_{7/2}$	1409(14)	22	158
Sm ¹⁴⁺	$4f^2^3H_4 \rightarrow 5s4f^3F^2$	2614(470)	-66	158
Ir ¹⁷⁺	$4f^{13}5s^3F_4 \rightarrow 4f^{14}^1S_0$	1978	145	159
Cf ¹⁵⁺	$6p^25f^2F_{5/2} \rightarrow 6p^25f^4I_{9/2}$	812	57	160
Cf ¹⁶⁺	$5f6p(J=3) \rightarrow 6p^2(J=0)$	1899	-140	161
Cf ¹⁶⁺	$5f6p(J=3) \rightarrow 5f^2(J=4)$	1030	85	161
Es ¹⁶⁺	$6p5f^24I_{9/2} \rightarrow 6p^25f^2F_{5/2}$	1430	-53	160
²²⁹ Th	nuclear clock transition	148 5900(2300)	156	

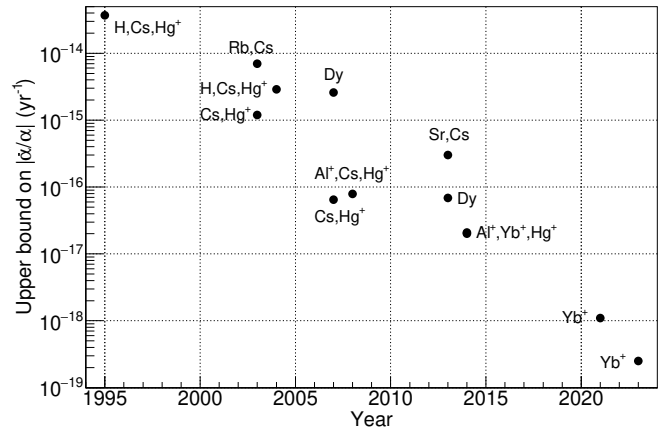


FIG. 3. Historical development of the constraint on time variation of the fine structure constant set by atomic spectroscopy.: atoms and ions next to data points show the atomic species used to obtain the corresponding data points.

the variation of α of the $6s^2^1S_0 \rightarrow 4f^{13}5d6s^2(J=2)$ transition is equivalent to that of the $6s6p^3P_0 \rightarrow 4f^{13}5d6s^2(J=2)$ transition, as far as the $6s^2^1S_0 \rightarrow 6s6p^3P_0$ transition is used as the reference. One might outperform the other only if there is a technical advantage in the clock stability for one of the two transitions. To make use of transitions with large K , tran-

sitions in highly charged ions and ^{229}Th are promising.

Another popular fundamental constant for the search for time variation is $\mu = m_p/m_e$. Same as α , dependence on μ differs between transitions and are calculated theoretically. Refs.^{163,164} perform combined analysis on the constraint on $\dot{\alpha}/\alpha$ and $\dot{\mu}/\mu$, resulting in $\dot{\mu}/\mu = 0.2(1.1) \times 10^{-16} \text{ yr}^{-1}$ and $\dot{\mu}/\mu = -0.5(1.6) \times 10^{-16} \text{ yr}^{-1}$, respectively, consistent with zero. More stringent constraints of $\dot{\mu}/\mu = 5.3(6.5) \times 10^{-17} \text{ yr}^{-1}$ and $\dot{\mu}/\mu = -0.8(3.6) \times 10^{-17} \text{ yr}^{-1}$ are reported by frequency comparison between Yb, Sr, and Cs clocks¹⁶⁵ and the E3 transitions in Yb^+ ion and a Cs clock¹⁶⁶, respectively. In addition, to search for the time variation of μ , molecules are widely used because the motional degrees of freedom for molecules show different dependence on μ . Energy differences for purely electronic, vibrational, and rotational transitions E_{el} , E_{vib} , and E_{rot} scale to μ in the following way:

$$\begin{aligned} E_{\text{el}} &\sim 1 \\ E_{\text{vib}} &\sim \mu^{-1/2} \\ E_{\text{rot}} &\sim \mu^{-1} \end{aligned} \quad (7)$$

Laboratory based reports utilize SF_6 molecules¹⁶⁷ and ultra-cold KRB molecules¹⁶⁸. The most stringent constraint based on the molecular measurements is $\dot{\mu}/\mu = 0.30(1.0) \times 10^{-14} / \text{yr}$ ¹⁶⁸, which is worse than the best constraint from the Yb^+ ion clock. However, the method with molecular vibrational levels is independent of optical clock frequency comparisons, serving as a good cross-check.

V. SPECTROSCOPY OF HIGHLY CHARGED IONS

A. Highly charged ion

Major systematic uncertainties in optical clocks arise from the ac Stark shift. It is induced by the deformation of the electronic cloud around the nucleus in an atom due to an external electric field and can be reduced by suppressing the deformation by holding electrons more tightly in an atom. Such tight confinement of electrons can be achieved in a highly charged ion (HCI)¹⁶⁹; qualitatively, by removing the outer-shell electrons that are loosely bound, only those with strong binding remain. The optical clock using HCIs is proposed as a next-generation clock that can go beyond the limit of optical lattice clocks and ion clocks.

The qualitative behavior of the energy levels in HCIs can be understood through the Z dependence of various energy scales, where Z is the atomic number, as summarized in Table III. For hydrogen-like ions, Z scaling of physical quantities can be derived from the Schrödinger equation and other exact solutions. This shows that the energy difference for the $1S - 2P$ transition increases proportional to Z^2 , but the ac Stark shift reduces with Z^{-4} scaling. For HCIs, the Z dependence originates from three different charges, Z , Z_a , and Z_{ion} , where Z_a is the effective charge that keeps the energy level scaling of an external electron for the HCI at $\sim 1/n^2$ and Z_{ion} is the charge of the ion. The scaling summarized in Table III is consistent with hydrogen-like ions when $Z \sim Z_a \sim Z_{\text{ion}}$.

TABLE III. Z dependence of the energy scales in hydrogen-like ions and HCI: dependence for HCI is cited from Ref.¹⁷⁰. More detailed scaling for the Lamb shift for the hydrogen-like atoms is described in Ref.¹⁷¹.

	hydrogen like ion	highly charged ion
binding energy	$\sim Z^2$	$\sim Z_a^{-4}$
fine structure	$\sim Z^4$	$\sim Z^2 Z_a^3 / (Z_{\text{ion}} + 1)$
hyperfine structure	$\sim Z^3$	$\sim Z Z_a^3 / (Z_{\text{ion}} + 1)$
Lamb shift	$\sim Z^4$	
ac Stark shift	$\sim Z^{-4}$	$\sim Z_a^{-4}$
BBR shift	$\sim Z^{-4}$	$\sim Z_a^{-4}$
electric quadrupole shift	$\sim Z^{-2}$	$\sim Z_a^{-2}$

The tradeoff of HCI clocks compared to optical lattice clocks is the number of ions that can be interrogated at once. HCI clocks typically trap a single HCI, and thus the stability of the clock limited by the SQL is low. A HCI is more likely to be deionized by a collision with residual gas than a singly-charged ion, which potentially can limit the duration of long-term operation.

Not only for a next-generation atomic clock, HCIs are also useful for various fundamental physics searches. One example is the test for QED in strong fields. The strong electric field experienced by electrons in U^{90+} is utilized to test QED in strong fields¹⁷². Another example is searches for the variation of α . The high velocities of the tightly-bound electrons lead to high sensitivities to relativistic effects that has larger α dependence. Following a pioneering work¹⁷³, various ionic species are proposed to be suitable for searching for the variation of α . Some transitions with large K are listed in Table II, and more transitions are listed in Table V. Also, transition with longer wavelengths tend to have large K , which can be understood by Eq. 6. The third example is the search for fifth force between an electron and a neutron (See Sec. VIII for details on this topic). The electronic structure different from neutral atoms by large amount provides high sensitivities to the search for new forces by isotope shift measurements^{174,175}.

To perform laser spectroscopy on HCIs, atoms and the number of electrons removed from the atom must be properly selected. The Z scaling of the binding energy suggests that electronic transitions between different n states in the range of visible light for neutral atoms go into the X-ray region for HCIs. Instead, the energy differences between hyperfine structures or fine structures increase to an energy where laser spectroscopy is possible. For hyperfine structures, hydrogen-like ions of heavy atoms have ~ 1 eV energy differences. Ions with nuclear spin $I = 1/2$ and visible light transition frequencies, which can be regarded as a two-level system as a quantum sensor, are summarized in Table. IV. For fine structures, ~ 1 eV energy differences are realized at $Z_{\text{ion}} \sim 10$. Examples of such transitions between fine structures are shown in Fig. 4; the 256 nm transition is between two fine-structure levels. The two $5s^2 4f$ states are another pair of fine structures. The transition between $J=3$ and $J=2$ states in the $5f 6p$ state of Cf^{16+} in Table V is also a transition between fine-structure levels.

Naively, electronic transitions between different orbitals have energy differences larger than energy for visible light.

TABLE IV. Hyperfine structures suitable for laser spectroscopy with $I = 1/2$. γ is the decay constant.¹⁶⁹

ion	wavelength λ (μm)	$\gamma/2\pi$ (s^{-1})
$^{171}\text{Yb}^{69+}$	2160	0.43
$^{195}\text{Pt}^{77+}$	1080	3.4
$^{199}\text{Hg}^{79+}$	1150	2.8
$^{203}\text{Tl}^{80+}$	338	111.2
$^{205}\text{Tl}^{80+}$	335	114.2
$^{207}\text{Pb}^{81+}$	886	6.2

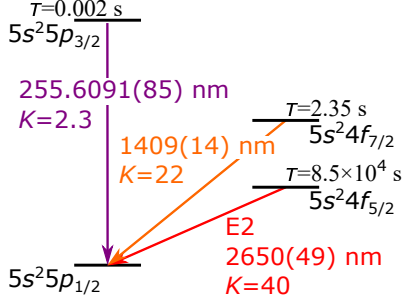


FIG. 4. Energy levels for Pr^{10+} : E2 shows an electric quadrupole transition. τ shows the lifetime of the excited states. K is the sensitivity coefficient for the variation of α .

An exceptional situation where visible light can drive electronic transitions in HCIs is called level crossing. Fig. 5 shows an intuitive understanding of this phenomenon. In a hydrogen atom, different l states for the same n are degenerated, where l is the azimuthal quantum number. However, in multielectron atoms, the nl states are ordered as $1s, 2s, 2p, 3s, 3p, 4s, 3d, 4p, 5s, 4d, 5p, 6s, 4f, 5d, 6p$. Let us take energy of the $5p$ and $4f$ orbitals as an example. In the hydrogen-like ion, the $5p$ orbital has a higher energy than the $4f$ orbital, but in the neutral atom, the energy of the $4f$ orbital is higher. At a certain Z_{ion} for the HCI, the energy differences between these two states changes its sign, and around Z_{ion} , the energy of these two orbitals are approximately the same, as shown in Fig. 5. This phenomenon is called level crossing, and here the transition energy between different electronic orbitals can be in the visible light range.

In the case of Pr, level crossing occurs around $Z_{\text{ion}} = 10$. As shown in Fig. 4, Pr^{10+} has two low-energy transitions between the $5s^25p$ ground state and $5s^24f$ states, in addition to a transition between fine-structure levels. The two $5s^24f$ states have long lifetimes suitable for clock states. Transitions from these states to the ground state have high sensitivity to the variation of α (see Table II for a comparison between neutral atoms and singly-ionized ions).

B. Experimental methods for precision spectroscopy of HCI

Experimentally, HCIs are generated by electron beam ion traps (EBITs)¹⁸¹. An EBIT is an electromagnetic trap for ions formed by a strong electron beam and electrodes. The negative charge of the electron beam confines the ions radially, and

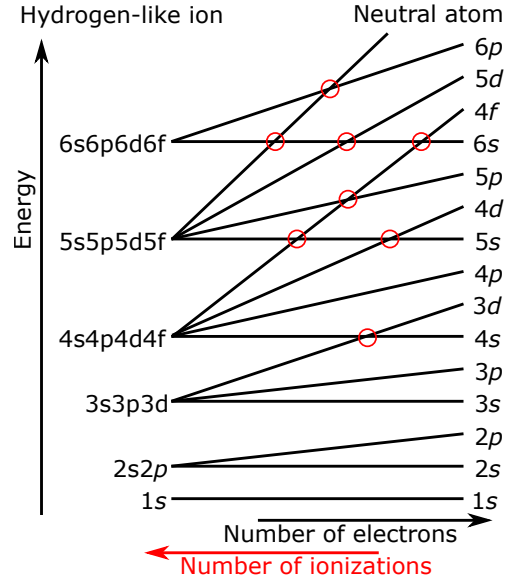


FIG. 5. Conceptual drawing for level crossing: the vertical axis shows relative energy. Red circles show level crossings.

axial confinement is provided by electrodes. The energy of the electron beam determines the maximum number of electrons that can be stripped from neutral atoms.

The generated HCI is extracted from an EBIT and then transferred to a Paul trap. At this point, the HCI is hot and therefore has to be cooled down to its motional ground state for precision spectroscopy. Due to the lack of broad-linewidth transitions suitable for laser cooling in HCIs, cooling is typically performed by sympathetic cooling. Such sympathetic cooling and high-precision spectroscopy are demonstrated in Ar^{13+182} . An Ar^{13+} ion is stopped by a Coulomb crystal of Be^+ , and subsequently laser-cooled using a broad transition in Be^+ . Note that the trap used in this experiment is cryogenic to suppress the BBR shift¹⁸³. The $^2P_{1/2} \rightarrow ^2P_{3/2}$ transition at 441 nm is used as the clock transition, and its transition frequency is measured with a relative uncertainty of 1.5×10^{-16} referenced to the state-of-the-art $^{171}\text{Yb}^+$ clock. The dominant source of uncertainty is the statistical uncertainty and the total systematic uncertainty for the Ar^{13+} system is 2.2×10^{-17} . The majority of the systematic uncertainty in the Ar^{13+} system originates from micromotions, which can be suppressed in the future work¹⁸⁴.

Other ionic species are also investigated, motivated by the theoretical proposals. One of the intensively investigated species is Pr ions. Pr^{9+} was first experimentally investigated¹⁸⁵. Although $K = 6.32(5.28)$ for the $5p4f\ ^3G_3(^3F_2)$ state is smaller than K 's listed in Table V, energies of the long-lived $5p4f\ ^3G_3$ states are determined with a $\sim 10^{-6}$ relative uncertainty. Pr^{10+} also has an early spectroscopy report¹⁷⁶. Together with an improved theoretical calculation for the energy of the metastable excited states¹⁵⁸, the energy of the $5s^25p_{3/2}$ state is determined with a 3×10^{-7} relative uncertainty. Further spectroscopy for the narrow-linewidth transition with high sensitivity to the variation of α is expected. Determination of transition frequencies is also

TABLE V. Some narrow-linewidth transitions in HCIs potentially useful for clock operation and the search for variation of α : Configurations 1 and 2 are the configurations of two states that are connected by the transition. J shows total angular momentum if it is described by a number, or angular momentum in spectroscopic notation. λ and τ are the wavelength and lifetime of the transition. K is the sensitivity coefficient for the variation of α defined in Eq. 6.

Atom	configuration 1	J	configuration 2	J	λ (nm)	τ (s)	K	Ref.
Pr ¹⁰⁺	5p	1/2	4f	5/2	2650(49)	8.5×10^4	40	176
Pr ¹⁰⁺	5p	1/2	4f	7/2	1409(14)	2.35	22	176
Nd ¹⁰⁺	4f ²		³ H ₄	5p4f	¹ D ₂	2200(430)	25	-24 158
Nd ¹⁰⁺	4f ²		³ H ₄	5p4f	³ F ₃	1480(240)	3.9	-18 158
Pm ¹⁴⁺	5s	1/2	4f	7/2	966		24	173
Sm ¹³⁺	5s ² 4f		² F _{5/2}	5s4f ²	⁴ H _{7/2}	494(22)	0.367	12 158
Sm ¹³⁺	5s ² 4f		² F _{5/2}	5s4f ²	⁴ H _{9/2}	444(18)	0.133	11 158
Sm ¹³⁺	5s ² 4f		² F _{5/2}	5s4f ²	⁴ H _{11/2}	386(14)	0.141	10 158
Sm ¹⁴⁺	4f ²		³ H ₄	5s4f	³ F ₂	2614(470)	8.515	-66 158
Sm ¹⁴⁺	4f ²		³ H ₄	5s4f	³ F ₄	1182(100)	0.556	-29 158
Eu ¹⁴⁺	4f ² 5s	7/2	4f ³	11/2	1657(330)		47	177
Eu ¹⁴⁺	4f ² 5s	7/2	4f ³	13/2	971(130)		28	177
Ho ¹⁴⁺	5s4f ⁶		⁸ F _{1/2}	4f ⁵ 5s ²	⁶ H _{5/2}	420	37	-16 178
W ⁸⁺	4f ¹⁴ 5p ⁴		³ P ₂	4f ¹³ 5p ⁵	³ F ₄	1646		-27 159
W ⁸⁺	4f ¹⁴ 5p ⁴		³ P ₂	4f ¹³ 5p ⁵	³ G ₃	1573		-26 159
W ⁸⁺	4f ¹⁴ 5p ⁴		³ P ₂	4f ¹³ 5p ⁵	³ G ₅	899		-15 159
Ir ¹⁶⁺	4f ¹³ 5s ²		² F _{7/2}	4f ¹⁴ 5s	² S _{1/2}	267		22 159
Ir ¹⁷⁺	4f ¹³ 5s		³ F ₄	4f ¹² 5s ²	³ H ₆	283		-22 159
Ir ¹⁷⁺	4f ¹³ 5s		³ F ₄	4f ¹⁴	¹ S ₀	1978		145 159
Pt ¹⁷⁺	4f ¹³ 5s ²		² F _{7/2}	4f ¹⁴ 5s	² S _{1/2}	402.2	4.05×10^9	-33 179
Pu ⁸⁺	6p ⁶	0	6p ⁵ 5f	1	654		11	180
Pu ⁹⁺	6p ⁵	3/2	6p ⁴ 5f	5/2	1172		19	180
Pu ⁹⁺	6p ⁵	3/2	6p ⁴ 5f	7/2	872		14	180
Pu ⁹⁺	6p ⁵	3/2	6p ⁴ 5f	3/2	862		14	180
Pu ¹⁰⁺	6p ⁴	2	6p ³ 5f	3	1989		25	180
Pu ¹⁰⁺	6p ⁴	2	6p ³ 5f	2	866		11	180
Pu ¹⁰⁺	6p ⁴	2	6p ³ 5f	4	817		11	180
Pu ¹¹⁺	6p ² 5f	5/2	6p ³	3/2	1461		-15	180
Am ⁹⁺	6p ⁵ 5f	1	6p ⁴ 5f ²	0	974		12	180
Am ⁹⁺	6p ⁵ 5f	1	6p ⁴ 5f ²	4	905		13	180
Bk ¹⁵⁺	6p ²	0	6p5f	3	483		14	180
Bk ¹⁵⁺	6p ²	0	6p5f	2	340		13	180
Cf ¹⁵⁺	6p ² 5f		² F _{5/2}	6p ² 5f	4I _{9/2}	812	6900	57 160
Cf ¹⁶⁺	5f6p	3	6p ²	0	1899	3.7×10^{16}	-140	161
Cf ¹⁶⁺	5f6p	3	5f6p	2	1638	0.178	35	161
Cf ¹⁷⁺	5f	5/2	6p	1/2	535		-48	161
Es ¹⁶⁺	6p5f ²		4I _{9/2}	6p ² 5f	² F _{5/2}	1430	16000	-53 160
Es ¹⁷⁺	5f ²		3H ₄	6p5f	³ F ₂	1343	11000	-13 160

performed for a narrow-linewidth transition in Ni⁺¹²¹⁸⁶ and many charge states for Xe¹⁷⁵ and Ca¹⁷⁴ ions. The Xe and Ca ions are investigated with the motivation of searching for the fifth force through isotope shift measurements (see Sec. VIII).

VI. NUCLEAR CLOCK

An even stiffer object against external electric fields than the inner-shell electronic cloud is the nucleus. It is challenging to make use of a typical nuclear transition at ~ 100 keV energy for precision spectroscopy with a laser. However, one exceptionally low-lying nuclear state in ²²⁹Th can be barely

accessible by a laser from the ground state. Previously, the energy of this transition was known with only one- or two-digit precision, but in the past couple of years, substantial advancements were made. The transition frequency is now known to be 2 020 407 384 335(2) kHz, corresponding to the energy of 148.38 nm and 8.3557 eV and the relative uncertainty of 9.9×10^{-13} . Note that the next lowest-energy nuclear excited state known today is in ^{235m}U, which is 76.7 eV above the ground state. With this state in ²²⁹Th, a clock can be operated with a nuclear transition. Because the nucleus is $\sim 10^5$ times smaller than the atom, it is approximately free from the ac Stark shift.

Details of the transition are summarized in Fig. 6. The

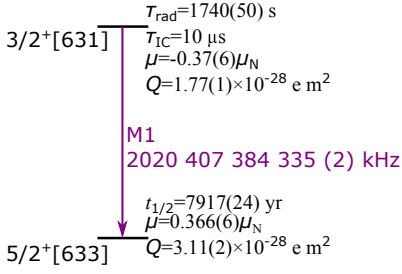


FIG. 6. Details of the nuclear transition in ^{229}Th : τ_{rad} : the decay constant for the radiative decay, τ_{IC} : the decay constant for the internal conversion, μ : the magnetic moment, μ_N : the nuclear magneton, Q : the quadrupole moment, $t_{1/2}$: the half lifetime. The notation of the angular momentum is $J^P[Nn_z\Lambda]$, where J is the total angular momentum, P is the parity, N and n_z are the deformed oscillator quantum number and its z component, and Λ is the projection of the valence neutron orbital angular momentum on the nuclear symmetry axis.

energy of the excited state was initially estimated by measuring the low-energy gamma rays emitted at the decay of ^{233}U to ^{229}Th ^{187,188}. Recent more precise measurements utilized the internal conversion and X-ray excitation of the nucleus to a higher excited state than the excited state of the clock transition¹⁸⁹. Spectroscopy of photons emitted by the relaxation of the clock state further reduced the uncertainty of the transition energy further^{190,191}. These efforts improved the uncertainty on the transition frequency to 4 digit precision. Finally, laser excitation of the transition by laser and subsequent decay of the excited state is observed for $^{229}\text{Th}^{3+}$ ions doped in two different crystals transparent to vacuum ultraviolet light^{192,193}. These studies measured the wavelength with 7 digit precision. A few months later, spectroscopy using the seventh harmonic generation of a frequency comb determined the transition energy with 2 kHz uncertainty¹⁹⁴. Further characterizations of the fine structure¹⁵⁶ and thermal effects¹⁹⁵ are performed, and now the path to the state-of-the-art precision laser spectroscopy with < 1 Hz uncertainty is paved.

The nuclear clock can be implemented in two different ways. To prevent the ^{229}Th nucleus from quickly decaying through internal conversion, the ^{229}Th atoms must be ionized to $^{229}\text{Th}^{3+}$ ions. For these ions, an ion trap similar to the one used in HCI clocks works well. This approach has an advantage that the methodology of spectroscopy is well established in ion clocks, making it easier to estimate systematic uncertainties. Spectroscopy of $^{229}\text{Th}^{3+}$ ions in a Paul trap is recently performed¹⁹⁶. However, the SQL is large, due to small number of ions in the system. The other method, which is unique to nuclear clocks, is to dope a crystal with $^{229}\text{Th}^{3+}$ ions. Because nucleus is highly isolated from the electrons, the effects being in a crystal are minimal compared to on those atoms. A large number of ions, e.g., $5 \times 10^{18} \text{ cm}^{-3}$ ¹⁹², can be doped, which is advantageous for suppressing QPN. However, a strong temperature dependence of the transition frequency is observed¹⁹⁵ recently, which is attributed to the change in the electric field induced by the thermal expansion of the lattice constant.

For fundamental physics purposes, the nuclear clock is expected to be highly sensitive to the variation of fundamental constants. Because the nuclear structure depends on the coupling constant for the strong force α_s , it should be sensitive to the variation of α_s ¹⁹⁷. In addition, it is theoretically predicted that it also has a high sensitivity to the variation of α , with $K = 5700(2300)$ ¹⁵⁶. Intuitively, this large K can be understood because the small transition energy is realized by a cancellation of a large repulsive Coulomb energy by another large attractive energy by the strong force. The large K is also suitable for the search for ultralight dark matter (see Sec. VII). Another direction of the future research on this nuclear clock is a system without vacuum chamber¹⁹⁸. This proposed system can be beneficial for compact portable optical clock.

VII. ULTRALIGHT DARK MATTER

A. Theoretical backgrounds

Dark matter is massive objects in the universe that do not interact with light. It was first proposed to explain the rotation curve in a galaxy¹⁹⁹. Today, multiple observations strongly support its existence, such as gravitational lensing²⁰⁰ and fluctuations in the cosmic microwave background²⁰¹. Dark matter is estimated to exist five times more than the ordinary matter.

Various candidates for dark matter are examined, e.g., massive compact halo objects²⁰² that have an astronomical mass scale, weakly interacting massive particle that are typically searched in the mass range from 0.1 GeV to 1000 GeV²⁰³, and axions and axion-like particles that are typically searched in the mass region below 1 eV²⁰³. Among these candidates, those with masses of 1 eV or smaller have to be bosonic due to the expected number density, the energy density of dark matter, and the Pauli exclusion principle. Such low-mass dark matter as a whole is referred to as ultralight dark matter^{204,205}. Searches for ultralight dark matter are conducted with various methods such as astronomical observation^{206–210}, microwave technology^{211–214}, laser technology^{215,216}, accelerometer^{217–219}, nuclear EDM searches²²⁰, and so on. In particular, atomic clocks have a sensitivity to topological dark matter, which is the dark matter in the form of topological defects in the universe, that has spin 0 and couples to the terms without derivatives in the Lagrangian for Standard Model (SM)²²¹.

Searches for such ultralight dark matter with atomic clocks is sensitive to the mass range whose energy scale is the same as or smaller than the single cycle of the clock operation, which is ~ 1 s. This corresponds to the mass of $10^{-15} \text{ eV}/c^2$ or less. The lower bound for this mass is set by the overall duration of clock operation. From a perspective of cosmology, the mass of the dark matter is expected to be larger than 10^{-22} eV to explain all phenomena with a single candidate, because at this mass, its de Broglie wavelength exceeds the size of dwarf galaxies. However, if dark matter is composed of multiple components, the mass range below 10^{-22} eV is still meaningful.

The first proposal for searching for ultralight dark matter

with atomic clocks was to search for topological dark matter that induces time dilation using an array of atomic clocks²²². This concept assumed the use of GPS satellites²²³, and experimental realization in the lab required the collaboration of multiple groups at geographically different locations^{112,224}. Later, it was proposed to detect ultralight dilaton dark matter that couples to fundamental constants²²¹. This proposal is easier for a single laboratory to implement.

For dark matter that couples to fundamental constants, a scalar field is typically assumed. The interaction between this field and ordinary matter is characterized by the following Lagrangian density²²¹:

$$\mathcal{L}_{\text{int}} = \phi \left[\frac{d_\alpha}{4\mu_0} F_{\mu\nu} F^{\mu\nu} - \frac{d_g \beta_g}{2g_3} F_{\mu\nu}^A F^{A\mu\nu} - c^2 \sum_{i=e,u,d} (d_{m_i} + \gamma_{m_i} d_g) m_i \bar{\Psi}_i \Psi_i \right] \quad (8)$$

$F^{\mu\nu}$ is the electromagnetic field tensor, $F^{A\mu\nu}$ is the intensity tensor for the gluon field, g_3 is the coupling constant for quantum chromodynamics (QCD), β_g is the β function for the running coupling constant for g_3 , γ_{m_i} is the anomalous dimension characterizing m_i , and Ψ_i is the spinor for fermions. Each term describes the tree-level interaction where a particle in the SM emits an ultralight dark matter particle, with the coupling constant for this interaction being d_i . A quadratic coupling, i.e., terms proportional to ϕ^2 can also be defined in a similar way as Eq. 8²²⁵. Well-known particles that satisfy these properties are the dilaton and moduli. Similar interactions can be assumed for axions when CP symmetry is violated²²⁶.

When ϕ couples to ordinary matter, fundamental constants vary due to the coupling constants in the Lagrangian in the following way.

$$\begin{aligned} \alpha(\phi) &= \alpha(1 + d_\alpha \phi), \\ m_e(\phi) &= m_e(1 + d_{m_e} \phi), \\ m_q(\phi) &= m_q(1 + d_{m_q} \phi), \\ \Lambda_{\text{QCD}}(\phi) &= \Lambda_{\text{QCD}}(1 + d_g \phi) \end{aligned}$$

Here, m_e is the electron mass, m_q ($q = u, d$) are the mass of up and down quark, respectively, and Λ_{QCD} is the energy scale for QCD, which dominates the mass of a proton. The dark matter field oscillates at a frequency $f = m_\phi c^2/h$ and amplitude ϕ_0 , and the dark matter density corresponds to $\rho_\phi = c^2 \pi f^2 \phi_0^2 / G$ (G : the Newtonian constant of gravitation). In general, atomic transitions depend on fundamental constants in different ways. These dependence can be calculated numerically for multi-electron system to evaluate the sensitivity of various transitions to the variation of fundamental constants.

Searches for ultralight dark matter through this interaction are easy to implement at a laboratory because atomic transitions and the size of an atom depend on fundamental constants in different ways²²⁷. Take α as an example. The wavelength of a narrow-linewidth laser for precision spectroscopy is locked to a stable reference cavity, where the distance L between two mirrors is set by the material used as the spacer. Wavelength of the laser is proportional to L ,

and the wavenumber k scales $k \propto 1/L \sim 1/a_B \sim \alpha$, where $a_B = \hbar/(m_e \alpha c)$ is the Bohr radius. An atomic transition is in general not proportional to α , as discussed in Sec. IV. This difference in α -scaling results in a periodic variation of the atomic resonance relative to the cavity resonance when α couples to the ultralight dark matter field ϕ . This means that the two-level system for the clock transition serves as a quantum sensor for the ϕ field. Because the measurement is performed differentially, a reference is required, which can be either a second clock transition or a reference cavity.

Three other fundamental constants can also affect the atomic transition frequency. In general, when the frequencies of two atomic transition A and B are monitored, their ratio ν_A/ν_B is depicted as

$$\frac{\delta(\nu_A/\nu_B)}{\nu_A/\nu_B} = k_\alpha \frac{\delta\alpha}{\alpha} + k_{m_e} \frac{\delta(m_e/\Lambda_{\text{QCD}})}{m_e/\Lambda_{\text{QCD}}} + k_{m_q} \frac{\delta(m_q/\Lambda_{\text{QCD}})}{m_q/\Lambda_{\text{QCD}}}, \quad (9)$$

where δX denotes the change in X . Because four fundamental constants can vary while the quantity experimentally measured is a single ratio, when a constraint is set for one fundamental constant, coupling constants for three other fundamental constants are assumed to be zero.

B. Status of experimental searches

In the end of the analysis of an experimental result, amplitudes of a sinusoidal oscillation in the frequency ratio are obtained. The frequency f assumed for the sinusoidal fit can be arbitrarily set within the range up to the Nyquist frequency. Therefore a single dataset for ν_A/ν_B versus time can provide constraints for dilaton ultralight dark matter over a wide range of mass as shown in Fig. 7. So far, no experimental result observed sinusoidal oscillations with amplitudes significantly larger than their statistical uncertainties. The resulting constraints excludes coupling constants stronger than a lower bound for a given mass. In Fig. 7, such excluded regions are shown as shaded area. In this kind of searches for new particles, it is very common to plot a possible mass on the horizontal axis and a coupling constant for a certain interaction on the vertical axis.

Figure 7(a) shows the constraints d_α . Because most electronic transitions have finite sensitivity to the modulation of α , state-of-the-art atomic clock comparisons contributes to this constraint^{113,162,228}. Particularly impressive is the result from PTB¹⁶², which surpasses other reports by an order of magnitude by combining two pairs of clock comparisons.

These comparisons between optical clocks do not have any sensitivity to d_{m_e} , mainly because all optical transitions more or less proportional to m_e , resulting in a constant when frequency ratio is taken. Instead, comparisons between an electronic transition or a reference cavity and a hyperfine transition have a high sensitivity. The comparison between an Si cavity and a hydrogen maser²²⁹ reported constraints down to 10^{-21} eV. A lower bound of the mass is limited by their measurement time. The long term comparison between an Yb optical lattice clock and a Cs fountain clock provides constraints

for smaller masses²³⁰, thanks to overall measurement period of 298 days.

For d_g and d_{m_q} , the contributions of clock comparisons are relatively small, compared to the satellite^{218,231} and torsion balance^{219,232} experiments, because of the large mass involved in these macroscopic experiments. Although Fig. 7(c) and (d) shows slight excess in the performance of the clock comparisons at low masses, the final result of the MICROSCOPE experiment²³¹, which has a factor of 4.6 improvement compared to the initial result shown in the plot, is not included in the plot. With this updated result, most of the clock comparison results become marginal. Note that the constraint by Yb⁺E2/E3 are not simply through the formalism shown in the previous subsection but through the modulation in nuclear charge radii²³³.

C. Future proposals

To increase the search region, three factors are important. One is the measurement time. A longer measurement time allows us to search for smaller masses. In principle, ultralight dark matter with arbitrarily small masses can be searched given a sufficiently long measurement time. However, masses below 10^{-22} eV require careful interpretation, as discussed in Sec. VII A. The second factor is the stability of the clock. To investigate smaller coupling constants, the stability of the clocks needs to be improved, as far as the same atomic clock is used. The third factor is the sensitivity of a transition to the coupling constant. Even if the stability of the clock is the same, transitions with high sensitivity to the variation of fundamental constants enhance the sensitivity to ultralight dark matter. For example, for d_α , transitions with large K listed in Table II are suitable for high-sensitivity measurements of d_α .

There are various proposals for searching for ultralight dark matter using different systems. One is molecular spectroscopy²³⁴. Microwave spectroscopy of a rovibrational transition in SrOH has a strong sensitivity to d_{m_e} and d_g . Spectroscopy of Ca⁺ ion and I₂⁺ ion is expected to provide a comparable constraint on d_g ²³⁵. Another proposal is to load an atomic clock on a satellite orbiting close to the sun²³⁶. The higher density of dark matter bound to the sun enhances sensitivity, offering constraints particularly higher than the existing limit in the high-mass range, from 10^{-16} to 10^{-14} eV. Some other molecular and atomic spectroscopy reports put constraints in the higher-mass region^{237,238}. Atom interferometry can also contribute to the same mass range as atomic clock comparisons²³⁹. The ²²⁹Th nuclear clock has high sensitivity to ultralight dark matter^{240,241}. Ref.²⁴⁰ discusses sensitivity to the coupling to d_g , and the large K shown in Table II results in high sensitivity to d_α ²⁴¹.

VIII. FIFTH FORCE SEARCH WITH ISOTOPE SHIFTS

A. Theoretical background

Searches for new forces using isotope shift measurements were theoretically proposed around 2018²⁴². Since then, various experimental reports ranging from simple isotope shift measurements to full analysis using new isotope shift measurements appeared, motivated by this theoretical proposal. The isotope shift is the frequency difference of an atomic transition between isotopes. For optical transitions with $\nu \sim 500$ THz, the amount of isotope shifts is on the order of from 10 MHz to 1 GHz. The isotope shift is induced by two main sources. One is the variation of the nuclear charge radius due to the difference in the number of neutrons. This is called the field shift. The other is difference in the nuclear mass, referred to as the mass shift. This can be phenomenologically described as

$$\nu_\alpha^{AA'} = K_\alpha \mu^{AA'} + F_\alpha \langle r^2 \rangle^{AA'}, \quad (10)$$

In the following discussion, subscribed α labels a transition, and $X^{AA'} = X^A - X^{A'}$, unless otherwise specified. For example, ν_α^A is the transition frequency for the transition α of the isotope with mass number A . $\mu^A = 1/m^A$ is the inverse mass for the isotope with mass number A , $\langle r^n \rangle^A$ is the n th moment of charge radii for the isotopes with mass number A , and K_α and F_α are constants characterizing the mass and field shifts. $\langle r^2 \rangle^{AA'}$ can be eliminated from two equations for the isotope shifts for transitions α and β in the following way.

$$\frac{\nu_\beta^{AA'}}{\mu^{AA'}} = \frac{F_\beta}{F_\alpha} \frac{\nu_\alpha^{AA'}}{\mu^{AA'}} + K_{\beta,\alpha} \quad (11)$$

Here, $K_{\beta,\alpha} = K_\beta - K_\alpha F_\beta / F_\alpha$, and the equation shows that $\nu_\beta^{AA'} / \mu^{AA'}$ is a linear function of $\nu_\alpha^{AA'} / \mu^{AA'}$. The two-dimensional plot of $\nu_\beta^{AA'} / \mu^{AA'}$ versus $\nu_\alpha^{AA'} / \mu^{AA'}$ is called the King plot²⁴³.

The linear relation described in Eq. 11 holds true, as long as broad-linewidth transitions are used in the plot. Narrow-linewidth transitions can resolve effects other than the field shift and the mass shift. Suppose an additional term $X_\alpha^{AA'}$ in Eq. 10. This term adds $X_{\beta,\alpha}^{AA'} / \mu^{AA'}$ to the right-hand side of Eq. 11, making the King plot nonlinear. An example of the source of such an additional term is a hypothetical force between an electron and a neutron, which forms the following Yukawa-type potential energy for an electron:

$$V(r) = (-1)^{s+1} \frac{y_n y_e}{4\pi} \frac{e^{-m_\phi cr/\hbar}}{r}, \quad (12)$$

where s is the spin for the new boson mediating the force, y_e and y_n are the coupling constant of the boson to an electron and a neutron, respectively, and m_ϕ is the mass of the new boson. If the plot shows nonlinearity, it is possible that the nonlinearity is induced by this new force. If not, it is proved that such a force does not exist.

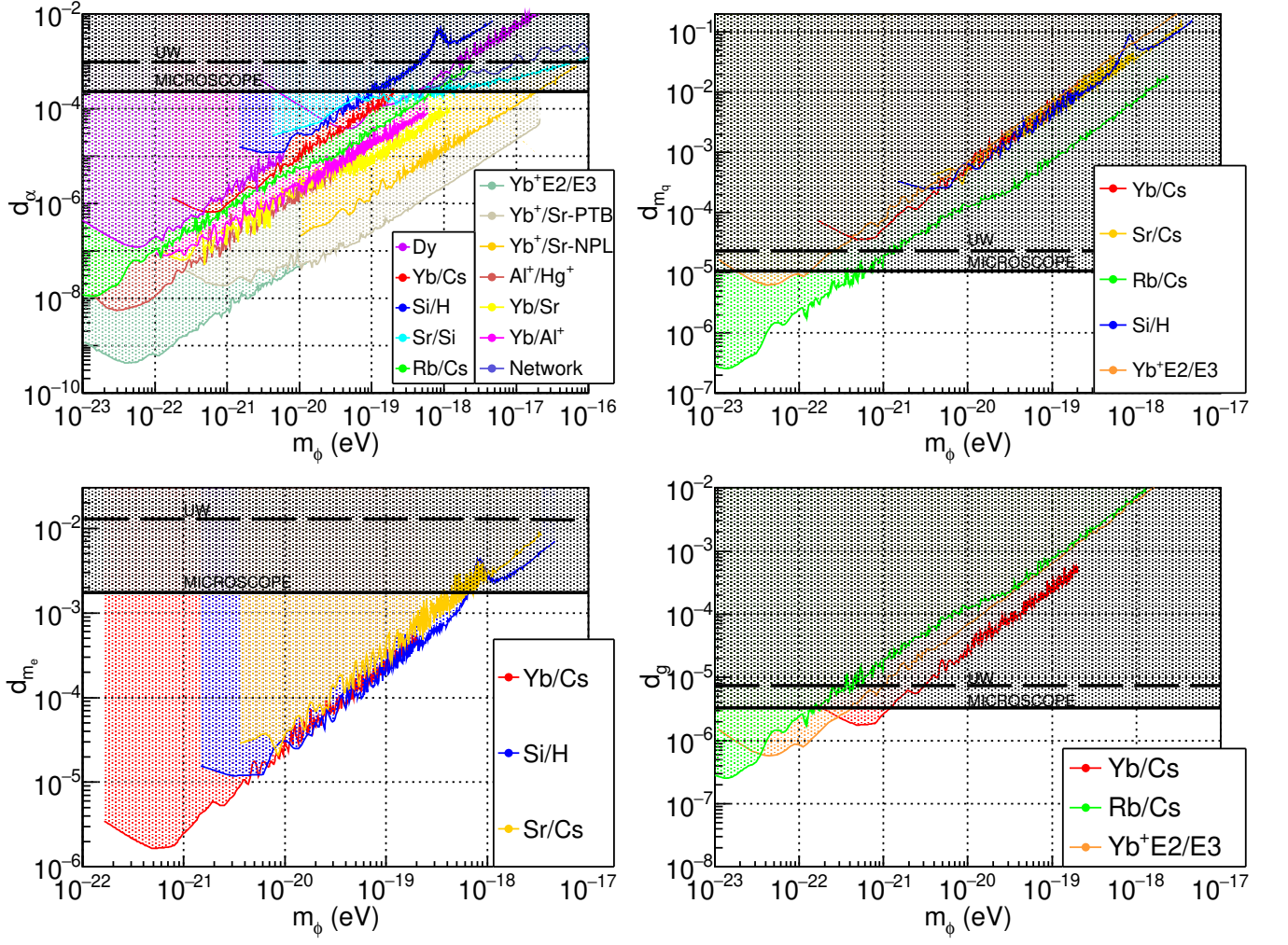


FIG. 7. Constraints on the coupling of ultralight dark matter to (a) the fine structure constant, (b) the electron mass, (c) the quark mass, and (d) the gluon field. The legends show two atoms utilized to obtain the constraint. Si refers to a silicon cavity, and Dy shows two different transitions in dysprosium. UW and MICROSCOPE refer to a torsion balance and a satellite experiment, respectively. In this plot, the final result of MICROSCOPE experiment²³¹ is not included.

The reality is more complex even within the SM; higher order effects of the nuclear charge radius also induce nonlinearity. The following equation is typically assumed in the state-of-the-art analysis.

$$v_{\alpha}^{AA'} = F_{\alpha} \langle r^2 \rangle^{AA'} + K_{\alpha} \mu^{AA'} + G_{\alpha}^{(4)} \langle r^4 \rangle^{AA'} + G_{\alpha}^{(2)} [\langle r^2 \rangle^2]^{AA'} + v_{ne} D_{\alpha} N^{AA'} \quad (13)$$

The third and fourth terms are the 4th-moment shift and the quadratic field shift, where $[\langle r^2 \rangle^2]^{AA'} = (\langle r^2 \rangle^{AA'})^2 - \langle (\langle r^2 \rangle^{AA'})^2 \rangle$ is the second order perturbative effect by $\langle r^2 \rangle^{AA'}$. The resulting equation corresponding to Eq. 11 is

$$\frac{v_{\beta}^{AA'}}{\mu^{AA'}} = \frac{F_{\beta}}{F_{\alpha}} \frac{v_{\alpha}^{AA'}}{\mu^{AA'}} + K_{\beta,\alpha} + \frac{\langle r^4 \rangle^{AA'}}{\mu^{AA'}} G_{\beta,\alpha}^{(4)} + \frac{[\langle r^2 \rangle^2]^{AA'}}{\mu^{AA'}} G_{\beta,\alpha}^{(2)} + \frac{v_{ne} N^{AA'}}{\mu^{AA'}} D_{\beta,\alpha}. \quad (14)$$

In this equation, all of the third, fourth, and fifth terms induce the nonlinearity, and thus proper subtraction of backgrounds from the SM is essential for the search for new forces.

There are some conditions for high-sensitivity measurements. The search for new forces through the nonlinearity of the King plot requires four or more stable isotopes in an element. The larger the number of isotopes and transitions, the more information can be extracted. Narrow-linewidth transitions are preferred for high-precision measurements. In addition, spinless nuclei are favored to avoid any spin-spin interactions that are difficult to precisely estimate. In fact, large nonlinearity is observed when isotopes with nonzero spin are included in the King plot^{65,244}, and the nonlinearity is fully explained by the second-order hyperfine interaction for Sr²⁴⁵. For high sensitivity, it is better to use transitions with excited states that have a large difference in the radial wave functions. For example, it is likely to have a higher sensitivity when the $S \rightarrow D$ and $S \rightarrow F$ transitions are plotted on the King plot than

when the $S \rightarrow ^2D_{5/2}$ and the $S \rightarrow ^2D_{3/2}$ transitions are plotted. To suppress any unwanted backgrounds arising from the SM, light nuclei are preferred, because of the small charge radii and insignificant relativistic effects. One of the sources of uncertainty is $\mu^{AA'}$, which can be eliminated by using three narrow-linewidth transitions²⁴⁶. Also, another way of analyzing isotope shift data sorted by isotopes instead of transitions is proposed²⁴⁷, where constraints on the new bosons comparable to the conventional analysis with the King plot is claimed.

It should be noted that this new force coupling to an electron and a neutron is phenomenologically introduced, and strong theoretical motivations do not necessarily underlie this force. One benefit is that it is sensitive to the X17 particle²⁴⁸.

To the extent that the fifth force changes the transition energy, the quantum sensor for the force between an electron and a neutron is the narrow-linewidth transition for which precision spectroscopy is performed. The transition also can be regarded as a quantum sensor for the nuclear charge radius. Using nonlinearity in the King plot described in this section is a methodology for discriminating the signal from the backgrounds.

B. Experimental results

A large number of experimental results are reported on this topic, ranging from only isotope shift measurements to constraints on the existence of new forces. For some atomic species, such as Xe¹⁷⁵, Cd^{249,250}, and Nd²⁵¹, isotope shifts are reported in the context of the search for new bosons. The constraints on the existence of new bosons are summarized in Fig. 8. The first experimental constraints on the new bosons are set by isotope shift measurements for Yb⁺²⁵² and Ca⁺²⁵³. In these reports, isotope shift measurements with a 20-Hz uncertainty for Ca⁺ excluded the existence of new bosons based on the observed King's linearity, whereas nonlinearity is observed in the isotope shift measurements for Yb⁺ with a 300-Hz uncertainty. The first report on Yb⁺ was for two E2 transitions, and later, isotope shifts for the E3 transition with an uncertainty of 500 Hz²⁵⁴ were reported. Additionally, multiple transitions in neutral Yb were carefully analyzed^{65,255,256}. The latest result for the E2 and E3 transitions of Yb⁺ has uncertainties of 5 and 16 Hz, respectively²⁵⁷. Ca⁺ and some Yb measurements did not observe nonlinearity, which is consistent with the constraint based on the $g-2$ measurement for an electron and neutron scattering. However, for some combinations of Yb data, nonlinearity is observed, which provides allowed regions for the new bosons. These allowed regions and excluded regions contradict each other. This potentially means that the observed nonlinearity is induced by some background phenomena within the SM, and further investigation is desired.

When the E3 transition for Yb⁺ is utilized, and the uncertainty of the isotope shift reaches ~ 10 Hz, the observed nonlinearity is so large that we have to carefully consider the effect of the higher order field shifts. For this analysis, the nonlinearity is decomposed into the following two components: $\zeta_{\pm} = d^{168} - d^{170} \pm (d^{172} - d^{174})$, where d^A is the resid-

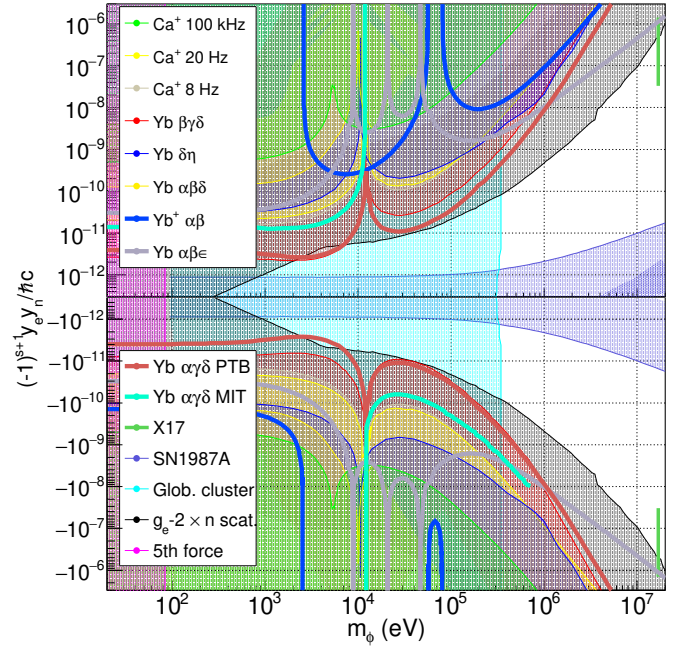


FIG. 8. Constraints on the new boson mediating forces between an electron and a neutron: shaded areas are excluded regions, and thick solid lines show the best fit for allowed regions. Greek letters in the legend shows the following transitions in Yb: α , β , γ are the $^2S_{1/2} \rightarrow ^2D_{5/2}$, $^2S_{1/2} \rightarrow ^2D_{3/2}$, and $^2S_{1/2} \rightarrow ^2F_{7/2}$ transitions in Yb⁺ ions, and δ , ϵ , η , are the $6s^2 \ ^1S_0 \rightarrow 6s6p^3P_0$, the $6s^2 \ ^1S_0 \rightarrow 5d6s \ ^1D_2$, and $6s^2 \ ^1S_0 \rightarrow 4f^{13}5d6s^2(J=2)$ transitions in neutral Yb, respectively. Glob. cluster shows the constraint from globular cluster, and $g_e - 2 \times n$ scat. shows the constraint based on the $g-2$ measurement for electrons and neutron scattering experiments.

ual of four data points from the linear fit²⁵² (Note that λ_{\pm} in Ref.²⁵⁴ is equivalent to ζ_{\pm}). On the $\zeta_+ - \zeta_-$ plane, a single source of nonlinearity of different strength forms a line passing through the origin. When the residuals of King plots for various combination of transitions in Yb are plotted on the $\zeta_+ - \zeta_-$ plane, the points are approximately on a single line. This suggests that the nonlinearity is mainly caused by a single source, which can be explained by nuclear density function theory calculations with the Fayan functional including several factors such as the surface thickness of nuclear density, relativistic corrections, nuclear deformation, and pairing effects²⁵⁴. The isotope shift measurements are so precise that from this information we can select a nuclear model to correctly describe the experimental results^{254,257}.

After subtracting the influence of the nuclear charge distribution, we still can seek an explanation for the remaining nonlinearity. Attributing this to new bosons, constraints on the existence of new bosons mediating forces between a neutron and an electron are obtained by isotope shift measurements of Yb. Some analyses in the currently available data show statistically significant nonlinearity, but other data are linear. These result in the allowed regions and excluded regions from different combinations of the transitions in Fig. 8.

The rapid development in the field motivated precise mass

measurements^{258,259}. Because the difference in the inverse mass comes into play, it is crucial to have very precise mass measurements for different isotopes to prevent the uncertainty of the mass measurement from limiting the uncertainty for the search for new bosons. After the first report on Yb²⁵² comes out, the uncertainty of the mass for ¹⁶⁸Yb is improved²⁶⁰, and recent report on Yb also includes more precise mass measurements²⁵⁷. For isotope shift measurements with even smaller uncertainties, further improvements in mass measurements are desired. To expand the sensitivity of the search, the use of new species such as HCl^{174,175} and radioactive isotopes^{244,246} are discussed.

IX. ATOMIC PARITY VIOLATION

A. Theoretical background

The parity (P) transformation refers to a flip of the sign of one spatial coordinate. In three dimensions, this is equivalent to the transformation of $\mathbf{x} \rightarrow -\mathbf{x}$. Under this transformation, basic equations of motion, such as the Newton's equation of motion, the Schrödinger equation, and the Dirac equation, are conserved. This symmetry under P transformation is called P symmetry. However, among the four fundamental forces, parity symmetry is fully violated in the weak force. Historically, the original theory was published by T.D. Lee and C. N. Yang²⁶¹, and C. S. Wu experimentally demonstrated the violation right after that²⁶². Later, the theory for the weak force was incorporated into the SM.

In atoms, where the electromagnetic force is dominant, P symmetry is naively conserved. Higher-order perturbations by the weak force or BSM physics manifest themselves as P violation. Examples of such interactions are summarized in the Feynman diagrams in Fig. 9. Here, instead of a photon mediating the force between an electron and a nucleus, a Z boson mediates the force, or a virtual W boson forms a loop in within a nucleon. Note that if a hypothetical boson make a loop or mediates the force between the nucleus and the electron, this involves BSM theories^{263,264}. The effective Hamiltonian for spin-independent atomic parity violation (APV) is expressed as

$$H_{\text{eff}} = e^\dagger \gamma^5 e \frac{G_F}{2\sqrt{2}} Q_W^{\text{eff}}(Z, N) \delta(\mathbf{r}), \quad (15)$$

where G_F is the Fermi constant for the weak force, $\gamma^5 = i\gamma^0\gamma^1\gamma^2\gamma^3$ with γ^μ being the Dirac matrices, and e^\dagger (e) is the creation (annihilation) operator for an electron. The effective weak charge $Q_W^{\text{eff}}(Z, N)$ is the following sum of the SM part and BSM part.

$$Q_W^{\text{eff}}(Z, N) = Q_W^{\text{SM}} + Q_W^{\text{BSM}} \quad (16)$$

$$= (Z(1 - 4\sin^2\theta_W) - N) + \frac{3}{\Lambda^2} f_{Vq}^{\text{eff}}, \quad (17)$$

with Z and N being number of protons and neutrons, respectively, θ_W being the Weinberg angle, and $f_{Vq}^{\text{eff}} = (f_{Vu}(2Z + N) + f_{Vd}(Z + 2N))/(3(Z + N))$ being the contribution of BSM

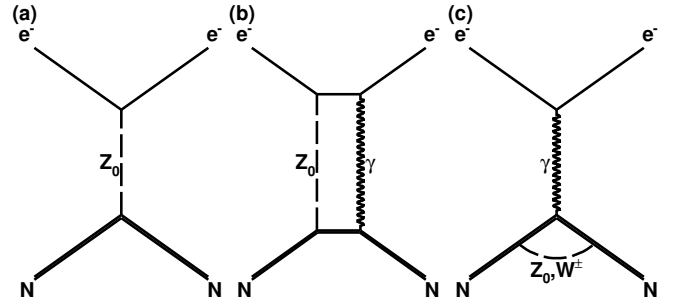


FIG. 9. Feynman diagrams contributing to atomic parity violation: (a) When the interaction is between a vector nucleon and an axial electron, the interaction is nuclear spin independent. When it is between an axial nucleon and a vector electron, it is spin dependent. (b) Hyperfine correction to the weak interaction, which is also nuclear spin dependent. (c) Diagram for the anapole moment, which is the main contribution to the nuclear spin dependent APV.

to the vector current ($f_{Vu, Vd}$ are the coupling of the BSM to up and down quarks, respectively). This equation tells that the test for the APV serves as the measurement of the Weinberg angle. The energy scale of the interaction is essentially at the size of the hydrogen-like 1S orbital of charge Z , i.e., the size of innermost electronic orbital, which results in a momentum transfer of $\hbar/(a_B/Z) = Zm_e\alpha^{265}$. Intuitively, this can be explained as electrons experiencing the potential due to the weak force only where the screening of the Coulomb potential induced by the nucleus is negligible. The momentum transfer is much lower than that in other measurements of θ_W performed by scattering experiments. The search for deviations of the Q_W^{eff} from Q_W^{SM} serves as a search for P-violating BSM physics, e.g., Z' boson and leptoquarks.

Spin-dependent APV originates from all three Feynman diagrams shown in Fig. 9. Diagram (c) shows the nuclear anapole moment contribution. A classical analogy for this moment is a solenoidal current bent into a torus, and the measurement of the anapole moment contributes to determining nuclear parity violation. The anapole moment is proportional to nuclear spin I . Some constraints are set from the Cs experiment described in the following section.

The effect of P violation can be observed as a nonzero transition amplitude for the electronic transition between states that have the same parity. For example, the ground state of alkali atoms is the 2S state. With the E1 transition, the state can be excited to 2P states. The transition to other states can be driven through either higher-order transition (e.g., the E2 transition) or mixing of the 2P states to other states due to the L-S coupling or a nuclear spin. P violation also mixes two states with opposite parity, which slightly allows some forbidden transitions. In practice, the measurement of APV is to evaluate the contribution of P-violating term in the total matrix element of the forbidden transition between electronic orbitals of the same parity. In other words, the quantum sensor for the APV measurement is the two-level system between the ground state and the excited state with the same parity, to which an opposite-parity state is mixed by the APV.

Because the effect of the APV is very small, multiple en-

hancements are utilized to magnify the signal to an observable amount. The amount of the mixing ε between an S state and a P state due to the APV satisfies the following equation.

$$\begin{aligned} |S\rangle &\rightarrow |S\rangle + i\varepsilon|P\rangle \\ |P\rangle &\rightarrow |P\rangle + i\varepsilon|S\rangle \\ \varepsilon &= \frac{\langle S|H_{\text{eff}}|P\rangle}{\Delta E} \sim \frac{Z^3}{\Delta E} \end{aligned} \quad (18)$$

Because of the Z^3 scaling^{266,267}, heavy atoms are preferred for the measurement of the APV. The measured quantity is the interference term between the P-conserving amplitude A_0 and P-violating amplitude A_{PV} :

$$\begin{aligned} R &= |A_0 + A_{\text{PV}}|^2 \simeq |A_0|^2 + (A_0 A_{\text{PV}} + c.c.) \\ &= \beta^2 E^2 \varepsilon^2 C_1 + 2\beta E E_{\text{osc}} \cdot 2p \text{Im}(E1_{\text{APV}}) C_2, \end{aligned} \quad (19)$$

where E is the dc electric field applied to mix the parity-odd and parity-even state, β is the tensor transition polarizability, p is the handedness of the polarization of the oscillating field, E_{osc} is the oscillating field perpendicular to E , and C_1 and C_2 are Clebsch-Gordan coefficients^{268,269}. $\text{Im}(E1_{\text{APV}}/\beta)$ is extracted from experimental measurements, and this is converted to Q_W^{SM} and θ_W .

B. Experimental reports

The two-level system that serves as the quantum sensor for APV consists of the ground state and an excited state that has the same parity as the ground state. Due to the enhancement, heavy atoms are preferred, and historically the measurements were mainly performed with Cs atoms, as shown in Table VI. In the latest experiment²⁶⁸, the 6S ground state and the 7S excited state are regarded as the two-level system. The E1 transition between these two state is forbidden, and these states can be driven as an M1 transition. In the experiment, the M1 transition is suppressed by generating a standing wave using a power build-up cavity. To drive the 6S-7S transition in a controlled way, they mix the 7P state with the 7S state by a static electric field (E in Eq. 19). By flipping the sign of E_{osc} and E , further discrimination of the background and the signal is performed. After estimating all systematic uncertainties, most of which are related to the M1 amplitude A_{M1} , $\text{Im}(E1_{\text{APV}}/\beta) = -1.5935(56)$ is obtained, which leads to $\theta_W = 0.2261(12)_{\text{exp}}(41)_{\text{theory}}$ around 2.4 MeV.

Another attempt to observe the APV is performed with Yb. In this case, the two-level system consists of the $6s^2 \ ^1S_0$ ground state and the $6s5d \ ^3D_1$ state. A large parity-violating effect is observed²⁷⁰ for this transition. An advantage of Yb compared to Cs is that the number of stable isotope is not one but five, even if the only bosonic isotopes are considered. In this case, the contribution of N on Q_W^{SM} can be estimated by measuring the P-violating effect for multiple isotopes²⁷¹.

The next generation experiment tries to measure the APV in Fr. Because all Fr isotopes are unstable, the experiments are performed at accelerator facilities such as TRIUMF and

TABLE VI. List of atomic parity violation measurements.

Atom	Year	$\text{Im}(E1_{\text{APV}})/\beta$ (mV/cm)	reference
Cs	1982	1.34(22) _{stat} (11) _{syst}	282
Cs	1986	1.52(18)	283
Cs	1988	1.65(13)	269
Cs	1988	1.576(34)	284
Cs	1997	1.5935(56)	268
Yb	2009	39(4) _{stat} (5) _{syst}	270

RIKEN RIBF. The loading of Fr atoms generated by nuclear reactions into a magneto-optical trap was achieved in the 1990s at Stony Brook²⁷², and relevant transitions have been characterized towards the measurement of the parity violation^{273,274}. An attempt to improve the uncertainty of the measurement with Cs is also ongoing²⁷⁵.

Another method to enhance sensitivity is to use small ΔE . For this purpose, the usage of diatomic molecule²⁷⁶⁻²⁷⁸ and dysprosium²⁷⁹ is proposed. Closely lying states for parity mixing in these species enhance the signal. Sensitivity is experimentally reported for a BaF molecule experiment²⁸⁰. In the case of BaF, the measured quantity is the nuclear spin dependent APV. A MOT for BaF is recently realized²⁸¹.

X. ELECTRIC DIPOLE MOMENT SEARCH

A. Introduction to electric dipole moment searches

Electric dipole moments (EDMs) of elementary particles serve as a probe for high-energy physics through the violation of time-reversal (T) symmetry. When an elementary particle with spin 1/2 has a finite EDM, this particle violates T operation, as the EDM remains the same but the magnetic dipole moment flips under the T operation. Assuming the CPT theorem^{285,286} (C stands for the charge conjugate operation), this results in a violation of the symmetry under the CP operation. Such a CP-violating moment is predicted in the framework of the SM of particle physics. For the electron, four-loop perturbations predict an EDM, and the magnitude is $d_e = 10^{-44} e\cdot\text{cm}$ ²⁸⁷⁻²⁸⁹. CP-violating interactions between electrons and nucleus mimics the electron EDM. This effect is estimated to range from $d_e^{\text{equiv}} = 10^{-35} e\cdot\text{cm}$ ²⁹⁰ to $d_e^{\text{equiv}} = 10^{-38} e\cdot\text{cm}$ ^{288,289}. In supersymmetric theories, such a CP-violating moments can be induced by one-loop diagrams, resulting in a much larger value. This argument holds for other elementary particles and nuclei. Therefore, the search for EDM serves as a search for supersymmetric particles. Also, the amount of CP-violation is closely related to the matter-antimatter asymmetry in the universe.

The search for EDM started from a theoretical proposal in 1950²⁹¹. Since then, it has been conducted for various particles, including the neutron²⁹², electron²⁹³, muon²⁹⁴, and nuclei²⁹⁵⁻²⁹⁸. Here, since quantum technologies related to atomic and molecular physics are focused on, only electron and nuclear EDM searches are dealt with, and refer to another review paper²⁹⁹ for EDMs on other particles.

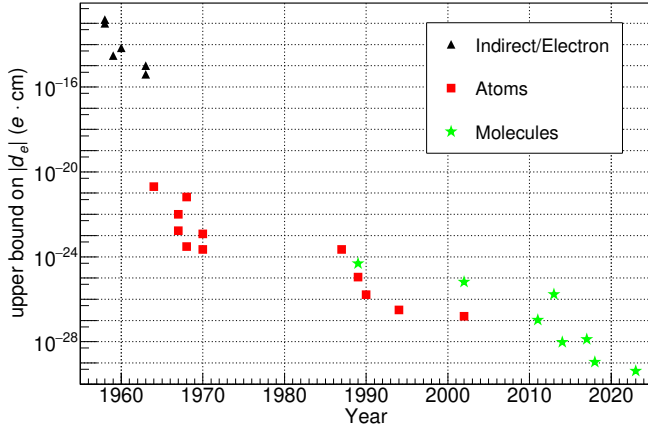


FIG. 10. Historical development of the constraint on electron EDM: black triangles indicate constraints obtained by theoretical calculations of atomic structure or measurements with electron scattering. Red squares and green stars show the constraints obtained by atomic and molecular spectroscopy, respectively. Constraints are either at the 90% or 95% confidence level, following the number in the original papers.

The Schiff's theorem³⁰⁰ plays an important role in EDM searches. It states that the overall EDM vanishes in an atom consisting of point-like nonrelativistic charged particles interacting with a static electric field. The measurable EDM arises due to relativistic effects, a nucleus of finite size, and an unpaired electron. Therefore, the electron EDM is always searched for in an atom or a molecule with an unpaired electron.

In experimental searches of EDM, the tiny effect of the EDM in a Ramsey sequence is investigated when both a magnetic field \mathbf{B} and an electric field \mathbf{E} are applied. If the particle is only with a magnetic moment μ by a spin, it precesses according to the Hamiltonian $H = -\mu \cdot \mathbf{B}$. If the particle has a finite EDM \mathbf{d} , the amount of precession changes according to $H = -\mu \cdot \mathbf{B} - \mathbf{d} \cdot \mathbf{E}$. Naively, this spin 1/2 state is regarded as the quantum sensor for the EDM, and the deviation of the precession from purely spin system is the signal for the EDM.

B. Electron EDM

An electron is one of the elementary particles for which EDM searches have long been performed, as shown in Fig. 10. Because it is a lepton, the resulting constraint on the EDM sets limits on the existence of supersymmetric particles corresponding to leptons. The EDM of an electron was first indirectly investigated by calculating its effect on the Lamb shift in hydrogen atoms³⁰¹. Although the first direct search was performed with bare electrons, neutral atoms and molecules are now widely used for the search to apply higher effective electric fields to enhance the amount of precession induced by the EDM through internal electric field.

For an atom with atomic number Z , the enhancement factor of the electron EDM is $10Z^3\alpha^{2.299,302}$. Because of this Z

dependence, heavy atoms are generally used for the search. Most of the measurements with atoms in Fig. 10 are performed with Cs and Tl.

To achieve an even higher internal electric field, polar molecules are utilized. Molecules consisting of a soft heavy atom and an atom with a high electronegativity induce a high internal electric field E_{eff} on the order of 10 GV/cm. Atoms are selected so that one extra electron remains in addition to fully closed inner shells and valence electrons filling orbitals for chemical bonding. This extra electron is utilized as the probe. The YbF experiment^{303,304} pioneered the work with molecules, and recent progresses are made with ThO and HfF⁺ molecules.

In these molecules, a set of states called the Ω -doublet states is utilized for EDM searches. $\Omega = \mathbf{J} \cdot \hat{n}$ is the projection of the angular momentum of an electron on the internuclear axis \hat{n} of the diatomic molecule. In the $J = 1$ case, $\Omega = \pm 1$ states are almost degenerated, forming two closely separated states with parity $(-1)^J$ and $(-1)^{J+1}$ ³⁰⁵. The Ω -doublet can be fully polarized by a small external electric field. When polarized, a pair of $m = \pm 1$ states at the same energy has the same E_{eff} orientation and opposite spin orientation. The Ramsey sequence is performed under external magnetic and electric fields. The recorded signal is the amount of the precession for the $m = 1$ state relative to the $m = -1$ state. To cancel systematic shifts and extract the EDM signal, the external electric and magnetic fields are flipped, as well as the orientation of the molecule by selecting the other pair of $m = \pm 1$ states in the Ω -doublet. The difference in the amount of precession in each combination of the flipping is properly processed to obtain desired quantities. The quantum sensor is the Ω doublet states, and the small perturbation of the energy level of the states when electric field is applied serves as the signal for the EDM.

The figure of merit for the sensitivity is the same as the SQL for atomic clocks:

$$\delta d_e = \frac{\hbar}{2\tau_R E_{\text{eff}} \sqrt{NT}}, \quad (20)$$

where N is the number of molecules including their detection efficiency, τ_R scales to the coherence time for the EDM states, E_{eff} is the effective electric field the electron feels in the molecule, and T is the overall measurement time. The choice of molecule is based on E_{eff} and the coherence time of the Ω -doublet states. In the case of ThO, the coherence time is 4.2(5) ms³⁰⁶. In this case, a beam experiment is suitable, and a buffer gas-cooled cryogenic beam is utilized for the measurement³⁰⁷. It is relatively easy to increase the number of molecules to enhance the sensitivity by reduced SQL. The HfF⁺ ion has much longer lifetime for the Ω -doublet state, which extends the interrogation time up to 3 s³⁰⁸. This cancels the disadvantage of only a small number of ions being in the trap. As a result, the sensitivity for the two state-of-the-art results are different by only a factor of a few.

Once decent sensitivity is obtained, the remaining tasks to extract the electron EDM are to properly estimating and compensating all systematic shifts. Two major sources of uncertainty are the nonuniform magnetic field and the non-inverting

components of the electric and magnetic fields. The stability of the laser power, including the overlap of the light and the molecules, is another source of uncertainty. Because the HfF^+ experiment puts ions in circular motion, uncertainties specific to this circular motion also needs to be considered.

The currently available most stringent constraint is from the HfF^+ experiment, providing $|d_e| < 4.1 \times 10^{-30} e \cdot \text{cm}^{308}$. The ThO experiment gives the constraint of $|d_e| < 1.1 \times 10^{-29} e \cdot \text{cm}^{293}$. These constraints corresponds to > 10 TeV-scale physics when it is properly interpreted based on supersymmetric theories²⁸⁷. The naive supersymmetric theory is already excluded by previous experiments, and these experiments are excluding some more complicated theories. The attainable highest energy with these constraint is 40 TeV^{308} .

Upgrades for both ThO and HfF^+ experiments are ongoing³⁰⁹⁻³¹¹, as well as for YbF^{312} . At the proposal level, the enhancement of sensitivity with an entangled state is discussed³¹³. This proposal suggests combining a cavity QED system and the electron EDM measurement using Fr to generate a squeezed-spin state for Fr. Experimental investigations on future searches with radioactive isotopes are also ongoing for molecules. Particularly, RaF is attractive not only for the electron EDM search but also for APV. This was initially proposed theoretically³¹⁴, and experimental investigations of molecular spectroscopy are ongoing^{315,316}. In general, Ra-containing molecules attract much attention, and some other species are investigated both theoretically³¹⁷⁻³¹⁹ and experimentally³²⁰. Polyatomic molecules are also investigated as next-generation species for electron EDM searches. A theoretical proposal³²¹ pointed out that polyatomic molecules have the advantage that the states easy to polarize, equivalent to Ω doublets, are not associated with electronic spin, and therefore the spin does not affect laser cooling properties or sensitivity to EDM. This proposal triggered investigations on YbOH and YbOCH_3 ³²²⁻³²⁵. Recently, a MOT of SrOH is reported³²⁶ in the context of the search for an electron EDM. Also, enhancing the sensitivity of the electron EDM search with polyatomic molecules through entanglement is theoretically proposed³²⁷.

C. Nuclear EDM

Within the technology of atomic physics, nuclear EDMs can also be measured. The nuclear EDM is associated with supersymmetric particles in the hadronic sector. The available constraints have an access to 10-TeV physics. To measure the EDM of a nucleus, spin-polarized nuclei are used. One of the ways to prepare such a spin-polarized system and detect the spin state is optical pumping and optical detection with lasers. Such methods involve atomic physics techniques, and thus the nuclear EDM is within the scope of this paper.

Nuclear EDM measurements are performed with atomic or molecular systems where electrons are fully paired to cancel out the potential effect of the electron EDM. Also, nuclei with spin 1/2 are preferred, due to the simplicity of the system and the absence of the potential effects of higher-order deformations of the nucleus. As a result, popular species for

nuclear EDM searches are ^{199}Hg , ^{171}Yb , ^{129}Xe , ^{225}Ra , and the neutron. Among them, ^{199}Hg , ^{171}Yb , and ^{225}Ra experiments utilize atomic physics techniques for the measurements, these species are focused on. For other systems, some review papers²⁹⁹ provide a thorough summary of the topic.

In the measurement sequence, nuclei are placed under magnetic and electric fields, and a Ramsey sequence is performed to detect the tiny phase difference when the direction of the electric field is flipped. The relevant energy level is the nuclear spin 1/2 in a strong magnetic field, and thus the energy scale for the Ramsey sequence is in the range of NMR spectroscopy, not laser spectroscopy. Because the internal electric field for the nucleus is zero, the applied electric field comes from electrodes, and thus the field is substantially smaller than E_{eff} in the electron EDM search case. Nevertheless, thanks to the very long coherence time of the nuclear spin, the interrogation time can be ~ 100 s, resulting in the constraint of $|d_{\text{Hg}}| < 7.4 \times 10^{-30} e \cdot \text{cm}$ for $^{199}\text{Hg}^{295}$ and $|d_{\text{Yb}}| < 1.5 \times 10^{-26} e \cdot \text{cm}^{296}$ for ^{171}Yb , which are comparable to the constraint on the electron EDM.

The Hg experiment uses a vapor cell, and thus the major systematic uncertainty is related to the motion of the atoms. For Yb, the atoms are laser-cooled and trapped in an optical dipole trap. This removes the uncertainty related to the motion. However, the optical dipole trap introduces different sources of uncertainty. The ^{225}Ra experiment²⁹⁸ has a similar configuration as the Yb experiment. This first report sets the constraint at $|d_{\text{Ra}}| < 1.4 \times 10^{-26} e \cdot \text{cm}$ and the major source of the uncertainty is related to the phase shift proportional to the square of the electric field and the magnetic field correlated to the electric field.

XI. SUMMARY AND OUTLOOK

High precision measurements with quantum states are applied to nuclear and particle physics in various ways. It is essential for the precision of the measurements to be high enough to enable such applications, and quantum sensors have been playing an important role in their development.

For further advancement in the future, a few aspects are important. One is the further improvement in the precision of the measurement. Even within the same experimental system, when the precision of the measurement improves, the sensitivity to nuclear and particle physics phenomena increases for most of the topics covered in this paper. In the past, advancements in clock uncertainty contributed to the search for ultralight dark matter and the time variation of fundamental constants. Secondly, the use of quantum sensors with high sensitivity can drastically improve the sensitivity. A good example is the search for variation of the fine structure constant. Switching from conventional ion clocks to HCI clocks or nuclear clocks would enhance the sensitivity by orders of magnitude. In addition, a good understanding of theory behind the measurements is crucial. Theoretical calculations of atomic or molecular structure determine sensitivity of a quantum sensor to the quantity of interest. Sensitivity coefficient K for the variation of the fine structure constant and internal electric

field E_{eff} for the electron EDM search are good examples. Further improvements in the accuracy of theoretical calculations for these quantities can contribute to a more precise determination of the parameters in nuclear and particle physics. Also, new theoretical proposals can trigger intensive experimental searches for a new parameter spaces. In the past, searches for the fifth force with isotope shifts and ultralight dark matter increased after the initial theoretical proposals. With a combination of these factors, further contributions of quantum sensors to nuclear and particle physics are expected.

ACKNOWLEDGMENTS

The author thanks Takashi Higuchi, Joonseok Hur, and Takumi Kobayashi for helpful discussions and comments on the manuscript. A.K. acknowledges the support of Japan Society for the Promotion of Science KAKENHI Grants No. JP22H01161, and Japan Science and Technology Agency FOREST Grant No. JPMJFR212S. Data sharing is not applicable to this article as no new data were created or analyzed in this study.

- ¹C. L. Degen, F. Reinhard, and P. Cappellaro, “Quantum sensing,” *Rev. Mod. Phys.* **89**, 035002 (2017).
- ²M. Kjaergaard, M. E. Schwartz, J. Braumüller, P. Krantz, J. I.-J. Wang, S. Gustavsson, and W. D. Oliver, “Superconducting qubits: Current state of play,” *Annu. Rev. Condens. Matter Phys.* **11**, 369–395 (2020).
- ³P. Krantz, M. Kjaergaard, F. Yan, T. P. Orlando, S. Gustavsson, and W. D. Oliver, “A quantum engineer’s guide to superconducting qubits,” *Appl. Phys. Rev.* **6**, 021318 (2019).
- ⁴S. Barzanjeh, A. Xuereb, S. Gröblacher, M. Paternostro, C. A. Regal, and E. M. Weig, “Optomechanics for quantum technologies,” *Nat. Phys.* **18**, 15–24 (2022).
- ⁵J. Millen, T. S. Monteiro, R. Pettit, and A. N. Vamivakas, “Optomechanics with levitated particles,” *Rep. Prog. Phys.* **83**, 026401 (2020).
- ⁶R. Schirhagl, K. Chang, M. Loretz, and C. L. Degen, “Nitrogen-vacancy centers in diamond: Nanoscale sensors for physics and biology,” *Annu. Rev. Phys. Chem.* **65**, 83–105 (2014).
- ⁷M. W. Doherty, N. B. Manson, P. Delaney, F. Jelezko, J. Wrachtrup, and L. C. Hollenberg, “The nitrogen-vacancy colour centre in diamond,” *Phys. Rep.* **528**, 1–45 (2013).
- ⁸J. F. Barry, J. M. Schloss, E. Bauch, M. J. Turner, C. A. Hart, L. M. Pham, and R. L. Walsworth, “Sensitivity optimization for NV-diamond magnetometry,” *Rev. Mod. Phys.* **92**, 015004 (2020).
- ⁹C. Gross and I. Bloch, “Quantum simulations with ultracold atoms in optical lattices,” *Science* **357**, 995–1001 (2017).
- ¹⁰J. L. Bohn, A. M. Rey, and J. Ye, “Cold molecules: Progress in quantum engineering of chemistry and quantum matter,” *Science* **357**, 1002–1010 (2017).
- ¹¹C. D. Bruzewicz, J. Chiaverini, R. McConnell, and J. M. Sage, “Trapped-ion quantum computing: Progress and challenges,” *Appl. Phys. Rev.* **6**, 021314 (2019).
- ¹²C. Monroe and J. Kim, “Scaling the ion trap quantum processor,” *Science* **339**, 1164–1169 (2013).
- ¹³W. D. Phillips and H. Metcalf, “Laser deceleration of an atomic beam,” *Phys. Rev. Lett.* **48**, 596–599 (1982).
- ¹⁴E. L. Raab, M. Prentiss, A. Cable, S. Chu, and D. E. Pritchard, “Trapping of neutral sodium atoms with radiation pressure,” *Phys. Rev. Lett.* **59**, 2631–2634 (1987).
- ¹⁵J. Dalibard and C. Cohen-Tannoudji, “Laser cooling below the doppler limit by polarization gradients: simple theoretical models,” *J. Opt. Soc. Am. B* **6**, 2023–2045 (1989).
- ¹⁶R. Grimm, M. Weidemüller, and Y. B. Ovchinnikov, “Optical dipole traps for neutral atoms,” (Academic Press, 2000) pp. 95–170.
- ¹⁷W. Ketterle and N. V. Druten, “Evaporative cooling of trapped atoms,” (Academic Press, 1996) pp. 181–236.
- ¹⁸C. Monroe, D. M. Meekhof, B. E. King, S. R. Jefferts, W. M. Itano, D. J. Wineland, and P. Gould, “Resolved-sideband Raman cooling of a bound atom to the 3D zero-point energy,” *Phys. Rev. Lett.* **75**, 4011–4014 (1995).
- ¹⁹W. Neuhauser, M. Hohenstatt, P. Toschek, and H. Dehmelt, “Optical-sideband cooling of visible atom cloud confined in parabolic well,” *Phys. Rev. Lett.* **41**, 233–236 (1978).
- ²⁰S. E. Hamann, D. L. Haycock, G. Klose, P. H. Pax, I. H. Deutsch, and P. S. Jessen, “Resolved-sideband Raman cooling to the ground state of an optical lattice,” *Phys. Rev. Lett.* **80**, 4149–4152 (1998).
- ²¹X. Zhang, K. Beloy, Y. S. Hassan, W. F. McGrew, C.-C. Chen, J. L. Siegel, T. Grogan, and A. D. Ludlow, “Subrecoil clock-transition laser cooling enabling shallow optical lattice clocks,” *Phys. Rev. Lett.* **129**, 113202 (2022).
- ²²C.-C. Chen, J. L. Siegel, B. D. Hunt, T. Grogan, Y. S. Hassan, K. Beloy, K. Gibble, R. C. Brown, and A. D. Ludlow, “Clock-line-mediated Sisyphus cooling,” *Phys. Rev. Lett.* **133**, 053401 (2024).
- ²³W. Happer, “Optical pumping,” *Rev. Mod. Phys.* **44**, 169–249 (1972).
- ²⁴N. V. Vitanov, A. A. Rangelov, B. W. Shore, and K. Bergmann, “Stimulated Raman adiabatic passage in physics, chemistry, and beyond,” *Rev. Mod. Phys.* **89**, 015006 (2017).
- ²⁵U. Gaubatz, P. Rudecki, S. Schiemann, and K. Bergmann, “Population transfer between molecular vibrational levels by stimulated Raman scattering with partially overlapping laser fields. A new concept and experimental results,” *J. Chem. Phys.* **92**, 5363–5376 (1990).
- ²⁶E. Treacy and A. Demaria, “Adiabatic inversion in the infrared,” *Phys. Lett. A* **29**, 369–370 (1969).
- ²⁷M. M. T. Loy, “Observation of population inversion by optical adiabatic rapid passage,” *Phys. Rev. Lett.* **32**, 814–817 (1974).
- ²⁸R. M. B. J. Dalton and P. Knight, “Coherent population trapping,” *Optica Acta: Int. J. Optics* **32**, 61–70 (1985).
- ²⁹C. Cohen-Tannoudji, J. Dupont-Roc, and G. Grynberg, *Atom—Photon Interactions* (Wiley, 1998).
- ³⁰S. Wimperis, “Broadband, narrowband, and passband composite pulses for use in advanced NMR experiments,” *J. Magn. Reson. Ser. A* **109**, 221–231 (1994).
- ³¹H. K. Cummins, G. Llewellyn, and J. A. Jones, “Tackling systematic errors in quantum logic gates with composite rotations,” *Phys. Rev. A* **67**, 042308 (2003).
- ³²M. Bando, T. Ichikawa, Y. Kondo, and M. Nakahara, “Concatenated composite pulses compensating simultaneous systematic errors,” *J. Phys. Soc. Jpn.* **82**, 014004 (2013).
- ³³H. Katori, M. Takamoto, V. G. Pal’chikov, and V. D. Ovsiannikov, “Ultra-stable optical clock with neutral atoms in an engineered light shift trap,” *Phys. Rev. Lett.* **91**, 173005 (2003).
- ³⁴M. Takamoto, F.-L. Hong, R. Higashi, and H. Katori, “An optical lattice clock,” *Nature* **435**, 321–324 (2005).
- ³⁵A. D. Ludlow, M. M. Boyd, J. Ye, E. Peik, and P. O. Schmidt, “Optical atomic clocks,” *Rev. Mod. Phys.* **87**, 637–701 (2015).
- ³⁶N. Poli, C. W. Oates, P. Gill, and G. M. Tino, “Optical atomic clocks,” *La Rivista del Nuovo Cimento* **036**, 555–624 (2013).
- ³⁷D. Allan, “Statistics of atomic frequency standards,” *Proc. IEEE* **54**, 221–230 (1966).
- ³⁸W. M. Itano, J. C. Bergquist, J. J. Bollinger, J. M. Gilligan, D. J. Heinzen, F. L. Moore, M. G. Raizen, and D. J. Wineland, “Quantum projection noise: Population fluctuations in two-level systems,” *Phys. Rev. A* **47**, 3554–3570 (1993).
- ³⁹D. J. Wineland, J. J. Bollinger, W. M. Itano, and D. J. Heinzen, “Squeezed atomic states and projection noise in spectroscopy,” *Phys. Rev. A* **50**, 67–88 (1994).
- ⁴⁰E. Pedrozo-Peñafiel, S. Colombo, C. Shu, A. F. Adiyatullin, Z. Li, E. Mendez, B. Braverman, A. Kawasaki, D. Akamatsu, Y. Xiao, *et al.*, “Entanglement on an optical atomic-clock transition,” *Nature* **588**, 414–418 (2020).
- ⁴¹F. T. Arecchi, E. Courtens, R. Gilmore, and H. Thomas, “Atomic coherent states in quantum optics,” *Phys. Rev. A* **6**, 2211–2237 (1972).
- ⁴²Y. Huang, B. Zhang, M. Zeng, Y. Hao, Z. Ma, H. Zhang, H. Guan, Z. Chen, M. Wang, and K. Gao, “Liquid-nitrogen-cooled Ca^+ optical clock with systematic uncertainty of 3×10^{-18} ,” *Phys. Rev. Appl.* **17**, 034041 (2022).
- ⁴³M. Steinel, H. Shao, M. Filzinger, B. Lipphardt, M. Brinkmann, A. Didier,

- T. E. Mehlstäubler, T. Lindvall, E. Peik, and N. Huntemann, "Evaluation of a $^{88}\text{Sr}^+$ optical clock with a direct measurement of the blackbody radiation shift and determination of the clock frequency," *Phys. Rev. Lett.* **131**, 083002 (2023).
- ⁴⁴K. J. Arnold, R. Kaewuam, S. R. Chanu, T. R. Tan, Z. Zhang, and M. D. Barrett, "Precision measurements of the $^{138}\text{Ba}^+ 6s^2S_{1/2} - 5d^2D_{5/2}$ clock transition," *Phys. Rev. Lett.* **124**, 193001 (2020).
- ⁴⁵C. A. Holliman, M. Fan, A. Contractor, S. M. Brewer, and A. M. Jayich, "Radium ion optical clock," *Phys. Rev. Lett.* **128**, 033202 (2022).
- ⁴⁶T. Rosenband, D. B. Hume, P. O. Schmidt, C. W. Chou, A. Brusch, L. Lorini, W. H. Oskay, R. E. Drullinger, T. M. Fortier, J. E. Stalnaker, and others, "Frequency ratio of Al^+ and Hg^+ single-ion optical clocks; metrology at the 17th decimal place," *Science* **319**, 1808–1812 (2008).
- ⁴⁷R. Lange, A. A. Peshkov, N. Huntemann, C. Tamm, A. Surzhykov, and E. Peik, "Lifetime of the $^2F_{7/2}$ level in Yb^+ for spontaneous emission of electric octupole radiation," *Phys. Rev. Lett.* **127**, 213001 (2021).
- ⁴⁸T. Rosenband, P. O. Schmidt, D. B. Hume, W. M. Itano, T. M. Fortier, J. E. Stalnaker, K. Kim, S. A. Diddams, J. C. J. Koelemeij, J. C. Bergquist, *et al.*, "Observation of the $^1S_0 \rightarrow ^3P_0$ clock transition in $^{27}\text{Al}^+$," *Phys. Rev. Lett.* **98**, 220801 (2007).
- ⁴⁹L. Pelzer, K. Dietze, J. Kramer, F. Dawel, L. Krinner, N. Spethmann, V. Martinez, N. Aharon, A. Retzker, K. Hammerer, *et al.*, "Tailored optical clock transition in $^{40}\text{Ca}^+$," *Measurement: Sensors* **18**, 100326 (2021).
- ⁵⁰P. Dubé, A. A. Madej, and B. Jian, " Sr^+ single-ion clock," *J. Phys. Conf. Ser.* **723**, 012018 (2016).
- ⁵¹M. Schacht, J. R. Danielson, S. Rahaman, J. R. Torgerson, J. Zhang, and M. M. Schauer, " $^{171}\text{Yb}^+ 5D_{3/2}$ hyperfine state detection and $F = 2$ lifetime," *J. Phys. B: At. Mol. Opt. Phys.* **48**, 065003 (2015).
- ⁵²A. G. Calamai and C. E. Johnson, "Radiative lifetimes of metastable states of Hg^+ and Hg^{2+} ," *Phys. Rev. A* **42**, 5425–5432 (1990).
- ⁵³J. A. Muniz, D. J. Young, J. R. K. Cline, and J. K. Thompson, "Cavity-QED measurements of the ^{87}Sr millihertz optical clock transition and determination of its natural linewidth," *Phys. Rev. Res.* **3**, 023152 (2021).
- ⁵⁴C.-Y. Xu, J. Singh, J. C. Zappala, K. G. Bailey, M. R. Dietrich, J. P. Greene, W. Jiang, N. D. Lemke, Z.-T. Lu, P. Mueller, *et al.*, "Measurement of the hyperfine quenching rate of the clock transition in ^{171}Yb ," *Phys. Rev. Lett.* **113**, 033003 (2014).
- ⁵⁵F. Schäfer, H. Konishi, A. Bouscal, T. Yagami, and Y. Takahashi, "Spin dependent inelastic collisions between metastable state two-electron atoms and ground state alkali-atoms," *New J. Phys.* **19**, 103039 (2017).
- ⁵⁶F. Schäfer, H. Konishi, A. Bouscal, T. Yagami, and Y. Takahashi, "Spectroscopic determination of magnetic-field-dependent interactions in an ultracold $\text{Yb}(^3P_2)\text{-Li}$ mixture," *Phys. Rev. A* **96**, 032711 (2017).
- ⁵⁷H. Konishi, F. Schäfer, S. Ueda, and Y. Takahashi, "Collisional stability of localized $\text{Yb}(^3P_2)$ atoms immersed in a Fermi sea of Li ," *New J. Phys.* **18**, 103009 (2016).
- ⁵⁸K. Honda, Y. Takasu, Y. Haruna, Y. Nishida, and Y. Takahashi, "Evidence of a four-body force in an interaction-tunable trapped cold-atom system," (2024), arXiv:2402.16254 [cond-mat.quant-gas].
- ⁵⁹V. A. Dzuba, V. V. Flambaum, and S. Schiller, "Testing physics beyond the standard model through additional clock transitions in neutral ytterbium," *Phys. Rev. A* **98**, 022501 (2018).
- ⁶⁰M. S. Safronova, S. G. Porsev, C. Sanner, and J. Ye, "Two clock transitions in neutral Yb for the highest sensitivity to variations of the fine-structure constant," *Phys. Rev. Lett.* **120**, 173001 (2018).
- ⁶¹Z.-M. Tang, Y.-m. Yu, B. K. Sahoo, C.-Z. Dong, Y. Yang, and Y. Zou, "Simultaneous magic trapping conditions for three additional clock transitions in Yb to search for variation of the fine-structure constant," *Phys. Rev. A* **107**, 053111 (2023).
- ⁶²A. Kawasaki, T. Kobayashi, A. Nishiyama, T. Tanabe, and M. Yasuda, "Observation of the $4f^{14}6s^2\ ^1S_0 - 4f^{13}5d6s^2\ (J = 2)$ clock transition at 431 nm in ^{171}Yb ," *Phys. Rev. A* **107**, L060801 (2023).
- ⁶³T. Ishiyama, K. Ono, T. Takano, A. Sunaga, and Y. Takahashi, "Observation of an inner-shell orbital clock transition in neutral ytterbium atoms," *Phys. Rev. Lett.* **130**, 153402 (2023).
- ⁶⁴H. Qiao, D. Ai, C.-Y. Sun, C.-Q. Peng, Q.-C. Qi, C.-C. Zhao, L.-M. Luo, T.-Y. Jin, T. Zhang, M. Zhou, *et al.*, "Investigation of the $6s6p\ ^3P_0 - 4f^{13}5d6s^2\ (J = 2)$ clock transition in ^{171}Yb atoms," *Phys. Rev. X* **14**, 011023 (2024).
- ⁶⁵A. Kawasaki, T. Kobayashi, A. Nishiyama, T. Tanabe, and M. Yasuda, "Isotope-shift analysis with the $4f^{14}6s^2\ ^1S_0 - 4f^{13}5d6s^2\ (J = 2)$ transition in ytterbium," *Phys. Rev. A* **109**, 062806 (2024).
- ⁶⁶A. P. Kulosa, D. Fim, K. H. Zipfel, S. Rühmann, S. Sauer, N. Jha, K. Gible, W. Ertmer, E. M. Rasel, M. S. Safronova, *et al.*, "Towards a Mg lattice clock: Observation of the $^1S_0 - ^3P_0$ transition and determination of the magic wavelength," *Phys. Rev. Lett.* **115**, 240801 (2015).
- ⁶⁷G. Wilpers, C. W. Oates, S. A. Diddams, A. Bartels, T. M. Fortier, W. H. Oskay, J. C. Bergquist, S. R. Jefferts, T. P. Heavner, T. E. Parker, *et al.*, "Absolute frequency measurement of the neutral ^{40}Ca optical frequency standard at 657 nm based on microkelvin atoms," *Metrologia* **44**, 146 (2007).
- ⁶⁸A. Aeppli, K. Kim, W. Warfield, M. S. Safronova, and J. Ye, "Clock with 8×10^{-19} systematic uncertainty," *Phys. Rev. Lett.* **133**, 023401 (2024).
- ⁶⁹W. F. McGrew, X. Zhang, R. J. Fasano, S. A. Schäffer, K. Beloy, D. Nicolodi, R. C. Brown, N. Hinkley, G. Milani, M. Schioppo, *et al.*, "Atomic clock performance enabling geodesy below the centimetre level," *Nature* **564**, 87–90 (2018).
- ⁷⁰A. Yamaguchi, M. S. Safronova, K. Gible, and H. Katori, "Narrow-line cooling and determination of the magic wavelength of Cd ," *Phys. Rev. Lett.* **123**, 113201 (2019).
- ⁷¹K. Yamanaka, N. Ohmae, I. Ushijima, M. Takamoto, and H. Katori, "Frequency ratio of ^{199}Hg and ^{87}Sr optical lattice clocks beyond the si limit," *Phys. Rev. Lett.* **114**, 230801 (2015).
- ⁷²L. Wu, X. Wang, T. Wang, J. Jiang, and C. Dong, "Be optical lattice clocks with the fractional stark shift up to the level of 10^{-19} ," *New J. Phys.* **25**, 043011 (2023).
- ⁷³M. Abe, P. Adamson, M. Borcean, D. Bortoletto, K. Bridges, S. P. Carman, S. Chattopadhyay, J. Coleman, N. M. Curfman, K. DeRose, *et al.*, "Matter-wave atomic gradiometer interferometric sensor (MAGIS-100)," *Quantum Sci. Technol.* **6**, 044003 (2021).
- ⁷⁴D. González-Cuadra, D. Bluvstein, M. Kalinowski, R. Kaubuegger, N. Maskara, P. Naldesi, T. V. Zache, A. M. Kaufman, M. D. Lukin, H. Pichler, *et al.*, "Fermionic quantum processing with programmable neutral atom arrays," *Proc. Natl. Acad. Sci.* **120**, e2304294120 (2023).
- ⁷⁵S. M. Brewer, J.-S. Chen, A. M. Hankin, E. R. Clements, C. W. Chou, D. J. Wineland, D. B. Hume, and D. R. Leibbrandt, " $^{27}\text{Al}^+$ quantum-logic clock with a systematic uncertainty below 10^{-18} ," *Phys. Rev. Lett.* **123**, 033201 (2019).
- ⁷⁶H. N. Hausser, J. Keller, T. Nordmann, N. M. Bhatt, J. Kiethe, H. Liu, M. von Boehn, J. Rahm, S. Weyers, E. Benkler, *et al.*, "An $^{115}\text{In}^+ - ^{172}\text{Yb}^+$ coulomb crystal clock with 2.5×10^{-18} systematic uncertainty," (2024), arXiv:2402.16807 [physics.atom-ph].
- ⁷⁷Z. Zhang, K. J. Arnold, R. Kaewuam, and M. D. Barrett, " $^{176}\text{Lu}^+$ clock comparison at the 10^{-18} level via correlation spectroscopy," *Sci. Adv.* **9**, eadg1971 (2023).
- ⁷⁸H. Katori, "Spectroscopy of strontium atoms in the lamb-diche confinement, in proc. 6th symp. on frequency standards and metrology (ed. gill, p.)," in *Frequency Standards and Metrology* (World Scientific, 2002) pp. 323–330.
- ⁷⁹N. Hinkley, J. A. Sherman, N. B. Phillips, M. Schioppo, N. D. Lemke, K. Beloy, M. Pizzocaro, C. W. Oates, and A. D. Ludlow, "An atomic clock with 10^{-18} instability," *Science* **341**, 1215–1218 (2013).
- ⁸⁰W. Zhang, J. M. Robinson, L. Sonderhouse, E. Oelker, C. Benko, J. L. Hall, T. Legero, D. G. Matei, F. Riehle, U. Sterr, *et al.*, "Ultrastable silicon cavity in a continuously operating closed-cycle cryostat at 4 K," *Phys. Rev. Lett.* **119**, 243601 (2017).
- ⁸¹J. M. Robinson, E. Oelker, W. R. Milner, W. Zhang, T. Legero, D. G. Matei, F. Riehle, U. Sterr, and J. Ye, "Crystalline optical cavity at 4 K with thermal-noise-limited instability and ultralow drift," *Optica* **6**, 240–243 (2019).
- ⁸²T. Bothwell, C. J. Kennedy, A. Aeppli, D. Kedar, J. M. Robinson, E. Oelker, A. Staron, and J. Ye, "Resolving the gravitational redshift across a millimetre-scale atomic sample," *Nature* **602**, 420–424 (2022).
- ⁸³T. L. Nicholson, S. L. Campbell, R. B. Hutson, G. E. Marti, B. J. Bloom, R. L. McNally, W. Zhang, M. D. Barrett, M. S. Safronova, G. F. Strouse, *et al.*, "Systematic evaluation of an atomic clock at 2×10^{-18} total uncertainty," *Nat. Commun.* **6**, 6896 (2015).
- ⁸⁴J. Lodewyck, M. Zawada, L. Lorini, M. Gurov, and P. Lemonde, "Observation and cancellation of a perturbing dc stark shift in strontium optical lattice clocks," *IEEE Trans. Ultrason. Ferroelectr. Freq. Control* **59**, 411–

- 415 (2012).
- ⁸⁵K. Beloy, X. Zhang, W. F. McGrew, N. Hinkley, T. H. Yoon, D. Nicolodi, R. J. Fasano, S. A. Schäffer, R. C. Brown, and A. D. Ludlow, “Faraday-shielded dc stark-shift-free optical lattice clock,” *Phys. Rev. Lett.* **120**, 183201 (2018).
- ⁸⁶S. Vogt, S. Häfner, J. Grotti, S. Koller, A. Al-Masoudi, U. Sterr, and C. Lisdat, “A transportable optical lattice clock,” *J. Phys. Conf. Ser.* **723**, 012020 (2016).
- ⁸⁷A. Zhang, Z. Xiong, X. Chen, Y. Jiang, J. Wang, C. Tian, Q. Zhu, B. Wang, D. Xiong, L. He, *et al.*, “Ytterbium optical lattice clock with instability of order 10^{-18} ,” *Metrologia* **59**, 065009 (2022).
- ⁸⁸K. Beloy, J. A. Sherman, N. D. Lemke, N. Hinkley, C. W. Oates, and A. D. Ludlow, “Determination of the $5d_{5/2} \ ^3D_1$ state lifetime and blackbody-radiation clock shift in Yb,” *Phys. Rev. A* **86**, 051404 (2012).
- ⁸⁹K. Beloy, N. Hinkley, N. B. Phillips, J. A. Sherman, M. Schioppo, J. Lehman, A. Feldman, L. M. Hanssen, C. W. Oates, and A. D. Ludlow, “Atomic clock with 1×10^{-18} room-temperature blackbody stark uncertainty,” *Phys. Rev. Lett.* **113**, 260801 (2014).
- ⁹⁰I. Ushijima, M. Takamoto, M. Das, T. Ohkubo, and H. Katori, “Cryogenic optical lattice clocks,” *Nat. Photon.* **9**, 185–189 (2015).
- ⁹¹M. Takamoto, Y. Tanaka, and H. Katori, “A perspective on the future of transportable optical lattice clocks,” *Appl. Phys. Lett.* **120**, 140502 (2022).
- ⁹²J. J. McFerran, L. Yi, S. Mejri, S. Di Manno, W. Zhang, J. Guéna, Y. Le Coq, and S. Bize, “Neutral atom frequency reference in the deep ultraviolet with fractional uncertainty = 5.7×10^{-15} ,” *Phys. Rev. Lett.* **108**, 183004 (2012).
- ⁹³A. Golovizin, D. Mishin, D. Provorchenko, D. Tregubov, and N. Kolachevsky, “Synchronous comparison of two thulium optical clocks,” *JETP Lett.* **119**, 659–664 (2024).
- ⁹⁴A. Golovizin, E. Fedorova, D. Tregubov, D. Sukachev, K. Khabarova, V. Sorokin, and N. Kolachevsky, “Inner-shell clock transition in atomic thulium with a small blackbody radiation shift,” *Nat. Commun.* **10**, 1724 (2019).
- ⁹⁵M. M. Boyd, A. D. Ludlow, S. Blatt, S. M. Foreman, T. Ido, T. Zelevinsky, and J. Ye, “ ^{87}Sr lattice clock with inaccuracy below 10^{-15} ,” *Phys. Rev. Lett.* **98**, 083002 (2007).
- ⁹⁶N. D. Lemke, A. D. Ludlow, Z. W. Barber, T. M. Fortier, S. A. Diddams, Y. Jiang, S. R. Jefferts, T. P. Heavner, T. E. Parker, and C. W. Oates, “Spin- $1/2$ optical lattice clock,” *Phys. Rev. Lett.* **103**, 063001 (2009).
- ⁹⁷P. G. Westergaard, J. Lodewyck, L. Lorini, A. Lecallier, E. A. Burt, M. Zawada, J. Millo, and P. Lemonde, “Lattice-induced frequency shifts in Sr optical lattice clocks at the 10^{-17} level,” *Phys. Rev. Lett.* **106**, 210801 (2011).
- ⁹⁸I. Ushijima, M. Takamoto, and H. Katori, “Operational magic intensity for Sr optical lattice clocks,” *Phys. Rev. Lett.* **121**, 263202 (2018).
- ⁹⁹K. Kim, A. Aeppli, T. Bothwell, and J. Ye, “Evaluation of lattice light shift at low 10^{-19} uncertainty for a shallow lattice Sr optical clock,” *Phys. Rev. Lett.* **130**, 113203 (2023).
- ¹⁰⁰T. Bothwell, B. D. Hunt, J. L. Siegel, Y. S. Hassan, T. Grogan, T. Kobayashi, K. Gibble, S. G. Porsev, M. S. Safronova, R. C. Brown, *et al.*, “Lattice light shift evaluations in a dual-ensemble Yb optical lattice clock,” (2024), arXiv:2409.10782 [physics.atom-ph].
- ¹⁰¹V. D. Ovsiannikov, S. I. Marmo, V. G. Palchikov, and H. Katori, “Higher-order effects on the precision of clocks of neutral atoms in optical lattices,” *Phys. Rev. A* **93**, 043420 (2016).
- ¹⁰²S. L. Campbell, R. B. Hutson, G. E. Marti, A. Goban, N. D. Oppong, R. L. McNally, L. Sonderhouse, J. M. Robinson, W. Zhang, B. J. Bloom, *et al.*, “A Fermi-degenerate three-dimensional optical lattice clock,” *Science* **358**, 90–94 (2017).
- ¹⁰³A. Cidrim, A. Piñeiro Orioli, C. Sanner, R. B. Hutson, J. Ye, R. Bachelard, and A. M. Rey, “Dipole-dipole frequency shifts in multilevel atoms,” *Phys. Rev. Lett.* **127**, 013401 (2021).
- ¹⁰⁴J. L. Siegel, W. F. McGrew, Y. S. Hassan, C.-C. Chen, K. Beloy, T. Grogan, X. Zhang, and A. D. Ludlow, “Excited-band coherent delocalization for improved optical lattice clock performance,” *Phys. Rev. Lett.* **132**, 133201 (2024).
- ¹⁰⁵Y. S. Hassan, T. Kobayashi, T. Bothwell, J. L. Siegel, B. D. Hunt, K. Beloy, K. Gibble, T. Grogan, and A. D. Ludlow, “Ratchet loading and multi-ensemble operation in an optical lattice clock,” *Quantum Science and Technology* **9**, 045023 (2024).
- ¹⁰⁶S. B. Koller, J. Grotti, S. Vogt, A. Al-Masoudi, S. Dörscher, S. Häfner, U. Sterr, and C. Lisdat, “Transportable optical lattice clock with 7×10^{-17} uncertainty,” *Phys. Rev. Lett.* **118**, 073601 (2017).
- ¹⁰⁷M. Takamoto, I. Ushijima, N. Ohmae, T. Yahagi, K. Kokado, H. Shinkai, and H. Katori, “Test of general relativity by a pair of transportable optical lattice clocks,” *Nat. Photon.* **14**, 411–415 (2020).
- ¹⁰⁸T. Bothwell, W. Brand, R. Fasano, T. Akin, J. Whalen, T. Grogan, Y.-J. Chen, M. Pomponio, T. Nakamura, B. Rauf, *et al.*, “Deployment of a transportable Yb optical lattice clock,” (2024), arXiv:2409.16264 [physics.atom-ph].
- ¹⁰⁹A. Amy-Klein, E. Benkler, P. Blondé, K. Bongs, E. Cantin, C. Chardonnet, H. Denker, S. Dörscher, C.-H. Feng, J.-O. Gaudron, *et al.* (International Clock and Oscillator Networking (ICON) Collaboration), “International comparison of optical frequencies with transportable optical lattice clocks,” (2024), arXiv:2410.22973 [physics.atom-ph].
- ¹¹⁰C. Lisdat, G. Grosche, N. Quintin, C. Shi, S. M. F. Raupach, C. Grebing, D. Nicolodi, F. Stefani, A. Al-Masoudi, S. Dörscher, *et al.*, “A clock network for geodesy and fundamental science,” *Nature Communications* **7**, 12443 (2016).
- ¹¹¹C. Clivati, M. Pizzocaro, E. Bertacco, S. Condio, G. Costanzo, S. Donadello, I. Goti, M. Gozzelino, F. Levi, A. Mura, *et al.*, “Coherent optical-fiber link across Italy and France,” *Phys. Rev. Appl.* **18**, 054009 (2022).
- ¹¹²B. M. Roberts, P. Delva, A. Al-Masoudi, A. Amy-Klein, C. Bärentsen, C. F. A. Baynham, E. Benkler, S. Bilicki, S. Bize, W. Bowden, *et al.*, “Search for transient variations of the fine structure constant and dark matter using fiber-linked optical atomic clocks,” *New J. Phys.* **22**, 093010 (2020).
- ¹¹³K. Beloy, M. I. Bodine, T. Bothwell, S. M. Brewer, S. L. Bromley, J.-S. Chen, J.-D. Deschênes, S. A. Diddams, R. J. Fasano, T. M. Fortier, *et al.* (BACON Collaboration), “Frequency ratio measurements at 18-digit accuracy using an optical clock network,” *Nature* **591**, 564–569 (2021).
- ¹¹⁴T. Takano, M. Takamoto, I. Ushijima, N. Ohmae, T. Akatsuka, A. Yamaguchi, Y. Kuroishi, H. Munekane, B. Miyahara, and H. Katori, “Geopotential measurements with synchronously linked optical lattice clocks,” *Nat. Photon.* **10**, 662–666 (2016).
- ¹¹⁵X. Zheng, J. Dolde, V. Lochab, B. N. Merriman, H. Li, and S. Kolkowitz, “Differential clock comparisons with a multiplexed optical lattice clock,” *Nature* **602**, 425–430 (2022).
- ¹¹⁶X. Zheng, J. Dolde, M. C. Cambria, H. M. Lim, and S. Kolkowitz, “A lab-based test of the gravitational redshift with a miniature clock network,” *Nat. Commun.* **14**, 4886 (2023).
- ¹¹⁷X. Zheng, J. Dolde, and S. Kolkowitz, “Reducing the instability of an optical lattice clock using multiple atomic ensembles,” *Phys. Rev. X* **14**, 011006 (2024).
- ¹¹⁸G. J. Dick, “Local oscillator induced instabilities in trapped ion frequency standards,” *Proceedings of the 19th Annual Precise Time and Time Interval Systems and Applications Meeting*, 133–147 (1987).
- ¹¹⁹G. Santarelli, C. Audoin, A. Makdissi, P. Laurent, G. Dick, and A. Clairon, “Frequency stability degradation of an oscillator slaved to a periodically interrogated atomic resonator,” *IEEE Trans. Ultrason. Ferroelect. Freq. Contr.* **45**, 887–894 (1998).
- ¹²⁰S. Okaba, R. Takeuchi, S. Tsuji, and H. Katori, “Continuous generation of an ultracold atomic beam using crossed moving optical lattices,” *Phys. Rev. Appl.* **21**, 034006 (2024).
- ¹²¹M. A. Norcia, A. W. Young, W. J. Eckner, E. Oelker, J. Ye, and A. M. Kaufman, “Seconds-scale coherence on an optical clock transition in a tweezer array,” *Science* **366**, 93–97 (2019).
- ¹²²J. P. Covey, I. S. Madjarov, A. Cooper, and M. Endres, “2000-times repeated imaging of strontium atoms in clock-magic tweezer arrays,” *Phys. Rev. Lett.* **122**, 173201 (2019).
- ¹²³A. Cooper, J. P. Covey, I. S. Madjarov, S. G. Porsev, M. S. Safronova, and M. Endres, “Alkaline-earth atoms in optical tweezers,” *Phys. Rev. X* **8**, 041055 (2018).
- ¹²⁴M. A. Norcia, A. W. Young, and A. M. Kaufman, “Microscopic control and detection of ultracold strontium in optical-tweezer arrays,” *Phys. Rev. X* **8**, 041054 (2018).
- ¹²⁵S. Sasaki, J. T. Wilson, B. Grinkemeyer, and J. D. Thompson, “Narrow-line cooling and imaging of ytterbium atoms in an optical tweezer array,” *Phys. Rev. Lett.* **122**, 143002 (2019).
- ¹²⁶A. W. Young, W. J. Eckner, W. R. Milner, D. Kedar, M. A. Norcia,

- E. Oelker, N. Schine, J. Ye, and A. M. Kaufman, “Half-minute-scale atomic coherence and high relative stability in a tweezer clock,” *Nature* **588**, 408–413 (2020).
- ¹²⁷I. D. Leroux, M. H. Schleier-Smith, and V. Vuletić, “Orientation-dependent entanglement lifetime in a squeezed atomic clock,” *Phys. Rev. Lett.* **104**, 250801 (2010).
- ¹²⁸O. Hosten, N. J. Engelsen, R. Krishnakumar, and M. A. Kasevich, “Measurement noise 100 times lower than the quantum-projection limit using entangled atoms,” *Nature* **529**, 505–508 (2016).
- ¹²⁹B. Braverman, A. Kawasaki, E. Pedrozo-Peñafiel, S. Colombo, C. Shu, Z. Li, E. Mendez, M. Yamoah, L. Salvi, D. Akamatsu, *et al.*, “Near-unitary spin squeezing in ^{171}Yb ,” *Phys. Rev. Lett.* **122**, 223203 (2019).
- ¹³⁰J. M. Robinson, M. Miklos, Y. M. Tso, C. J. Kennedy, T. Bothwell, D. Kedar, J. K. Thompson, and J. Ye, “Direct comparison of two spin-squeezed optical clock ensembles at the 10^{-17} level,” *Nat. Phys.* **20**, 208–213 (2024).
- ¹³¹R. Finkelstein, R. B.-S. Tsai, X. Sun, P. Scholl, S. Direkci, T. Gefen, J. Choi, A. L. Shaw, and M. Endres, “Universal quantum operations and ancilla-based read-out for tweezer clocks,” *Nature* **634**, 321–327 (2024).
- ¹³²A. Cao, W. J. Eckner, T. Lukin Yelin, A. W. Young, S. Jandura, L. Yan, K. Kim, G. Pupillo, J. Ye, N. Darkwah Oppong, *et al.*, “Multi-qubit gates and schrödinger cat states in an optical clock,” *Nature* **634**, 315–320 (2024).
- ¹³³W. Paul, “Electromagnetic traps for charged and neutral particles,” *Rev. Mod. Phys.* **62**, 531–540 (1990).
- ¹³⁴E. Fischer, “Die dreidimensionale stabilisierung von ladungsträgern in einem vierpolfeld,” *Zeitschrift für Physik* **156**, 1–26 (1959).
- ¹³⁵W. Paul, O. Osberghaus, and E. Fischer, *Berichte Des Wirtschaftsministeriums Nordrhein-Westfalen Nr. 415* (1958).
- ¹³⁶A. Tofful, C. F. A. Baynham, E. A. Curtis, A. O. Parsons, B. I. Robertson, M. Schioppa, J. Tunesi, H. S. Margolis, R. J. Hendricks, J. Whale, *et al.*, “ $^{171}\text{Yb}^+$ optical clock with 2.2×10^{-18} systematic uncertainty and absolute frequency measurements,” *Metrologia* **61**, 045001 (2024).
- ¹³⁷N. Huntemann, C. Sanner, B. Lipphardt, C. Tamm, and E. Peik, “Single-ion atomic clock with 3×10^{-18} systematic uncertainty,” *Phys. Rev. Lett.* **116**, 063001 (2016).
- ¹³⁸A. A. Madej, P. Dubé, Z. Zhou, J. E. Bernard, and M. Gertsch, “ $^{88}\text{Sr}^+$ 445-THz single-ion reference at the 10^{-17} level via control and cancellation of systematic uncertainties and its measurement against the si second,” *Phys. Rev. Lett.* **109**, 203002 (2012).
- ¹³⁹P. O. Schmidt, T. Rosenband, C. Langer, W. M. Itano, J. C. Bergquist, and D. J. Wineland, “Spectroscopy using quantum logic,” *Science* **309**, 749–752 (2005).
- ¹⁴⁰K. J. Arnold, R. Kaewuam, A. Roy, T. R. Tan, and M. D. Barrett, “Black-body radiation shift assessment for a lutetium ion clock,” *Nat. Commun.* **9**, 1650 (2018).
- ¹⁴¹P. Zhang, J. Cao, H. Lin Shu, J. bo Yuan, J. Juan Shang, K. feng Cui, S. jia Chao, S. mao Wang, D. xin Liu, and X. ren Huang, “Evaluation of black-body radiation shift with temperature-associated fractional uncertainty at 10^{-18} level for $^{40}\text{Ca}^+$ ion optical clock,” *J. Phys. B: At. Mol. Opt. Phys.* **50**, 015002 (2016).
- ¹⁴²V. I. Yudin, A. V. Taichenachev, C. W. Oates, Z. W. Barber, N. D. Lemke, A. D. Ludlow, U. Sterr, C. Lisdat, and F. Riehle, “Hyper-ramsey spectroscopy of optical clock transitions,” *Phys. Rev. A* **82**, 011804 (2010).
- ¹⁴³N. Huntemann, B. Lipphardt, M. Okhapkin, C. Tamm, E. Peik, A. V. Taichenachev, and V. I. Yudin, “Generalized Ramsey excitation scheme with suppressed light shift,” *Phys. Rev. Lett.* **109**, 213002 (2012).
- ¹⁴⁴M. E. Kim, W. F. McGrew, N. V. Nardelli, E. R. Clements, Y. S. Hassan, X. Zhang, J. L. Valencia, H. Leopardi, D. B. Hume, T. M. Fortier, *et al.*, “Improved interspecies optical clock comparisons through differential spectroscopy,” *Nat. Phys.* **19**, 25–29 (2023).
- ¹⁴⁵N. Herschbach, K. Pyka, J. Keller, and T. E. Mehlstäubler, “Linear Paul trap design for an optical clock with Coulomb crystals,” *Appl. Phys. B* **107**, 891–906 (2012).
- ¹⁴⁶N. Aharon, N. Spethmann, I. D. Leroux, P. O. Schmidt, and A. Retzker, “Robust optical clock transitions in trapped ions using dynamical decoupling,” *New J. Phys.* **21**, 083040 (2019).
- ¹⁴⁷K. Arnold, E. Hajiyev, E. Paez, C. H. Lee, M. D. Barrett, and J. Bollinger, “Prospects for atomic clocks based on large ion crystals,” *Phys. Rev. A* **92**, 032108 (2015).
- ¹⁴⁸R. Shaniv, N. Akerman, T. Manovitz, Y. Shapira, and R. Ozeri, “Quadrupole shift cancellation using dynamic decoupling,” *Phys. Rev. Lett.* **122**, 223204 (2019).
- ¹⁴⁹R. Kaewuam, T. R. Tan, K. J. Arnold, S. R. Chanu, Z. Zhang, and M. D. Barrett, “Hyperfine averaging by dynamic decoupling in a multi-ion lutetium clock,” *Phys. Rev. Lett.* **124**, 083202 (2020).
- ¹⁵⁰K. Cui, J. Valencia, K. T. Boyce, E. R. Clements, D. R. Leibbrandt, and D. B. Hume, “Scalable quantum logic spectroscopy,” *Phys. Rev. Lett.* **129**, 193603 (2022).
- ¹⁵¹A. Chodos and S. Detweiler, “Where has the fifth dimension gone?” *Phys. Rev. D* **21**, 2167–2170 (1980).
- ¹⁵²Y.-S. Wu and Z. Wang, “Time variation of Newton’s gravitational constant in superstring theories,” *Phys. Rev. Lett.* **57**, 1978–1981 (1986).
- ¹⁵³E. Kiritsis, “Supergravity, D-brane probes and thermal super Yang-Mills: a comparison,” *J. High Energy Phys.* **1999**, 010 (1999).
- ¹⁵⁴C. J. A. P. Martins, “The status of varying constants: a review of the physics, searches and implications,” *Rep. Prog. Phys.* **80**, 126902 (2017).
- ¹⁵⁵J. K. Webb, M. T. Murphy, V. V. Flambaum, V. A. Dzuba, J. D. Barrow, C. W. Churchill, J. X. Prochaska, and A. M. Wolfe, “Further evidence for cosmological evolution of the fine structure constant,” *Phys. Rev. Lett.* **87**, 091301 (2001).
- ¹⁵⁶K. Beeks, G. A. Kazakov, F. Schaden, I. Morawetz, L. T. de Col, T. Riebner, M. Bartokos, T. Sikorsky, T. Schumm, C. Zhang, *et al.*, “Fine-structure constant sensitivity of the Th-229 nuclear clock transition,” (2024), arXiv:2407.17300 [nucl-th].
- ¹⁵⁷M. S. Safronova, D. Budker, D. DeMille, D. F. J. Kimball, A. Derevianko, and C. W. Clark, “Search for new physics with atoms and molecules,” *Rev. Mod. Phys.* **90**, 025008 (2018).
- ¹⁵⁸M. S. Safronova, V. A. Dzuba, V. V. Flambaum, U. I. Safronova, S. G. Porsev, and M. G. Kozlov, “Highly charged ions for atomic clocks, quantum information, and search for α variation,” *Phys. Rev. Lett.* **113**, 030801 (2014).
- ¹⁵⁹J. C. Berengut, V. A. Dzuba, V. V. Flambaum, and A. Ong, “Electron-hole transitions in multiply charged ions for precision laser spectroscopy and searching for variations in α ,” *Phys. Rev. Lett.* **106**, 210802 (2011).
- ¹⁶⁰V. A. Dzuba, M. S. Safronova, U. I. Safronova, and V. V. Flambaum, “Actinide ions for testing the spatial α -variation hypothesis,” *Phys. Rev. A* **92**, 060502 (2015).
- ¹⁶¹J. C. Berengut, V. A. Dzuba, V. V. Flambaum, and A. Ong, “Optical transitions in highly charged californium ions with high sensitivity to variation of the fine-structure constant,” *Phys. Rev. Lett.* **109**, 070802 (2012).
- ¹⁶²M. Filzinger, S. Dörscher, R. Lange, J. Klose, M. Steinle, E. Benkler, E. Peik, C. Lisdat, and N. Huntemann, “Improved limits on the coupling of ultralight bosonic dark matter to photons from optical atomic clock comparisons,” *Phys. Rev. Lett.* **130**, 253001 (2023).
- ¹⁶³R. M. Godun, P. B. R. Nisbet-Jones, J. M. Jones, S. A. King, L. A. M. Johnson, H. S. Margolis, K. Szymaniec, S. N. Lea, K. Bongs, and P. Gill, “Frequency ratio of two optical clock transitions in $^{171}\text{Yb}^+$ and constraints on the time variation of fundamental constants,” *Phys. Rev. Lett.* **113**, 210801 (2014).
- ¹⁶⁴N. Huntemann, B. Lipphardt, C. Tamm, V. Gerginov, S. Weyers, and E. Peik, “Improved limit on a temporal variation of m_p/m_e from comparisons of Yb^+ and Cs atomic clocks,” *Phys. Rev. Lett.* **113**, 210802 (2014).
- ¹⁶⁵W. F. McGrew, X. Zhang, H. Leopardi, R. J. Fasano, D. Nicolodi, K. Boley, J. Yao, J. A. Sherman, S. A. Schäffer, J. Savory, *et al.*, “Towards the optical second: verifying optical clocks at the si limit,” *Optica* **6**, 448–454 (2019).
- ¹⁶⁶R. Lange, N. Huntemann, J. M. Rahm, C. Sanner, H. Shao, B. Lipphardt, C. Tamm, S. Weyers, and E. Peik, “Improved limits for violations of local position invariance from atomic clock comparisons,” *Phys. Rev. Lett.* **126**, 011102 (2021).
- ¹⁶⁷A. Shelkovich, R. J. Butcher, C. Chardonnet, and A. Amy-Klein, “Stability of the proton-to-electron mass ratio,” *Phys. Rev. Lett.* **100**, 150801 (2008).
- ¹⁶⁸J. Kobayashi, A. Ogino, and S. Inouye, “Measurement of the variation of electron-to-proton mass ratio using ultracold molecules produced from laser-cooled atoms,” *Nat. Commun.* **10**, 3771 (2019).
- ¹⁶⁹M. G. Kozlov, M. S. Safronova, J. R. Crespo López-Urrutia, and P. O. Schmidt, “Highly charged ions: Optical clocks and applications in fundamental physics,” *Rev. Mod. Phys.* **90**, 045005 (2018).

- ¹⁷⁰J. C. Berengut, V. A. Dzuba, V. V. Flambaum, and A. Ong, “Highly charged ions with E1, M1, and E2 transitions within laser range,” *Phys. Rev. A* **86**, 022517 (2012).
- ¹⁷¹W. Johnson and G. Soff, “The Lamb shift in hydrogen-like atoms, $1 \leq Z \leq 110$,” *At. Data Nucl. Data Tables* **33**, 405–446 (1985).
- ¹⁷²R. Loetzsch, H. F. Beyer, L. Duval, U. Spillmann, D. Banaś, P. Dergham, F. M. Kröger, J. Glorius, R. E. Grisenti, M. Guerra, *et al.*, “Testing quantum electrodynamics in extreme fields using helium-like uranium,” *Nature* **625**, 673–678 (2024).
- ¹⁷³J. C. Berengut, V. A. Dzuba, and V. V. Flambaum, “Enhanced laboratory sensitivity to variation of the fine-structure constant using highly charged ions,” *Phys. Rev. Lett.* **105**, 120801 (2010).
- ¹⁷⁴N.-H. Rehbehn, M. K. Rosner, H. Bekker, J. C. Berengut, P. O. Schmidt, S. A. King, P. Micke, M. F. Gu, R. Müller, A. Surzhykov, *et al.*, “Sensitivity to new physics of isotope-shift studies using the coronal lines of highly charged calcium ions,” *Phys. Rev. A* **103**, L040801 (2021).
- ¹⁷⁵N.-H. Rehbehn, M. K. Rosner, J. C. Berengut, P. O. Schmidt, T. Pfeifer, M. F. Gu, and J. R. C. López-Urrutia, “Narrow and ultranarrow transitions in highly charged Xe ions as probes of fifth forces,” *Phys. Rev. Lett.* **131**, 161803 (2023).
- ¹⁷⁶S. G. Porsev, C. Cheung, M. S. Safronova, H. Bekker, N.-H. Rehbehn, J. R. C. López-Urrutia, and S. M. Brewer, “Pr¹⁰⁺ as a candidate for a high-accuracy optical clock for tests of fundamental physics,” *Phys. Rev. A* **110**, 042823 (2024).
- ¹⁷⁷M. S. Safronova, V. A. Dzuba, V. V. Flambaum, U. I. Safronova, S. G. Porsev, and M. G. Kozlov, “Highly charged Ag-like and In-like ions for the development of atomic clocks and the search for α variation,” *Phys. Rev. A* **90**, 042513 (2014).
- ¹⁷⁸V. A. Dzuba, V. V. Flambaum, and H. Katori, “Optical clock sensitive to variations of the fine-structure constant based on the Ho¹⁴⁺ ion,” *Phys. Rev. A* **91**, 022119 (2015).
- ¹⁷⁹D. K. Nandy and B. K. Sahoo, “Highly charged W¹³⁺, Ir¹⁶⁺, and Pt¹⁷⁺ ions as promising optical clock candidates for probing variations of the fine-structure constant,” *Phys. Rev. A* **94**, 032504 (2016).
- ¹⁸⁰V. A. Dzuba and V. V. Flambaum, “Highly charged ions of heavy actinides as sensitive probes for time variation of the fine-structure constant,” *Phys. Rev. A* **110**, 012801 (2024).
- ¹⁸¹M. A. Levine, R. E. Marrs, J. R. Henderson, D. A. Knapp, and M. B. Schneider, “The electron beam ion trap: A new instrument for atomic physics measurements,” *Phys. Sci.* **1988**, 157 (1988).
- ¹⁸²L. Schmöger, M. Schwarz, T. M. Baumann, O. O. Versolato, B. Piest, T. Pfeifer, J. Ullrich, P. O. Schmidt, and J. R. Crespo López-Urrutia, “Deceleration, precooling, and multi-pass stopping of highly charged ions in Be⁺ coulomb crystals,” *Rev. Sci. Instrum.* **86**, 103111 (2015).
- ¹⁸³T. Leopold, S. A. King, P. Micke, A. Bautista-Salvador, J. C. Heip, C. Ospelkaus, J. R. Crespo López-Urrutia, and P. O. Schmidt, “A cryogenic radio-frequency ion trap for quantum logic spectroscopy of highly charged ions,” *Rev. Sci. Instrum.* **90**, 073201 (2019).
- ¹⁸⁴S. A. King, L. J. Spieß, P. Micke, A. Wilzewski, T. Leopold, E. Benkler, R. Lange, N. Huntemann, A. Surzhykov, V. A. Yerokhin, *et al.*, “An optical atomic clock based on a highly charged ion,” *Nature* **611**, 43–47 (2022).
- ¹⁸⁵H. Bekker, A. Borschevsky, Z. Harman, C. H. Keitel, T. Pfeifer, P. O. Schmidt, J. R. Crespo López-Urrutia, and J. C. Berengut, “Detection of the 5p – 4f orbital crossing and its optical clock transition in Pr⁹⁺,” *Nat. Commun.* **10**, 5651 (2019).
- ¹⁸⁶S. Chen, Z. Zhou, J. Li, T. Zhang, C. Li, T. Shi, Y. Huang, K. Gao, and H. Guan, “Precision measurement of M1 optical clock transition in Ni¹²⁺,” *Phys. Rev. Res.* **6**, 013030 (2024).
- ¹⁸⁷A. Yamaguchi, H. Muramatsu, T. Hayashi, N. Yuasa, K. Nakamura, M. Takimoto, H. Haba, K. Konashi, M. Watanabe, H. Kikunaga, *et al.*, “Energy of the ²²⁹Th nuclear clock isomer determined by absolute γ -ray energy difference,” *Phys. Rev. Lett.* **123**, 222501 (2019).
- ¹⁸⁸T. Sikorsky, J. Geist, D. Hengstler, S. Kempf, L. Gastaldo, C. Enss, C. Mokry, J. Runke, C. E. Düllmann, P. Wobrauschek, *et al.*, “Measurement of the ²²⁹Th isomer energy with a magnetic microcalorimeter,” *Phys. Rev. Lett.* **125**, 142503 (2020).
- ¹⁸⁹B. Seiferle, L. von der Wense, P. V. Bilous, I. Amersdorffer, C. Lemell, F. Libisch, S. Stellmer, T. Schumm, C. E. Düllmann, A. Pálffy, *et al.*, “Energy of the ²²⁹Th nuclear clock transition,” *Nature* **573**, 243–246 (2019).
- ¹⁹⁰S. Kraemer, J. Moens, M. Athanasakis-Kaklamanakis, S. Bara, K. Beeks, P. Chhetri, K. Chrysalidis, A. Claessens, T. E. Cocolios, J. G. M. Correia, *et al.*, “Observation of the radiative decay of the ²²⁹Th nuclear clock isomer,” *Nature* **617**, 706–710 (2023).
- ¹⁹¹T. Hiraki, K. Okai, M. Bartokos, K. Beeks, H. Fujimoto, Y. Fukunaga, H. Haba, Y. Kasamatsu, S. Kitao, A. Leitner, *et al.*, “Controlling ²²⁹Th isomeric state population in a VUV transparent crystal,” *Nat. Commun.* **15**, 5536 (2024).
- ¹⁹²J. Tiedau, M. V. Okhapkin, K. Zhang, J. Thielking, G. Zitzer, E. Peik, F. Schaden, T. Pronebner, I. Morawetz, L. T. De Col, *et al.*, “Laser excitation of the Th-229 nucleus,” *Phys. Rev. Lett.* **132**, 182501 (2024).
- ¹⁹³R. Elwell, C. Schneider, J. Jeet, J. E. S. Terhune, H. W. T. Morgan, A. N. Alexandrova, H. B. Tran Tan, A. Derevianko, and E. R. Hudson, “Laser excitation of the ²²⁹Th nuclear isomeric transition in a solid-state host,” *Phys. Rev. Lett.* **133**, 013201 (2024).
- ¹⁹⁴C. Zhang, T. Ooi, J. S. Higgins, J. F. Doyle, L. von der Wense, K. Beeks, A. Leitner, G. A. Kazakov, P. Li, P. G. Thirolf, *et al.*, “Frequency ratio of the ^{229m}Th nuclear isomeric transition and the ⁸⁷Sr atomic clock,” *Nature* **633**, 63–70 (2024).
- ¹⁹⁵J. S. Higgins, T. Ooi, J. F. Doyle, C. Zhang, J. Ye, K. Beeks, T. Sikorsky, and T. Schumm, “Temperature sensitivity of a thorium-229 solid-state nuclear clock,” (2024), arXiv:2409.11590 [physics.atom-ph].
- ¹⁹⁶A. Yamaguchi, Y. Shigekawa, H. Haba, H. Kikunaga, K. Shirasaki, M. Wada, and H. Katori, “Laser spectroscopy of triply charged ²²⁹Th isomer for a nuclear clock,” *Nature* **629**, 62–66 (2024).
- ¹⁹⁷V. V. Flambaum, “Enhanced effect of temporal variation of the fine structure constant and the strong interaction in ²²⁹Th,” *Phys. Rev. Lett.* **97**, 092502 (2006).
- ¹⁹⁸H. W. T. Morgan, R. Elwell, J. E. S. Terhune, H. B. T. Tan, U. C. Perera, A. Derevianko, A. N. Alexandrova, and E. R. Hudson, “²²⁹Th-doped nonlinear optical crystals for compact solid-state clocks,” (2024), arXiv:2410.23364 [physics.optics].
- ¹⁹⁹E. Corbelli and P. Salucci, “The extended rotation curve and the dark matter halo of M33,” *Mon. Not. Roy. Astron. Soc.* **311**, 441–447 (2000).
- ²⁰⁰R. Massey, T. Kitching, and J. Richard, “The dark matter of gravitational lensing,” *Rep. Prog. Phys.* **73**, 086901 (2010).
- ²⁰¹Planck Collaboration, “Planck 2018 results - I. overview and the cosmological legacy of planck,” *Astron. Astrophys.* **641**, A1 (2020).
- ²⁰²T. D. Brandt, “Constraints on macho dark matter from compact stellar systems in ultra-faint dwarf galaxies,” *Astrophys. J. Lett.* **824**, L31 (2016).
- ²⁰³S. Navas, C. Amsler, T. Gutsche, C. Hanhart, J. J. Hernández-Rey, C. Lourenço, A. Masoni, M. Mikhasenko, R. E. Mitchell, C. Patrignani, *et al.* (Particle Data Group Collaboration), “Review of particle physics,” *Phys. Rev. D* **110**, 030001 (2024).
- ²⁰⁴W. Hu, R. Barkana, and A. Gruzinov, “Fuzzy cold dark matter: The wave properties of ultralight particles,” *Phys. Rev. Lett.* **85**, 1158–1161 (2000).
- ²⁰⁵E. G. M. Ferreira, “Ultra-light dark matter,” *Astron. and Astrophys. Rev.* **29**, 7 (2021).
- ²⁰⁶M. Aghaie, G. Armando, A. Dondarini, and P. Pani, “Bounds on ultralight dark matter from NANOGrav,” *Phys. Rev. D* **109**, 103030 (2024).
- ²⁰⁷K. Blum, R. T. D’Agnolo, M. Lisanti, and B. R. Safdi, “Constraining axion dark matter with big bang nucleosynthesis,” *Phys. Lett. B* **737**, 30–33 (2014).
- ²⁰⁸G. G. Raffelt, “Astrophysical methods to constrain axions and other novel particle phenomena,” *Phys. Rep.* **198**, 1–113 (1990).
- ²⁰⁹P. Carena, T. Fischer, M. Giannotti, G. Guo, G. Martínez-Pinedo, and A. Mirizzi, “Improved axion emissivity from a supernova via nucleon-nucleon bremsstrahlung,” *J. Cosmol. Astropart. Phys.* **2019**, 016 (2019).
- ²¹⁰M. Buschmann, C. Dessert, J. W. Foster, A. J. Long, and B. R. Safdi, “Upper limit on the QCD axion mass from isolated neutron star cooling,” *Phys. Rev. Lett.* **128**, 091102 (2022).
- ²¹¹N. Du, N. Force, R. Khatiwada, E. Lentz, R. Ottens, L. J. Rosenberg, G. Rybka, G. Carosi, N. Woollett, D. Bowring, *et al.* (ADMX Collaboration), “Search for invisible axion dark matter with the axion dark matter experiment,” *Phys. Rev. Lett.* **120**, 151301 (2018).
- ²¹²O. Kwon, D. Lee, W. Chung, D. Ahn, H. Byun, F. Caspers, H. Choi, J. Choi, Y. Chong, H. Jeong, *et al.*, “First results from an axion haloscope at capp around 10.7 μ eV,” *Phys. Rev. Lett.* **126**, 191802 (2021).
- ²¹³S. Chaudhuri, P. W. Graham, K. Irwin, J. Mardon, S. Rajendran, and Y. Zhao, “Radio for hidden-photon dark matter detection,” *Phys. Rev. D* **92**, 075012 (2015).

- ²¹⁴C. P. Salemi, J. W. Foster, J. L. Ouellet, A. Gavin, K. M. W. Pappas, S. Cheng, K. A. Richardson, R. Henning, Y. Kahn, R. Nguyen, *et al.*, “Search for low-mass axion dark matter with ABRACADABRA-10 cm,” *Phys. Rev. Lett.* **127**, 081801 (2021).
- ²¹⁵F. Della Valle, A. Ejlli, U. Gastaldi, G. Messineo, E. Milotti, R. Pengo, G. Ruoso, and G. Zavattini, “The PVLAS experiment: measuring vacuum magnetic birefringence and dichroism with a birefringent fabry-perot cavity,” *Eur. Phys. J. C* **76**, 24 (2016).
- ²¹⁶R. Ballou, G. Deferne, M. Finger, M. Finger, L. Flekova, J. Hosek, S. Kunc, K. Macuchova, K. A. Meissner, P. Pugnat, *et al.* (OSQAR Collaboration), “New exclusion limits on scalar and pseudoscalar axionlike particles from light shining through a wall,” *Phys. Rev. D* **92**, 092002 (2015).
- ²¹⁷P. W. Graham, D. E. Kaplan, J. Mardon, S. Rajendran, and W. A. Terrano, “Dark matter direct detection with accelerometers,” *Phys. Rev. D* **93**, 075029 (2016).
- ²¹⁸J. Bergé, P. Brax, G. Métris, M. Pernot-Borràs, P. Touboul, and J.-P. Uzan, “Microscope mission: First constraints on the violation of the weak equivalence principle by a light scalar dilaton,” *Phys. Rev. Lett.* **120**, 141101 (2018).
- ²¹⁹E. A. Shaw, M. P. Ross, C. A. Hagedorn, E. G. Adelberger, and J. H. Gundlach, “Torsion-balance search for ultralow-mass bosonic dark matter,” *Phys. Rev. D* **105**, 042007 (2022).
- ²²⁰C. Abel, N. J. Ayres, G. Ban, G. Bison, K. Bodek, V. Bondar, M. Daum, M. Fairbairn, V. V. Flambaum, P. Geltenbort, *et al.*, “Search for axionlike dark matter through nuclear spin precession in electric and magnetic fields,” *Phys. Rev. X* **7**, 041034 (2017).
- ²²¹A. Arvanitaki, J. Huang, and K. Van Tilburg, “Searching for dilaton dark matter with atomic clocks,” *Phys. Rev. D* **91**, 015015 (2015).
- ²²²A. Derevianko and M. Pospelov, “Hunting for topological dark matter with atomic clocks,” *Nat. Phys.* **10**, 933–936 (2014).
- ²²³B. M. Roberts, G. Blewitt, C. Dailey, M. Murphy, M. Pospelov, A. Rollings, J. Sherman, W. Williams, and A. Derevianko, “Search for domain wall dark matter with atomic clocks on board global positioning system satellites,” *Nat. Commun.* **8**, 1195 (2017).
- ²²⁴P. Wcisło, P. Ablewski, K. Belay, S. Bilicki, M. Bober, R. Brown, R. Fasano, R. Ciuryło, H. Hachisu, T. Ido, *et al.*, “New bounds on dark matter coupling from a global network of optical atomic clocks,” *Sci. Adv.* **4**, eaau4869 (2018).
- ²²⁵A. Banerjee, G. Perez, M. Safronova, I. Savoray, and A. Shalit, “The phenomenology of quadratically coupled ultra light dark matter,” *J. High Energy Phys.* **2023**, 42 (2023).
- ²²⁶H. Kim and G. Perez, “Oscillations of atomic energy levels induced by QCD axion dark matter,” *Phys. Rev. D* **109**, 015005 (2024).
- ²²⁷P. Wcisło, P. Morzyński, M. Bober, A. Cygan, D. Lisak, R. Ciuryło, and M. Zawada, “Experimental constraint on dark matter detection with optical atomic clocks,” *Nat. Astron.* **1**, 0009 (2016).
- ²²⁸N. Sherrill, A. O. Parsons, C. F. A. Baynham, W. Bowden, E. A. Curtis, R. Hendricks, I. R. Hill, R. Hobson, H. S. Margolis, B. I. Robertson, *et al.*, “Analysis of atomic-clock data to constrain variations of fundamental constants,” *New J. Phys.* **25**, 093012 (2023).
- ²²⁹C. J. Kennedy, E. Oelker, J. M. Robinson, T. Bothwell, D. Kedar, W. R. Milner, G. E. Marti, A. Derevianko, and J. Ye, “Precision metrology meets cosmology: Improved constraints on ultralight dark matter from atom-cavity frequency comparisons,” *Phys. Rev. Lett.* **125**, 201302 (2020).
- ²³⁰T. Kobayashi, A. Takamizawa, D. Akamatsu, A. Kawasaki, A. Nishiyama, K. Hosaka, Y. Hisai, M. Wada, H. Inaba, T. Tanabe, *et al.*, “Search for ultralight dark matter from long-term frequency comparisons of optical and microwave atomic clocks,” *Phys. Rev. Lett.* **129**, 241301 (2022).
- ²³¹P. Touboul, G. Métris, M. Rodrigues, J. Bergé, A. Robert, Q. Baghi, Y. André, J. Bedouet, D. Boulanger, S. Bremer, *et al.* (MICROSCOPE Collaboration), “MICROSCOPE mission: Final results of the test of the equivalence principle,” *Phys. Rev. Lett.* **129**, 121102 (2022).
- ²³²S. Schlamminger, K.-Y. Choi, T. A. Wagner, J. H. Gundlach, and E. G. Adelberger, “Test of the equivalence principle using a rotating torsion balance,” *Phys. Rev. Lett.* **100**, 041101 (2008).
- ²³³A. Banerjee, D. Budker, M. Filzinger, N. Huntemann, G. Paz, G. Perez, S. Porsev, and M. Safronova, “Oscillating nuclear charge radii as sensors for ultralight dark matter,” (2023), arXiv:2301.10784 [hep-ph].
- ²³⁴I. Kozyryev, Z. Lasner, and J. M. Doyle, “Enhanced sensitivity to ultralight bosonic dark matter in the spectra of the linear radical SrOH,” *Phys. Rev. A* **103**, 043313 (2021).
- ²³⁵E. Madge, G. Perez, and Z. Meir, “Prospects of nuclear-coupled-dark-matter detection via correlation spectroscopy of I_2^+ and Ca^+ ,” *Phys. Rev. D* **110**, 015008 (2024).
- ²³⁶Y.-D. Tsai, J. Eby, and M. S. Safronova, “Direct detection of ultralight dark matter bound to the sun with space quantum sensors,” *Nat. Astron.* **7**, 113–121 (2023).
- ²³⁷R. Oswald, A. Nevsky, V. Vogt, S. Schiller, N. L. Figueroa, K. Zhang, O. Tretiak, D. Antypas, D. Budker, A. Banerjee, *et al.*, “Search for dark-matter-induced oscillations of fundamental constants using molecular spectroscopy,” *Phys. Rev. Lett.* **129**, 031302 (2022).
- ²³⁸X. Zhang, A. Banerjee, M. Leysner, G. Perez, S. Schiller, D. Budker, and D. Antypas, “Search for ultralight dark matter with spectroscopy of radio-frequency atomic transitions,” *Phys. Rev. Lett.* **130**, 251002 (2023).
- ²³⁹Y. Zhou, R. Ranson, M. Panagiotou, and C. Overstreet, “Ytterbium atom interferometry for dark matter searches,” *Phys. Rev. A* **110**, 033313 (2024).
- ²⁴⁰E. Fuchs, F. Kirk, E. Madge, C. Paranjape, E. Peik, G. Perez, W. Ratzinger, and J. Tiedau, “Implications of the laser excitation of the Th-229 nucleus for dark matter searches,” (2024), arXiv:2407.15924 [hep-ph].
- ²⁴¹D. Antypas, A. Banerjee, C. Bartram, M. Baryakhtar, J. Betz, J. J. Bollinger, C. Boutan, D. Bowring, D. Budker, D. Carney, *et al.*, “New horizons: Scalar and vector ultralight dark matter,” (2022), arXiv:2203.14915 [hep-ex].
- ²⁴²J. C. Berengut, D. Budker, C. Delaunay, V. V. Flambaum, C. Frugieuele, E. Fuchs, C. Grojean, R. Harnik, R. Ozeri, G. Perez, *et al.*, “Probing new long-range interactions by isotope shift spectroscopy,” *Phys. Rev. Lett.* **120**, 091801 (2018).
- ²⁴³W. H. King, “Comments on the article ‘peculiarities of the isotope shift in the samarium spectrum,’” *J. Opt. Soc. Am.* **53**, 638–639 (1963).
- ²⁴⁴H. Miyake, N. C. Pisenti, P. K. Elgee, A. Sitarum, and G. K. Campbell, “Isotope-shift spectroscopy of the $^1S_0 \rightarrow ^3P_1$ and $^1S_0 \rightarrow ^3P_0$ transitions in strontium,” *Phys. Rev. Res.* **1**, 033113 (2019).
- ²⁴⁵J. C. Berengut and N. S. Oreshkina, “Second-order hyperfine structure in strontium and impact on new physics searches using isotope shift spectroscopy,” (2024), arXiv:2409.01530 [physics.atom-ph].
- ²⁴⁶J. C. Berengut, C. Delaunay, A. Geddes, and Y. Soreq, “Generalized King linearity and new physics searches with isotope shifts,” *Phys. Rev. Res.* **2**, 043444 (2020).
- ²⁴⁷Y. Yamamoto, “The dual King relation,” *Phys. Lett. B* **838**, 137682 (2023).
- ²⁴⁸Firak, D. S., Krasznahorkay, A. J., Csatlós, M., Csige, L., Gulyás, J., Koszta, M., Szihalmi, B., Timár, J., Nagy, Á., Sas, N. J., *et al.*, “Confirmation of the existence of the X17 particle,” *EPJ Web Conf.* **232**, 04005 (2020).
- ²⁴⁹S. Hofsäss, J. E. Padilla-Castillo, S. C. Wright, S. Kray, R. Thomas, B. G. Sartakov, B. Ohayon, G. Meijer, and S. Truppe, “High-resolution isotope-shift spectroscopy of Cd I,” *Phys. Rev. Res.* **5**, 013043 (2023).
- ²⁵⁰B. Ohayon, S. Hofsäss, J. E. Padilla-Castillo, S. C. Wright, G. Meijer, S. Truppe, K. Gibble, and B. K. Sahoo, “Isotope shifts in cadmium as a sensitive probe for physics beyond the standard model,” *New J. Phys.* **24**, 123040 (2022).
- ²⁵¹N. Bhatt, K. Kato, and A. C. Vutha, “Nd⁺ isotope shift measurements in a cryogenically cooled neutral plasma,” *Phys. Rev. A* **101**, 052505 (2020).
- ²⁵²I. Counts, J. Hur, D. P. L. Aude Craik, H. Jeon, C. Leung, J. C. Berengut, A. Geddes, A. Kawasaki, W. Jhe, and V. Vuletić, “Evidence for nonlinear isotope shift in Yb⁺ search for new boson,” *Phys. Rev. Lett.* **125**, 123002 (2020).
- ²⁵³C. Solaro, S. Meyer, K. Fisher, J. C. Berengut, E. Fuchs, and M. Drewsen, “Improved isotope-shift-based bounds on bosons beyond the standard model through measurements of the $^2D_{3/2} - ^2D_{5/2}$ interval in Ca⁺,” *Phys. Rev. Lett.* **125**, 123003 (2020).
- ²⁵⁴J. Hur, D. P. L. Aude Craik, I. Counts, E. Knyazev, L. Caldwell, C. Leung, S. Pandey, J. C. Berengut, A. Geddes, W. Nazarewicz, *et al.*, “Evidence of two-source King plot nonlinearity in spectroscopic search for new boson,” *Phys. Rev. Lett.* **128**, 163201 (2022).
- ²⁵⁵K. Ono, Y. Saito, T. Ishiyama, T. Higomoto, T. Takano, Y. Takasu, Y. Yamamoto, M. Tanaka, and Y. Takahashi, “Observation of nonlinearity of generalized King plot in the search for new boson,” *Phys. Rev. X* **12**, 021033 (2022).
- ²⁵⁶N. L. Figueroa, J. C. Berengut, V. A. Dzuba, V. V. Flambaum, D. Budker, and D. Antypas, “Precision determination of isotope shifts in ytterbium

- and implications for new physics,” *Phys. Rev. Lett.* **128**, 073001 (2022).
- ²⁵⁷M. Door, C.-H. Yeh, M. Heinz, F. Kirk, C. Lyu, T. Miyagi, J. C. Berengut, J. Bieroń, K. Blaum, L. S. Dreissen, *et al.*, “Search for new bosons with ytterbium isotope shifts,” (2024), arXiv:2403.07792 [physics.atom-ph].
- ²⁵⁸W. Huang, M. Wang, F. Kondev, G. Audi, and S. Naimi, “The AME 2020 atomic mass evaluation (I). Evaluation of input data, and adjustment procedures,” *Chin. Phys. C* **45**, 030002 (2021).
- ²⁵⁹M. Wang, W. Huang, F. Kondev, G. Audi, and S. Naimi, “The AME 2020 atomic mass evaluation (ii). tables, graphs and references*,” *Chin. Phys. C* **45**, 030003 (2021).
- ²⁶⁰D. Nesterenko, R. de Groote, T. Eronen, Z. Ge, M. Hukkanen, A. Jokinen, and A. Kankainen, “High-precision mass measurement of ^{168}Yb for verification of nonlinear isotope shift,” *Int. J. Mass Spectrom.* **458**, 116435 (2020).
- ²⁶¹T. D. Lee and C. N. Yang, “Question of parity conservation in weak interactions,” *Phys. Rev.* **104**, 254–258 (1956).
- ²⁶²C. S. Wu, E. Ambler, R. W. Hayward, D. D. Hoppes, and R. P. Hudson, “Experimental test of parity conservation in beta decay,” *Phys. Rev.* **105**, 1413–1415 (1957).
- ²⁶³C. Bouchiat and P. Fayet, “Constraints on the parity-violating couplings of a new gauge boson,” *Phys. Lett. B* **608**, 87–94 (2005).
- ²⁶⁴G. Arcadi, M. Lindner, J. Martins, and F. S. Queiroz, “New physics probes: Atomic parity violation, polarized electron scattering and neutrino-nucleus coherent scattering,” *Nucl. Phys. B* **959**, 115158 (2020).
- ²⁶⁵C. Bouchiat and C. Pickett, “Parity violation in atomic cesium and alternatives to the standard model of electroweak interactions,” *Phys. Lett. B* **128**, 73–78 (1983).
- ²⁶⁶M. A. Bouchiat and C. Bouchiat, “I. parity violation induced by weak neutral currents in atomic physics,” *J. Phys. France* **35**, 899 (1974).
- ²⁶⁷M. A. Bouchiat and C. Bouchiat, “Parity violation induced by weak neutral currents in atomic physics. part II,” *J. Phys. France* **36**, 493 (1975).
- ²⁶⁸C. S. Wood, S. C. Bennett, D. Cho, B. P. Masterson, J. L. Roberts, C. E. Tanner, and C. E. Wieman, “Measurement of parity nonconservation and an anapole moment in cesium,” *Science* **275**, 1759–1763 (1997).
- ²⁶⁹S. L. Gilbert and C. E. Wieman, “Atomic-beam measurement of parity nonconservation in cesium,” *Phys. Rev. A* **34**, 792–803 (1986).
- ²⁷⁰K. Tsigutkin, D. Dounas-Frazer, A. Family, J. E. Stalnaker, V. V. Yashchuk, and D. Budker, “Observation of a large atomic parity violation effect in ytterbium,” *Phys. Rev. Lett.* **103**, 071601 (2009).
- ²⁷¹D. Antypas, A. Fabricant, J. E. Stalnaker, K. Tsigutkin, V. V. Flambaum, and D. Budker, “Isotopic variation of parity violation in atomic ytterbium,” *Nat. Phys.* **15**, 120–123 (2019).
- ²⁷²J. E. Simsarian, A. Ghosh, G. Gwinner, L. A. Orozco, G. D. Sprouse, and P. A. Voytas, “Magneto-optic trapping of ^{210}Fr ,” *Phys. Rev. Lett.* **76**, 3522–3525 (1996).
- ²⁷³R. Collister, G. Gwinner, M. Tandecki, J. A. Behr, M. R. Pearson, J. Zhang, L. A. Orozco, S. Aubin, and E. Gomez (FrPNC Collaboration), “Isotope shifts in francium isotopes $^{206-213}\text{Fr}$ and ^{221}Fr ,” *Phys. Rev. A* **90**, 052502 (2014).
- ²⁷⁴M. R. Kalita, J. A. Behr, A. Gorelov, M. R. Pearson, A. C. DeHart, G. Gwinner, M. J. Kossin, L. A. Orozco, S. Aubin, E. Gomez, *et al.*, “Isotope shifts in the $7s \rightarrow 8s$ transition of francium: Measurements and comparison to ab initio theory,” *Phys. Rev. A* **97**, 042507 (2018).
- ²⁷⁵J. A. Quirk, A. Jacobsen, A. Damitz, C. E. Tanner, and D. S. Elliott, “Measurement of the static stark shift of the $7s^2S_{1/2}$ level in atomic cesium,” *Phys. Rev. Lett.* **132**, 233201 (2024).
- ²⁷⁶D. DeMille, S. B. Cahn, D. Murphree, D. A. Rahmlow, and M. G. Kozlov, “Using molecules to measure nuclear spin-dependent parity violation,” *Phys. Rev. Lett.* **100**, 023003 (2008).
- ²⁷⁷V. Flambaum and I. Khriplovich, “On the enhancement of parity nonconserving effects in diatomic molecules,” *Phys. Lett. A* **110**, 121–125 (1985).
- ²⁷⁸M. G. Kozlov and L. N. Labzowsky, “Parity violation effects in diatomics,” *J. Phys. B: At. Mol. Opt. Phys.* **28**, 1933 (1995).
- ²⁷⁹N. Leefer, L. Bougas, D. Antypas, and D. Budker, “Towards a new measurement of parity violation in dysprosium,” (2014), arXiv:1412.1245 [physics.atom-ph].
- ²⁸⁰E. Altuntaş, J. Ammon, S. B. Cahn, and D. DeMille, “Demonstration of a sensitive method to measure nuclear-spin-dependent parity violation,” *Phys. Rev. Lett.* **120**, 142501 (2018).
- ²⁸¹Z. Zeng, S. Deng, S. Yang, and B. Yan, “Three-dimensional magneto-optical trapping of barium monofluoride,” *Phys. Rev. Lett.* **133**, 143404 (2024).
- ²⁸²M. Bouchiat, J. Guena, L. Hunter, and L. Pottier, “Observation of a parity violation in cesium,” *Phys. Lett. B* **117**, 358–364 (1982).
- ²⁸³M. Bouchiat, J. Guena, and L. Pottier, “Atomic parity violation measurements in the highly forbidden $6S_{1/2}-7S_{1/2}$ caesium transition. II. analysis and control of systematic effects,” *J. Phys. France* **47**, 1175 (1986).
- ²⁸⁴M. C. Noecker, B. P. Masterson, and C. E. Wieman, “Precision measurement of parity nonconservation in atomic cesium: A low-energy test of the electroweak theory,” *Phys. Rev. Lett.* **61**, 310–313 (1988).
- ²⁸⁵G. Lüders, “On the equivalence of invariance under time reversal and under particle-antiparticle conjugation for relativistic field theories,” *Kgl. Danske Videnskab. Selskab. Mat.-Fys. Medd.* **28**, 1–17 (1954).
- ²⁸⁶G. Lüders, “Proof of the TCP theorem,” *Annals of Physics* **2**, 1–15 (1957).
- ²⁸⁷C. Cesarotti, Q. Lu, Y. Nakai, A. Parikh, and M. Reece, “Interpreting the electron EDM constraint,” *J. High Energy Phys.* **2019**, 59 (2019).
- ²⁸⁸M. Pospelov and A. Ritz, “CKM benchmarks for electron electric dipole moment experiments,” *Phys. Rev. D* **89**, 056006 (2014).
- ²⁸⁹D. V. Chubukov and L. N. Labzowsky, “ \mathcal{P} , \mathcal{T} -odd electron-nucleus interaction in atomic systems as an exchange by higgs bosons,” *Phys. Rev. A* **93**, 062503 (2016).
- ²⁹⁰Y. Ema, T. Gao, and M. Pospelov, “Standard model prediction for paramagnetic electric dipole moments,” *Phys. Rev. Lett.* **129**, 231801 (2022).
- ²⁹¹E. M. Purcell and N. F. Ramsey, “On the possibility of electric dipole moments for elementary particles and nuclei,” *Phys. Rev.* **78**, 807–807 (1950).
- ²⁹²C. Abel, S. Afach, N. J. Ayres, C. A. Baker, G. Ban, G. Bison, K. Bodek, V. Bondar, M. Burghoff, E. Chanel, *et al.*, “Measurement of the permanent electric dipole moment of the neutron,” *Phys. Rev. Lett.* **124**, 081803 (2020).
- ²⁹³V. Andreev, D. G. Ang, D. DeMille, J. M. Doyle, G. Gabrielse, J. Haefner, N. R. Hutzler, Z. Lasner, C. Meisenhelder, B. R. O’Leary, *et al.*, “Improved limit on the electric dipole moment of the electron,” *Nature* **562**, 355–360 (2018).
- ²⁹⁴G. W. Bennett, B. Bousquet, H. N. Brown, G. Bunce, R. M. Carey, P. Cushman, G. T. Danby, P. T. Debevec, M. Deile, H. Deng, *et al.* (Muon (g-2) Collaboration), “Improved limit on the muon electric dipole moment,” *Phys. Rev. D* **80**, 052008 (2009).
- ²⁹⁵B. Graner, Y. Chen, E. G. Lindahl, and B. R. Heckel, “Reduced limit on the permanent electric dipole moment of ^{199}Hg ,” *Phys. Rev. Lett.* **116**, 161601 (2016).
- ²⁹⁶T. A. Zheng, Y. A. Yang, S.-Z. Wang, J. T. Singh, Z.-X. Xiong, T. Xia, and Z.-T. Lu, “Measurement of the electric dipole moment of ^{171}Yb atoms in an optical dipole trap,” *Phys. Rev. Lett.* **129**, 083001 (2022).
- ²⁹⁷F. Allmendinger, I. Engin, W. Heil, S. Karpuk, H.-J. Krause, B. Niederländer, A. Offenhäusser, M. Repetto, U. Schmidt, and S. Zimmer, “Measurement of the permanent electric dipole moment of the ^{129}Xe atom,” *Phys. Rev. A* **100**, 022505 (2019).
- ²⁹⁸M. Bishof, R. H. Parker, K. G. Bailey, J. P. Greene, R. J. Holt, M. R. Kalita, W. Korsch, N. D. Lemke, Z.-T. Lu, P. Mueller, *et al.*, “Improved limit on the ^{225}Ra electric dipole moment,” *Phys. Rev. C* **94**, 025501 (2016).
- ²⁹⁹T. E. Chupp, P. Fierlinger, M. J. Ramsey-Musolf, and J. T. Singh, “Electric dipole moments of atoms, molecules, nuclei, and particles,” *Rev. Mod. Phys.* **91**, 015001 (2019).
- ³⁰⁰L. I. Schiff, “Measurability of nuclear electric dipole moments,” *Phys. Rev.* **132**, 2194–2200 (1963).
- ³⁰¹G. Feinberg, “Effects of an electric dipole moment of the electron on the hydrogen energy levels,” *Phys. Rev.* **112**, 1637–1642 (1958).
- ³⁰²E. D. Commins, J. D. Jackson, and D. P. DeMille, “The electric dipole moment of the electron: An intuitive explanation for the evasion of Schiff’s theorem,” *Am. J. Phys.* **75**, 532–536 (2007).
- ³⁰³J. J. Hudson, B. E. Sauer, M. R. Tarbutt, and E. A. Hinds, “Measurement of the electron electric dipole moment using YbF molecules,” *Phys. Rev. Lett.* **89**, 023003 (2002).
- ³⁰⁴J. J. Hudson, D. M. Kara, I. J. Smallman, B. E. Sauer, M. R. Tarbutt, and E. A. Hinds, “Improved measurement of the shape of the electron,” *Nature* **473**, 493–496 (2011).
- ³⁰⁵D. Kawall, F. Bay, S. Bickman, Y. Jiang, and D. DeMille, “Precision zeeman-stark spectroscopy of the metastable $a(1)[^3\Sigma^+]$ state of PbO ,” *Phys. Rev. Lett.* **92**, 133007 (2004).
- ³⁰⁶D. G. Ang, C. Meisenhelder, C. D. Panda, X. Wu, D. DeMille, J. M. Doyle,

- and G. Gabrielse, “Measurement of the $H\ ^3\Delta_1$ radiative lifetime in ThO,” *Phys. Rev. A* **106**, 022808 (2022).
- ³⁰⁷N. R. Hutzler, M. F. Parsons, Y. V. Gurevich, P. W. Hess, E. Petrik, B. Spaun, A. C. Vutha, D. DeMille, G. Gabrielse, and J. M. Doyle, “A cryogenic beam of refractory, chemically reactive molecules with expansion cooling,” *Phys. Chem. Chem. Phys.* **13**, 18976–18985 (2011).
- ³⁰⁸T. S. Roussy, L. Caldwell, T. Wright, W. B. Cairncross, Y. Shagam, K. B. Ng, N. Schlossberger, S. Y. Park, A. Wang, J. Ye, *et al.*, “An improved bound on the electron’s electric dipole moment,” *Science* **381**, 46–50 (2023).
- ³⁰⁹X. Wu, P. Hu, Z. Han, D. G. Ang, C. Meisenhelder, G. Gabrielse, J. M. Doyle, and D. DeMille, “Electrostatic focusing of cold and heavy molecules for the ACME electron EDM search,” *New J. Phys.* **24**, 073043 (2022).
- ³¹⁰A. Hiramoto, T. Masuda, D. Ang, C. Meisenhelder, C. Panda, N. Sasao, S. Uetake, X. Wu, D. Demille, J. Doyle, *et al.*, “SiPM module for the ACME III electron EDM search,” *Nucl. Instrum. Methods Phys. Res. Sect. A* **1045**, 167513 (2023).
- ³¹¹K. B. Ng, Y. Zhou, L. Cheng, N. Schlossberger, S. Y. Park, T. S. Roussy, L. Caldwell, Y. Shagam, A. J. Vigil, E. A. Cornell, *et al.*, “Spectroscopy on the electron-electric-dipole-moment-sensitive states of ThF^+ ,” *Phys. Rev. A* **105**, 022823 (2022).
- ³¹²N. J. Fitch, J. Lim, E. A. Hinds, B. E. Sauer, and M. R. Tarbutt, “Methods for measuring the electron’s electric dipole moment using ultracold YbF molecules,” *Quantum Sci. Technol.* **6**, 014006 (2020).
- ³¹³T. Aoki, R. Sreekantham, B. K. Sahoo, B. Arora, A. Kastberg, T. Sato, H. Ikeda, N. Okamoto, Y. Torii, T. Hayamizu, *et al.*, “Quantum sensing of the electron electric dipole moment using ultracold entangled Fr atoms,” *Quantum Sci. Technol.* **6**, 044008 (2021).
- ³¹⁴A. D. Kudashov, A. N. Petrov, L. V. Skripnikov, N. S. Mosyagin, T. A. Isaev, R. Berger, and A. V. Titov, “Ab initio study of radium monofluoride (RaF) as a candidate to search for parity- and time-and-parity-violation effects,” *Phys. Rev. A* **90**, 052513 (2014).
- ³¹⁵R. F. Garcia Ruiz, R. Berger, J. Billowes, C. L. Binnersley, M. L. Bissell, A. A. Breier, A. J. Brinson, K. Chrysalidis, T. E. Cocolios, B. S. Cooper, *et al.*, “Spectroscopy of short-lived radioactive molecules,” *Nature* **581**, 396–400 (2020).
- ³¹⁶S. M. Udrescu, A. J. Brinson, R. F. G. Ruiz, K. Gaul, R. Berger, J. Billowes, C. L. Binnersley, M. L. Bissell, A. A. Breier, K. Chrysalidis, *et al.*, “Isotope shifts of radium monofluoride molecules,” *Phys. Rev. Lett.* **127**, 033001 (2021).
- ³¹⁷P. Yu and N. R. Hutzler, “Probing fundamental symmetries of deformed nuclei in symmetric top molecules,” *Phys. Rev. Lett.* **126**, 023003 (2021).
- ³¹⁸T. Fleig and D. DeMille, “Theoretical aspects of radium-containing molecules amenable to assembly from laser-cooled atoms for new physics searches,” *New J. Phys.* **23**, 113039 (2021).
- ³¹⁹G. Arrowsmith-Kron, M. Athanasakis-Kaklamanakis, M. Au, J. Ballof, R. Berger, A. Borschevsky, A. A. Breier, F. Buchinger, D. Budker, L. Caldwell, *et al.*, “Opportunities for fundamental physics research with radioactive molecules,” *Rep. Prog. Phys.* **87**, 084301 (2024).
- ³²⁰M. Fan, C. A. Holliman, X. Shi, H. Zhang, M. W. Straus, X. Li, S. W. Buechele, and A. M. Jayich, “Optical mass spectrometry of cold RaOH^+ and RaOCH_3^+ ,” *Phys. Rev. Lett.* **126**, 023002 (2021).
- ³²¹I. Kozyryev and N. R. Hutzler, “Precision measurement of time-reversal symmetry violation with laser-cooled polyatomic molecules,” *Phys. Rev. Lett.* **119**, 133002 (2017).
- ³²²M. Denis, P. A. B. Haase, R. G. E. Timmermans, E. Eliav, N. R. Hutzler, and A. Borschevsky, “Enhancement factor for the electric dipole moment of the electron in the BaOH and YbOH molecules,” *Phys. Rev. A* **99**, 042512 (2019).
- ³²³B. L. Augenbraun, Z. D. Lasner, A. Frenett, H. Sawaoka, A. T. Le, J. M. Doyle, and T. C. Steimle, “Observation and laser spectroscopy of ytterbium monomethoxide, YbOCH_3 ,” *Phys. Rev. A* **103**, 022814 (2021).
- ³²⁴N. H. Pilgram, A. Jadbabaie, Y. Zeng, N. R. Hutzler, and T. C. Steimle, “Fine and hyperfine interactions in $^{171}\text{YbOH}$ and $^{173}\text{YbOH}$,” *J. Chem. Phys.* **154**, 244309 (2021).
- ³²⁵T. C. Steimle, C. Linton, E. T. Mengesha, X. Bai, and A. T. Le, “Field-free, stark, and zeeman spectroscopy of the $\tilde{A}\ ^2\Pi_{1/2} - \tilde{X}\ ^2\Sigma^+$ transition of ytterbium monohydroxide,” *Phys. Rev. A* **100**, 052509 (2019).
- ³²⁶Z. D. Lasner, A. Frenett, H. Sawaoka, L. Anderegg, B. Augenbraun, H. Lampson, M. Li, A. Lunstad, J. Mango, A. Nasir, *et al.*, “Magneto-optical trapping of a heavy polyatomic molecule for precision measurement,” (2024), arXiv:2409.04948 [physics.atom-ph].
- ³²⁷C. Zhang, P. Yu, A. Jadbabaie, and N. R. Hutzler, “Quantum-enhanced metrology for molecular symmetry violation using decoherence-free subspaces,” *Phys. Rev. Lett.* **131**, 193602 (2023).